DEVELOPMENT AND CHARACTERIZATION OF SILK FIBROIN AND CITRUS PECTIN BASED SCAFFOLDS FOR BONE TISSUE ENGINEERING

A THESIS SUBMITTED TO
THE GRADUATE SCHOOL OF NATURAL AND APPLIED SCIENCES
OF
MIDDLE EAST TECHNICAL UNIVERSITY

BY

SİBEL ATAOL

IN PARTIAL FULFILLMENT OF THE REQUIREMENTS
FOR
THE DEGREE OF MASTER OF SCIENCE
IN
BIOMEDICAL ENGINEERING

DECEMBER 2014

Approval of the thesis:

DEVELOPMENT AND CHARACTERIZATION OF SILK FIBROIN AND CITRUS PECTIN BASED SCAFFOLDS FOR BONE TISSUE ENGINEERING

submitted by **SİBEL ATAOL** in partial fulfillment of the requirements for the degree of **Master of Science in Biomedical Engineering Department, Middle East Technical University** by,

Prof. Dr. Gülbin Dural Ünver _____
Dean, Graduate School of **Natural and Applied Sciences**

Prof. Dr. Vasıf N. Hasırcı _____
Head of **Department, Biomedical Engineering**

Assoc. Prof. Dr. Ayşen Tezcaner _____
Supervisor, **Engineering Sciences Department, METU**

Assoc. Prof. Dr. Akın Akdağ _____
Co-supervisor, **Chemistry Department, METU**

Examining Committee Members:

Assoc. Prof. Dr. Dilek Keskin _____
Engineering Sciences Department, METU

Assoc. Prof. Dr. Ayşen Tezcaner _____
Engineering Sciences Department, METU

Assoc. Prof. Dr. Akın Akdağ _____
Chemistry Department, METU

Prof. Dr. Şükrü Talaş _____
Metallurgical and Materials Engineering Dept., Afyon Kocatepe University

Assist. Prof. Dr. Urartu Özgür Şafak Şeker _____
Institute of Materials Science and Nanotechnology, UNAM, Bilkent University

DATE: _____

I hereby declare that all information in this document has been obtained and presented in accordance with academic rules and ethical conduct. I also declare that, as required by these rules and conduct, I have fully cited and referenced all material and results that are not original to this work.

Name, Last name: Sibel Ataol

Signature:

ABSTRACT

DEVELOPMENT AND CHARACTERIZATION OF SILK FIBROIN AND CITRUS PECTIN BASED SCAFFOLDS FOR BONE TISSUE ENGINEERING

Ataol, Sibel

M.S., Department of Biomedical Engineering

Supervisor: Assoc. Prof. Dr. Ayşen Tezcaner
Co-supervisor: Assoc. Prof. Dr. Akın Akdağ

December 2014, 164 pages

Current strategies of tissue engineering aim to design and develop biologically, physicochemically and mechanically proper scaffolds. Natural polymers are gaining interest in applications since they have already many roles in biochemical pathways and have proper mechanical properties. The objective of this thesis is to develop natural silk fibroin (SF) and citrus pectin (PEC) based three-dimensional porous scaffolds for bone tissue engineering applications. Additionally, we aimed to synthesize nano calcium phosphates with different Ca/P ratios using Flame Spray Pyrolysis method for preparing polymer/bioceramic composite scaffolds for future studies. Human urine derived stem cells were used for testing the *in vitro* biocompatibility of scaffolds and synthesized particles.

The scaffolds were obtained by freeze-drying of chemically crosslinked scaffolds which prepared by three different methods; namely click reactions, carbodiimide reactions and imine formation reactions. The materials were chemically modified for these crosslinking processes. Further physical modifications were conducted by immersing into methanol and $CaCl_2$. FTIR-ATR analyses confirmed the chemical modifications. Degradation profiles of scaffolds were assessed to compare the crosslinking efficiency of the different crosslinking agents and *in vivo* stability of the

scaffolds. Silk fibroin-amidated pectin (SF:A.PEC) scaffolds crosslinked with EDC and oxidized pectin, amidated pectin and silk fibroin (O.PEC:A-PEC:SF) scaffolds pregelated with 0.015 M had lower weight loss after 1 week incubation and highest water adsorption. SEM analyses revealed that scaffolds had porous internal structures, with a polymer skin layer. To reinforce scaffolds with bioactive agents, nano sized calcium phosphates were synthesized. Nanoparticles were produced at different calcium to phosphorus ratios (1.20-2.19).

X-ray diffraction (XRD) patterns, high resolution transmission electron microscopy (HRTEM), and selected area electron diffraction (SAED) analyses revealed the amorphous nature of the particles at low Ca/P ratios. An increase in the specific surface area and crystallinity were observed with increasing Ca/P ratios. In vitro cytotoxicity studies using human derived stem cells showed that there was no composition and dose dependent cytotoxic effect of nanoparticles on stem cells (5-50 μg/ml). Cells treated with prepared nanoparticles had higher alkaline phosphatase (ALP) enzyme activity than the control cells, indicating positive effect on osteogenic differentiation of the cells. Future studies are suggested to be investigated on use of urine derived stem cells seeded silk fibroin and citrus pectin based scaffolds reinforced with calcium phosphate nanoparticles as a potential engineered construct for regeneration of bone.

Keywords: bone tissue engineering, silk fibroin, citrus pectin, flame spray pyrolysis, nano calcium phosphates, and urine derived cells.

ÖZ

KEMİK DOKU MÜHENDİSLİĞİNE YÖNELİK İPEK FİBROİNİ VE TURUNÇGİL PEKTİNİ TABANLI TAŞIYICILARIN GELİŞTİRİLMESİ VE KARAKTERİZASYONU

Ataol, Sibel
Yüksek Lisans, Biyomedikal Mühendisliği Bölümü
Tez Yöneticisi: Doç. Dr. Ayşen Tezcaner
Ortak Tez Yöneticisi: Doç. Dr. Akın Akdağ

Aralık 2014, 164 sayfa

Doku mühendisliği, biyolojik, fizikokimyasal ve mekanik özellikleri bakımından uygun, hücre yüklenmiş üç boyutlu taşıyıcı geliştirmeyi hedefler. Biyolojik kökenli malzemeler, vücutta birçok biyokimyasal reaksiyonda görev aldığı ve uygun mekanik dayanıma sahip olduğu için bu uygulama alanında ilgi görmektedir. Bu çalışmanın amacı, kemik doku mühendisliğine yönelik doğal malzemelerden ipek fibroin proteini ve turunçgil pektin polisakkariti ile üç boyutlu ve gözenekli taşıyıcılar geliştirmektir. Ayrıca ileriki çalışmalarda polimer/seramik kompozit yapıda taşıyıcı oluşturmak için Alev Sprey Pirolizi yöntemi ile nano boyutta kalsiyum fosfat tuzları sentezlenmesi amaçlanmıştır. Taşıyıcının ve sentezlenen partiküllerin biyolojik karakterizasyon çalışmaları için idrar örneklerinden izole edilen kök hücreler kullanılmıştır.

Taşıyıcılar, klik reaksiyonları, karbodiimit reaksiyonları ve imin bağı oluşturma reaksiyonları olmak üzere üç farklı kimyasal çapraz bağlama işlemi gerçekleştirildikten sonra dondurulup liyofilizasyon işlemi uygulanarak elde edilmiştir. Bu işlemler için polimerler kimyasal olarak modifiye edilmiştir. Metanol ve $CaCl_2$ uygulaması yapılarak polimerlerin fiziksel çapraz bağlanma işlemi indüklenmiştir. Taşıyıcı, FTIR ATR analizi ile karakterize edilmişlerdir. Çapraz bağlama işlemi sonrası taşıyıcıların bozunma profili incelenerek çapraz bağlama

işleminin verimi kullanılan farklı çapraz bağlayıcı ajana ve in vivo dayanıklılığına göre kıyaslanmıştır. EDC ile çapraz bağlanmış ipek fibroini ve amit bağı içeren turunçgil pektini taşıyıcıları ve 0.015 M borax varlığında önceden jelleşme uygulanan ipek fibroini, oksitlenmiş pektin ve amit bağı içeren pektin karışımı taşıyıcılar, 1 haftalık inkübasyon sonucunda daha düşük ağırlık kaybı ve en yüksek su tutabilme değerlerine sahiptir. SEM analizi sonuçlarına göre taşıyıcılar üst yüzeylerinde polimer katmanına sahiptir ve taşıyıcıların gözenekli bir yapısı olduğu gözlemlenmiştir Taşıyıcıları biyoaktif ajanlar ile güçlendirmek için nano boyutta kalsiyum fosfat tuzları sentezlenmiştir. Partiküller farklı kalsiyum fosfat mol oranlarında sentezlenmiştir (1.20-2.19).

XRD dağılımı, HRTEM, SAED analizi, TGA-DTA analizleri ile partiküllerin amorf yapısının düşük Ca/P oranlarında arttığı analiz edilmiştir. Artan Ca/P oranı ile partiküllerin spesifik yüzey alanında ve kristallin yapısında artış gözlemlenmiştir. İn vitro sitotoksisite çalışmaları, idrardan elde edilen kök hücreler ile yürütülmüş, partiküllerin kompozisyon ve doza bağlı sitotoksik etkisi gözlemlenmemiştir (5-50 µg/ml). Nanopartiküller ile test edilen hücrelerin, kontrol grubu hücrelerine göre daha fazla ALP enzim aktivitesine sahip olduğu gözlemlenmiştir. Bu sonuç, partiküllerin osteojenik değişimde indüktif etkisi olduğunu göstermektedir. Kemik dokusunun rejenerasyonunda kullanmak amacıyla tasarlanmış ipek fibroini ve turunçgil pektini tabanlı potansiyel taşıyıcıların sentezlenen nano boyuttaki kalsiyum fosfat tuzları ile güçlendirilmesi ve idrar kökenli kök hücreler ile yüklenme çalışmaları ve bu yapının geliştirilmesi önerilmektedir.

Anahtar Kelimeler: Kemik doku mühendisliği, ipek fibroini, turunçgil pektini, alev sprey pirolizi, nano boyutta kalsiyum fosfat tuzları, idrar kökenli kök hücre

ACKNOWLEDGEMENTS

I would like to express my special appreciation and sincere thanks to my advisor Assoc. Prof. Dr. Ayşen Tezcaner for her guidance, valuable academic advices and moral support. Moreover, I would like to thank her for encouraging my research in light of my demands and for allowing me to grow as a research scientist. I would like to express my special gratitude and sincere thanks to my co-advisor Assoc. Prof. Dr. Akın Akdağ for his guidance, encouragement on organic chemistry and science, and supportive academic advisory throughout this dissertation. His advices on both research as well as on my career have been priceless. I would like to thank Assoc. Prof. Dr. Dilek Keskin for her worthy mentoring throughout my study. I would also like to thank my committee members, Prof. Dr. Şükrü Talaş and Assist. Prof. Dr. Urartu Şeker for serving as my committee members and their brilliant comments and suggestions on my thesis.

I would like to deeply thank to Assoc. Prof. Dr. Nesrin Ekinci Machin for her guidance, worthy academic advisory and sharing her time and facilities for my research. I want to add my thanks to Sinem Sel from Machin Research Group for her assistance to me on Flame Spray Pyrolysis system and sharing her time and knowledge. I add my thanks to Dr. Özgür Duygulu from TUBİTAK-MAM for his support on TEM and SEM analyses.

I want to thank to Assoc. Prof. Dr. Zafer Evis for his sharing facilities and consumables in laboratory. I want to thank to the technical staff of Engineering Sciences department for their support on technical problems.

I would like to express appreciation to Prof. Dr. Vasıf Hasırcı allowing us to conduct our analyses in BIOMATEN and I would like to thank METU-BIOMATEN-Center of Excellence in Biomaterials and Tissue Engineering members Menekşe Ermiş and Esen Sayın for their assistance to me on Flow Cytometry analyses.

I would like to add my thanks to Assoc. Prof. Dr. Gülay Ertaş allowing me to perform ICP-MS analysis in her research laboratory. Also I would like to thank Emrah Yıldırım for his assistance to conduct the analysis.

I would like to thank Dr. İrem Gül Sancak and Prof. Dr. med. vet. Brigitte von Rechenberg allowing me to visit Competence Center for Applied Biotechnology and Molecular Medicine (CABMM) at University of Zurich. They encouraged me to give the shape of my thesis topic.

I am so pleasured to be a part of two big awesome research groups. First, I would thank to Biomaterials Research Laboratory group members (alphabetically), Ali Deniz Dalgıç, Alişan Kayabölen, Aydın Tahmasebifer, Dr. Ayşegül Kavas, Bengi Yılmaz, Deniz Atila, Engin Pazarçeviren, Hazal Aydoğdu, Merve Güldiken, Nil Göl, Dr. Özge Erdemli, Ömer Aktürk, Reza Moonesirad and Zeynep Barçin for their valuable friendship, supports in my depressions. Second, I would like to express my thanks to Akın Akdağ Research Group members; Kıvanç Akkaş, Halil İpek, Gizem Tekin, Perihan Öztürk, Gizem Çalışgan, Gözde Coşkun, Esra Nur Doğru, Milad Fathi, Duygu Tan for their valuable friendship and support to my organic chemistry inadequacy. They never made me feel alone in this research group. I have been blessed with a friendly and cheerful groups of students. I wish all the best for all of my labmates and hope all their dreams come true.

Also I would add my thanks to all of my friends who gave me their urine sample for conducting my stem cell studies.

I want to add my special thanks to my beloved Mustafa Nuri Türkkan for his love, kindness, motivation and support that he has shown during my undergraduate and graduate projects and finalize this thesis. Furthermore, I would like to add my thanks to my lovely family, Sırrı Ataol, Emine Ataol, Özlem Ataol Demirkan, Özge Ataol for their love and support throughout my life.

I would like to thank to The Scientific and Technological Research Council of Turkey for the support they provided (Project no: 112T749). I thank to METU GSNAS Biomedical Engineering Department allowing me to work as part time student assistant

TABLE OF CONTENTS

LIST OF TABLES

TABLES

LIST OF FIGURES

FIGURES

LIST OF ABBREVIATIONS

A	Absorbance of test wells
A'	Absorbance of negative control well
A-PEC	Amidated citrus peçtin
A-SF	Acylated Silk Fibroin
Alpha-TCP	Alpha tricalcium phosphate
ASC	Adipose derived stem cells
ALP	Alkaline Phosphatase
ANOVA	Analysis of Variance
BCA	Bicinchoninic Acid
Beta-CPP	Beta calcium pyrophosphate
BSA	Bovine Serum Albumin
BTE	Bone Tissue Engineering,
CaP	Calcium phosphate
$CDCl_3$	Deuterated chloroform
CuAAC	Copper catalyzed azide alkyne cycloaddition
$CuSO_4\,5H_2O$	Copper sulfate pentahydrate solution
d_{BET}	Primary particle size
d_{xrd}	Crystallite size
D_2O	Deuterated water
DMF	Dimethyl formamide
DMEM	Dulbecco's Modified Eagle Medium
DMSO	Dimethyl Sulfoxide
DMSO-D6	Deuterated Dimethyl Sulfoxide
DNPH	2,4-Dinitrophenylhydrazine
DTA-TGA	Differential Thermal Analysis-Thermogravimetric Analysis
EDC	1-Ethyl-3-(3-dimethylaminopropyl)carbodiimide

ELISA	Enzyme-Linked Immunosorbent Assay
ε_{red}	Molar extinction coefficient of Alamar Blue reduced form
ε_{ox}	Molar extinction coefficient of Alamar Blue oxidized form
FFT	Fast Fourier Transform
FBS	Fetal Bovine Serum
FT-IR ATR	Fourier Transform Infrared- Attenuated Total Reflectance
FSP	Flame Spray Pyrolysis
hMSC	Human mesenchymal stem cells
HA/HAp	Hydroxyapatite
HFIP	Hexafluoroisopropanol
HR TEM	High resolution Transmission Electron Microscopy
HRMS	High resolution mass spectroscopy
ICP-MS	Inductively coupled plasma mass spectroscopy
KSFM	Keratinocyte serum free medium
NMR	Nuclear Magnetic Resonance
NHS	N-hydroxysuccinimide
O-PEC	Oxidized citrus pectin
PBS	Phosphate Buffered Saline
pNPP	p-Nitrophenyl Phosphate
PCL	Poly(ε-caprolactone)
PEG	Poly(ethylene glycol)
PLA	Poly (lactic acid)
PLLA	Poly (L-lactic acid)
PLGA	Poly(lactic-co-glycolide)
PMMA	Poly(methyl methacrylate)
PVA	Poly(vinyl alcohol)
rt PCR	Real-Time Polymerase Chain Reaction
RGD	Arginine, Glycine, and Asparagine
SAED	Selected Area Diffraction
SBF	Simulated Body Fluid
SEM	Scanning Electron Microscopy
SF	Silk Fibroin

SPAAC	Strain promoted azide alkyne cycloaddition
TCPS	Tissue culture polystyrene plates without scaffolds
TLC	Thin layer chromatography
TGF-β	Transforming Growth Factor β
TEM	Transmission Electron Microscopy
USC	Urine derived stem cells
UV	Ultra Violet
W	Weight of the sample (g)
XRD	X-Ray Diffraction
VEGF	Vascular Endothelial Growth Factor
λ_1	570 nm
λ_2	600 nm

CHAPTER 1

INTRODUCTION

1.1. Bone

Structural skeletal tissues are the characteristics of the vertebrates and this tissue structure has evolved with them. Bone, cartilage, tendon and ligaments comprise the skeletal tissues of present day mammals. Among them bone is the principal calcified stiff skeletal tissue of many species. Adult human skeleton consists of 213 bones, excluding the sesamoid bones [1]. The size, structure and composition of bones in body differ with respect to age, gender, site of tissue, type and so the function of bone tissue. Bones have variety of functions. Bones serve as structural support for body, protect vital organs, provide the locomotion of musculoskeletal system, serve as reservoir for many minerals, and thereby play an important role in ion homeostasis and so acid base balance. Bones have a crucial role in active agent expression and hematopoiesis [2,3].

Bone tissue is termed as specialized connective tissue. From a structural point of view, bone and other calcified connective tissues are considered as natural anisotropic composites consisting of calcium phosphate nanoparticles that are embedded in a fibrous collagen matrix, other organic materials and water. The remarkable amount of water is found in bone tissue. Water molecules provide a mechanical strength to bone tissue [3,4]

1.1.1. Bone Structure and Composition

Bone tissue is a complex structure and can be classified according to macrostructure (whole bone), tissue structure, microstructure and ultrastructure (nanostructure). These levels are shown in Figure 1.1.

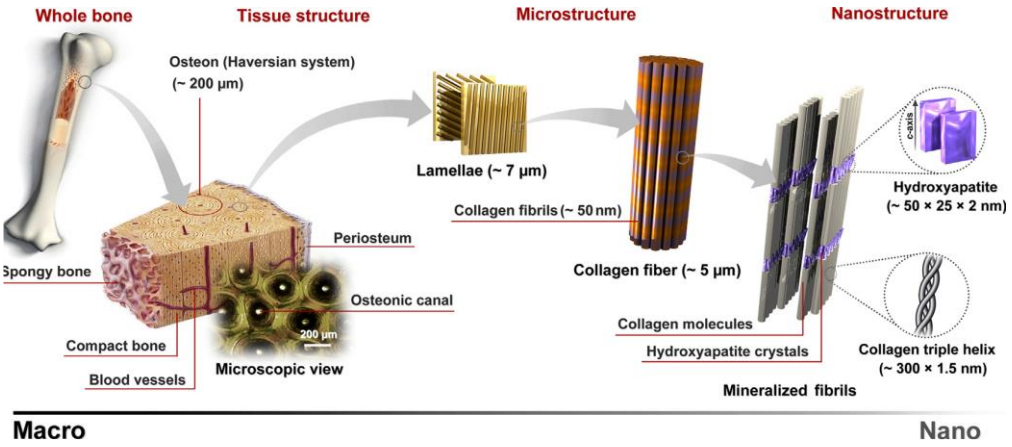

Figure 1.1 The hierarchical structure of bone in large scale [5]

There are main elements of bone tissue levels. The bone tissue shape is termed as the macrostructure of bone. The macroscopic structure differs with respect to tissue site in body as well as the function of bone. Bones can be classified as long and short bones based on sizes, and tubular, irregular and flat bones based on their shapes. According to structure there are two types of bones, namely compact bone and cancellous bones. Compact bone and cancellous bone comprise nearly 20% and 80% of bone tissue, respectively [2,3]. They show mechanical property differences. Compact bone is the solid phase of bone in which there is space only for microscopic channels, canaliculi, blood vessels and space for osteocytes [6]. Osteon is the fundamental functional unit of compact bone which consists of concentric layers that surrounds a central canal called the haversian canal. Blood vessels are located in Haverisan canals. Nutrition diffusion takes place through canaliculi. As shown in Figure 1.1, osteons are aligned in one direction.

An microscopic scale of bone is classified as woven and lamellar bone. Woven bone is the immature form of bone found in the fetus. The collagen content is variable. It contains osteocytes and blood vessels. Lamellar bone is the mature form of bone that is formed by remodeling of woven bone tissue. The collagen fibrils and minerals are arranged in sheet like lamella [6]. The ultrastructure level defines the chemical composition of bone tissue. In nanostructure, bone consists of organic phase (~25-30%), inorganic particles (~65-70%) and water. Fibrous collagen and non collagenous proteins comprise the organic phase of bone tissue. The proteins, tropocollagens

agglomerate and form collagen fibrils which comprise 90% of the bone protein. Remaining organic phase of bone is the non collagenous proteins that have key roles on bone biology. The inorganic crystals are some variety of calcium phosphates; mostly impure semi crystalline hydroxyapatites [6,7]. The main structures in each level of bone tissue are summarized in Table 1.1

Table 1.1 The levels of bone structure (Modified from [1,2,4,6])

Levels	Comprising elements
Macrostructure	Types of bone: flat, short, long, irregular
Tissue structure	Cancellous/Trabecular/Spongy bone
	Compact/Cortical bone: structural unit is cylindrical shaped osteon
Microstructure	Woven bone: found in embryo, immature bone
	Lamellar bone: mature bone
Submicrostructure	Lamella, Collagen fibers
Nanostructure	Collagen fibrils, tropocollagen molecules, mineral crystals

Bone tissue is lined with various kinds of specialized cells. These cells can be categorized with respect to their origin and specific activity. These cells are given in Table 1.2. Osteoclasts are responsible for resorbing bone tissue. They are large multinucleated cells originated from bone marrow hematopoietic stem cells which are macrophage and monocyte precursor cells. Osteoclasts are mobile cells that circulate in blood. Osteoprogenitor cells are derived from self-renewing pluripotent mesenchymal stem cells. Apart from hematopoietic stem cells bone marrow also contains mesenchymal stem cells. Osteoprogenitor cells maintain the osteoblasts, osteocytes, bone lining cells in bone matrix. Osteoblasts are bone forming cells and they are located in collagenous matrix, named as osteoid. These cells have role in type I collagen secretion and calcification through collagen fibrils [6,7]. Osteocytes are the body cells of bone, which are located in little channels called canaliculi. They are responsible for the support of bone structure and metabolism. The primary function of

osteocytes is the mechanosensation. In case of mechanical stress, osteocytes release cytokines and effects the bone biology [3]. Bone lining cells cover the surface of bone tissue and control the ionic exchange through bone to body and body to bone [6].

Table 1.2 The classification of bone cells

Origin	Osteoprogenitor cells: originate from pluripotent mesenchymal stem cells
	Osteoclasts: originate from hematopoietic stem cells
Function	Osteoprogenitor cells /Preosteoblasts
	Osteoblasts; forming bone
	Osteocytes; mechanosensation
	Osteoclasts; resorbing bone
	Bone lining cells; controlling ion movement

1.1.2. Bone Regeneration and Remodeling

Bone is a dynamic tissue that undergoes both longitudinal and radial growth, modeling and remodeling. All these processes embody new bone tissue. Bone growth takes place through childhood. The endosteum and periosteum surfaces increase, and mineralization occurs, then new bone tissue is formed. Modeling is the lifelong process of bone during which resorption and new bone formation take place in response to physiological influences such as hormonal changes, diet, drugs etc. In modeling process, the size and shape of bone changes as bone forms on or bone is removed from periosteal or endosteal surfaces. Three phases of modelling are activation, osteoclastic resorption and osteoblastic formation. In remodeling, there is no alteration in bone size and shape. The old or immature bone tissue is replaced in order to keep the mineral homeostasis and the mechanical strength of bone tissue. The bone remodeling process depends on tightly coupled activity of osteoclasts (resorption of old bone) and osteoblasts (formation of new bone)[3,6,7]. When compared, remodeling is a cyclic and slow process whereas modeling is continuous and fast.

In mechanism, firstly the activation step occurs, mononuclear monocyte-macrophage cells are recruited by physiological changes in tissue (damages, micro cracks in tissue etc.) during in circulation. These active cells accumulate on endosteum; bone surface containing bone lining cells. The multiples of these cells are fused and form multinucleated osteoclasts. Osteoclasts attach to bone matrix (Type I collagen, osteopontin etc.) by surface integrin receptors and RGD (arginine, glycine, and asparagine) containing peptides. This binding makes osteoclasts polarized and generates intracellular signals. The acidified vesicles containing metalloproteinases and cathepsin K are transported and H^+ ions are secreted after fusion with the membrane. As a result, pH is lowered causing exocytosis of cathepsin K, an enzyme that digests organic matrix. The acidification demineralizes the bone. Bone resorption takes place at the site with the activity of osteoclasts. This step takes about 2 to 4 weeks. At the end of resorption, bone formation step begins. Apart from controversies, TGF-β is admitted as the trigger of bone formation which is released from the matrix and inhibits the inhibitory effect of osteoblast formation [3]. Osteoblasts synthesize the collagenous matrix and mineralize the tissue. At the end of bone formation, osteoblasts undergo apoptosis or become osteocyte and bone lining cells. Osteoblasts which remain in the matrix become osteocytes [3,4,8].

1.1.3. Bone Defects and Treatment Strategies

Although bone tissue has a self-renewing capacity, these processes are often impaired in case of large amount of bone tissue loss due to trauma, tumors or diseases. Indeed, the estimated records for bone fractures only in United States are about 15 million of which 1.6 million and 2 million cases are hospital admissions and osteoporotic fractures, respectively. These treatments cost about 60 million dollars for a year [9,10]. Bone grafts are preferred for treatment and there is growing demand. Autologous bone grafts cannot always be applied since patients suffer from donor site morbidity. Allogeneic bone grafts have a risk of immune rejection or infection. Moreover, there are limited donors. Thereby, tissue engineering approach is required to support the clinical demand for bone defects as an alternative and cost effective way.

1.2. Scaffold Guided Bone Tissue Engineering

In tissue engineering, the main aim is to replace or repair the damaged tissues and organs. For achieving regeneration, either functional cells are transplanted or patient's own cells are recruited by inducing with the use of bioactive agents. The agents and cells should be carried to site properly and should stay in body for specified time. The damaged site also needs mechanically supportive network during regeneration. This scaffold should also act as a three-dimensional template for tissue ingrowth by mimicking the extracellular matrix for cell adhesion and proliferation.

There are criteria for scaffolds to be admitted as an ideal scaffold;

- Biocompatibility
- Biodegradability
- Three dimensional porous structures
- Mechanical stability

The scaffold material should be biocompatible. In order to enhance the integration of engineered scaffold with host tissue, the materials should degrade at a rate that new tissue is formed. Also the scaffolds should be porous and have high interconnectivity for cells to attach, proliferate and populate. The mechanical stability is also crucial especially for load bearing tissues as bone tissue. Each tissue is subject to mechanical stress as that directly affects the phenotype of cells. The implanted scaffold should have a capacity to withstand the stress as original tissue [11–13].

Since 1970s, the field of bone tissue engineering has shown tremendous advances over years with increasing number of research articles and reviews in Pubmed database [14]. The number of tissue engineered products on the market are also increasing each year.

Bone tissue engineering aims to present an alternative treatment to bone treatment modalities. For a tissue-engineered bone, the construct should satisfy the needs for a natural bone tissue. Therefore, the whole properties of bone tissue should be considered for the design of scaffolds.

1.2.1. Cell Source

In bone tissue engineering, osteoprogenitor cells, osteoblasts or their cell lines are used for *in vivo* and *in vitro* studies. Bone tissue and periosteum are the sites for isolation of these cells. If autologous grafts are used for clinical applications, cells are obtained by biopsies from the patient. The use of bone and periosteum derived cells have some limitations. In one of the previous studies, osteoblasts were photoencapsulated in RGD-modified PEG hydrogels to test the surface modification experiments [15]. PEG hydrogels were functionalized with RGD peptide sequence in order to enhance the cell adhesion. RGD sequence is specific cell adhesion integrins and found most of the cells. In this study, PEG was functionalized to maximize osteoblast adhesion for bone tissue engineering applications. In an another study, the periosteum derived osteoblasts were used as cell source and they were seeded on an absorbable polyglactin/polydioxanon scaffold (Ethisorb®) to investigate their potential for in vivo bone regeneration. 3 months after implantation the group observed the lamellar bone formation in the cell seeded scaffolds [16].

1.2.1.1. Stem Cells

Stem cells are defined as undifferentiated cells that have high proliferation rate and self-renewal capacity with a multi-lineage differentiation potential [17]. These properties of stem cells and limitation in the use of patients' mature cells make the stem cells most ideal cell source for tissue engineering approach. Stem cells have different capacities for differentiation or proliferation depending on their origin. There are two types of stem cells basically used for bone tissue engineering applications, namely adult stem cells and embryonic stem cells.

1.2.1.1.1. Embryonic Stem Cells

Embryonic stem cells are derived from early embryos. They have indefinite self-renewal capacity and higher differentiation capacity [18]. These stem cells reside in inner cell membrane of blastocysts [10]. The first *in vitro* cultivation studies of cells obtained from human blastocysts and studies on the developmental differentiation potential of all three germ lines were conducted nearly 20 years ago [19]. Embryonic stem cells mainly have been used to generate skeletal connective tissue cells, bone and

cartilage and also tissues derived from mesoderm. The osteogenic and chondrogenic differentiation of human embryonic stem cells in the presence of specific growth factors has been reported using ALP assay and mRNA expression level by RT-PCR analyses [20] Although embryonic stem cells have very high potential in tissue engineering approaches, there are still concerns on their use for both research and clinical usage purposes due to ethical issue related with their source and risk of teratomas and teratocarcinomas formation leading to tumors *in vivo* [21].

1.2.1.1.2. Adult Stem Cells

Each tissue has a population of progenitor cells that proliferates and differentiates in case of any defect in that tissue or organ. Adult stem cells are derived from these undifferentiated progenitor cells in body. The undifferentiated progenitor cells that have the capacity to differentiate into mesoderm derived lineages such as adipogenic, chondrogenic, osteogenic, myogenic and other type of mesoderm originated cells are defined as mesenchymal stem cells (MSC). Adult mesenchymal stem cells play vital role in bone tissue engineering applications. Adult mesenchymal stem cells can be derived from a variety of tissues such as adipose tissue, bone marrow, dental pulp, synovial fluid, blood etc. [22,23]. Among them, bone marrow mesenchymal stem cells are the most widely studied type of stem cells. Isolating bone marrow derived mesenchymal stem cells is less invasive than isolation of osteoblasts from periosteum or trabecular bone and these cells have high proliferative ability [24]. The *in vitro* osteogenic differentiation of bone marrow derived mesenchymal stem cells seeded on scaffolds and results of in vivo applications of these cell-polymer composites have been reported [25]. These stem cells were seeded onto electrospun PCL scaffolds and cultivated in perfusion bioreactor for 4 weeks. ALP staining was conducted to evaluate the osteogenic differentiation of bone marrow derived mesenchymal stem cells within the scaffolds. The results gave positive ALP staining showing their successful osteogenic differentiation. After 1 week of *in vitro* cultivation, the scaffolds were implanted. Histological analyses upon both after in vitro cultivation and 4 weeks implantation, showed that mineralization and type I collagen deposition inside scaffolds occurred. Such findings revealed that cells penetrated through the scaffold

matrix and differentiated towards osteogenic lineage. These results showed that PCL based scaffolds had a potential to be used use as bone grafts.

Adipose derived stem cells (ASC) are preferred for bone tissue engineering applications due to their accessibility and high proliferation capacity. Several groups conducted studies with adipose derived stem cells. In one of the studies ASCs were seeded on porous silk fibroin based three dimensional scaffolds [26]. The osteogenic differentiation of ASCs on four types of differently fabricated silk fibroin scaffolds. Two of these scaffolds had pore sizes of 250–500 μm and 500–1000 μm and the other two scaffolds prepared with hexafluoro-2-propanol (HFIP) had lamellar morohology. The scaffolds were compared in terms of mineralization by the seeded cells as well as, bone protein expression and alkaline phosphatase enzyme activity levels of these cells. In all scaffolds, adipose derived stem cells showed osteogenic differentiation. However, when compared with bone tissue, adipose derived stem cells seeded onto aqueous derived silk fibroin based lamellar scaffolds gave higher ALP expression levels, calcium change ratio and higher bone volume results.

1.2.1.1.2.1. Urine Derived Stem Cells

Current stem cell sources are obtained by invasive harvesting methods. Since these isolation processes require an operation, they have higher medical cost. There is also a risk of infection and local bleeding during these procedures. To overcome these problems, as a new stem cell source, human voided urine was discovered a decade ago. Obtaining cells from voided urine is an attractive method since the therapies can be patient oriented, and it is noninvasive method that will not disturb patient. The biological characterizations of these cells were conducted, and these cells were defined as mesenchymal stem cells [27–29]. The multilineage differentiation potential, self-renewal and clonogenicity of cells showed that they were stem cells [30,31]. The biological characteristics of urine derived stem cells were compared with adipose derived stem cells and the results gave similar stem cell characteristics [30]. In this study, mesodermal differentiation of urine derived stem cells has been reported. The cells were shown to differentiate into three lineages, namely osteogenic chondrogenic and adipogenic lineages. Especially, 3 weeks incubation of ASCs and USCs in osteogenic medium revealed that both urine and adipose derived stem cells showed

osteogenic differentiation. Calcium deposition assay, collagen type I expression and mRNA expression of cells confirmed this higher level osteogenic differentiation. Moreover, urological and myogenic differentiation potential of urine derived cells was reported [27]. For urological reconstruction, urine derived stem cells that were differentiated into smooth muscle cells were seeded into bacterial cellulose derived scaffolds. Cells seeded on these scaffolds were then cultivated in a bioreactor [32]. The results were promising and the group reported that these tissue engineered constructs have potential for use as grafts. *In vivo* studies of USCs were further conducted to examine their angiogenic and myogenic differentiation on VEGF loaded collagen based scaffolds. The group observed that angiogenic and myogenic differentiation of these cells were enhanced [33]. In one of the previous studies, the neurogenic differentiation of USCs was also accomplished by implanting these cells with neural cells into rat brain. In this study the group showed that human urine derived cells were reprogrammed to neural progenitor cells without transferring gene by implanting together with neural cells. Neural and glial cell differentiation of USCs was examined [34]. Recently, the urine derived stem cells-nanomaterial interaction studies were conducted with silver nanoparticles and their osteogenic differentiation was investigated. Osteogenesis related gene expressions, ALP activity of cells and calcium deposition by these cells proved the osteogenic differentiation capacity of urine derived stem cells [35].

1.2.2. Design and Processing of Scaffolds for Bone Tissue Engineering Applications

1.2.2.1. Design Criteria

The ultimate goal of scaffold based tissue engineering is to replace the damaged tissues by shaping scar with three dimensional scaffolds, to provide temporary mechanical strength and to induce the regeneration of tissues by the material content. The design and fabrication of three-dimensional scaffolds are important issues to be considered for tissue engineering applications. The mechanical and biochemical properties of the native tissue are the key factors to be considered for choosing among the variety of materials to develop scaffolds aimed to mimic cell and tissue specific niches. The choice of biomaterial is especially based on the material composition, structural

stability, surface properties, porosity and degradability in the body. It is also sought that the scaffold should accelerate the regeneration by inducing cellular interaction and its degradation rate should match the rate of new tissue formation.

For bone tissue engineering (BTE), porous three dimensional scaffolds with mechanical properties similar to bone tissue are aimed to be developed so that the engineered construct can withstand mechanical microenvironment. This fact led to the development of scaffolds from mechanically load bearable materials, which results with fabrication difficulties and pore connectivity problems. Moreover, bone tissue engineering comprises of not only long or short bone tissue specific treatments, orthopedic, spine and cranio maxillofacial tissues are also inclusive in BTE applications. In one of the studies engineered constructs for regeneration of bone were evaluated for clinical applications [36]. The design hypothesis of scaffolds for BTE was defined under 4 topics and 4F rule. The scaffold should fulfill these 4 topics for use in clinical therapies. This 4F rule consists of Form, Function, Fixation, and Formation needs of the bone defect. Form is used to define the ability of effective scaffold to conform the three dimensional shape of tissue. Function refers to the functionality of effective scaffold to provide optimally similar mechanical properties to damaged tissue as original tissue. Fixation means the integrity of scaffold with neighboring soft and hard tissue. Finally, formation rule is used to define the osteoconductive properties of effective scaffold. In this study, osteoconductive properties were described in terms of porosity, mass transport, perfusion and integration of cells and other bioactive molecules. When this 4F rule is accompanied with design and fabrication of scaffolds, the clinically applicable effective scaffolds would be produced. In another study these points were stated as the increase in complexity of scaffolds and new scaffold systems should be offered, and it is commented that bone tissue engineering field has promising ongoing studies [9].

1.2.2.2. Biomaterials Used For Scaffolding

Selection of biomaterial is important for tissue engineering applications. It determines the time for healing process by guiding the cells and efficiency of treatment by triggering the cellular organization. In tissue engineering applications, various

synthetic and natural biomaterials have been used for fabrication of functional three-dimensional scaffolds.

Natural biomaterials are obtained from plants, animals, and microorganism. These biomaterials are favorable for scaffolding since these scaffolds enable to mimic the natural tissue. Their effects on cellular activities as well as their recognition, degradation and remodeling are already well-known [37,38]. Since they are the materials that compose the native tissues; they provide enhanced cell adhesion, proliferation, migration and even differentiation. However, there are limitations on use of natural biomaterials. Either allogenic or xenogenic sources are used. Each has some limitations. Materials of xenogenic origin can have variability with respect to animal source. Their xenogenic nature (from animal to human) can lead to immunogenic responses after implantation. If decellurazitaion process is not performed well, remaining cell or debris can induce immunogenicity and antigenicity [39]. Synthetic biomaterials have been widely used for contact lenses, sutures etc. and have been developing since then. In regenerative medicine applications synthetic polymers are mostly preferred due to their physiological stability, biochemical activity and mechanical load capacity. However, synthetic materials also have disadvantages. The structure and composition of scaffolds made up of synthetic materials do not mimic the natural tissue. To gain cytocompatibility, the materials require further modifications to overcome the biocompatibility problems [40]. In Table 1.3 natural and synthetic polymers most commonly used in bone tissue engineering applications are summarized.

Table 1.3 Synthetic and natural polymers that are widely used in bone tissue engineering applications

Natural polymers	Collagen	[41]
	Silk Fibroin	[12]
	Alginate	[42]
	Chitosan	[43]
Synthetic polymers	Poly (methyl methacrylate) (PMMA)	[44]
	Poly (glycolic acid), Poly (lactic acid)	[45]
	Poly (Ɛ-caprolactone)	[15]
	Poly (propylene fumarate)	[46]

In this study naturally derived biomaterials were used for scaffold development. Natural biomaterials can be classified as protein based biomaterials such as collagen, gelatin, silk fibroin etc., polysaccharide based biomaterials such as alginate, starch, and citrus pectin etc. and decellularized tissue based biomaterials. Proteins and polysaccharides are obtained by either extraction from natural tissues by enzymes or chemicals or by production using recombinant DNA technology. Among protein and polysaccharide used for bone tissue engineering studies the most common ones; collagen and silk fibroin, citrus pectin and alginate are reviewed here.

1.2.2.2.1. Silk Fibroin

Silk is a protein that is produced by spiders, silkworms and scorpions. Due to its unique properties such as mechanical stability, aqueous or organic solvent processability, ability for chemical modifications, slow degradation rate in body and versatility in fabrication process [12,47,48] it is mostly favored in regenerative medicine and tissue engineering applications. Cocoons of domesticated silkworm, *Bombyx mori* are the most widely used silk protein source [37]. Cocoons consist of water soluble small globular protein sericin and fibrous fibroin protein. Cocoons mostly consist of fibroin protein. Fibroin gives structural and mechanical stability to cocoon form [12,49].

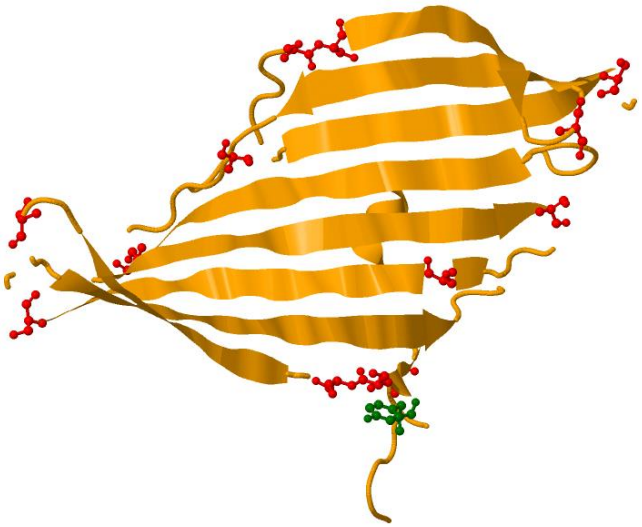

Figure 1.2 The heavy chain of silk fibroin (generated by Jmol [50]), yellow colored residues show β-sheet repeating structures, red colored residues are serine and green colored residues are tyrosine residues at the end of β-sheets [51]

Silk fibroin is highly insoluble protein that consists of ~ 350 kDa heavy chain and ~ 25 kDa light chain polypeptides. These chains are crosslinked by disulfide bonds [12,37]. The silk fibroin has a similar structure as the block copolymers since the hydrophobic β-sheet forming heavy chain is polymerized with little hydrophilic light chain. Nearly 90% of silk fibroin heavy chain is comprised of alanine, glycine and serine amino acid residues. These amino acids lead to antiparallel β-sheet structure in fibers as seen in Figure 1.2 which gives the mechanical strength and toughness to protein [49]. Silk fibroin has been reported as the toughest polymeric material in tissue engineering applications. In a previous study, silk fibroin was compared with synthetic polymer Kevlar® and it was shown that fibroin was tougher than Kevlar® [52]. In another study, the mechanical strength of silk fibroin was compared with collagen and poly (l-lactic acid) (PLA). The tensile strengths of *B. mori* silk fibroin, collagen and PLA were found as 740 MPa, 0.9-7.4 MPa and 28-50 MPa, respectively [47].

The unique properties make silk fibroin an attractive material for bone tissue engineering applications. Porous 3D cell culture carriers had been fabricated from silk fibroin alone and as composites. It was shown that human mesenchymal stem cells (hMSC) loaded fibroin based carriers induced osteogenic differentiation of stem cells

and bone formation in vivo [53]. Osteogenic differentiation factors like BMP-2 had been integrated with silk fibroin scaffolds for engineering of bone. It was shown that the efficient release of BMP-2 resulted with osteogenic differentiation of hMSCs and calcium deposition by these cells [54]. Additionally, mineralized silk fibroin scaffolds were investigated for engineering of bone in the absence of osteogenic factors. It has been showed that silk/HA composite scaffolds had improved the osteogenic differentiation of seeded hMSC cells [55].

1.2.2.2.2. Collagen

Collagen is a fibrous protein like silk fibroin and found in all connective tissues in human body. Fibrous nature of collagen originates from its highly repetitive primary sequence and its homogenous secondary α helix structure [56]. Like in the case of silk fibroin, this nature of the protein structure gives mechanical strength to this material. Collagen is easily purified from living organisms; it has slow biodegradation in body. It is metabolized and resorbed.

Collagen protein is a bundle of helically twisted three polypeptide chains. Each chain has α helix structure. Glycine- Proline and Hydroxyproline comprise the motifs in amino acid sequence of collagen protein (Figure 1.3). The polypeptide chains are connected to each other by hydrogen bonds.

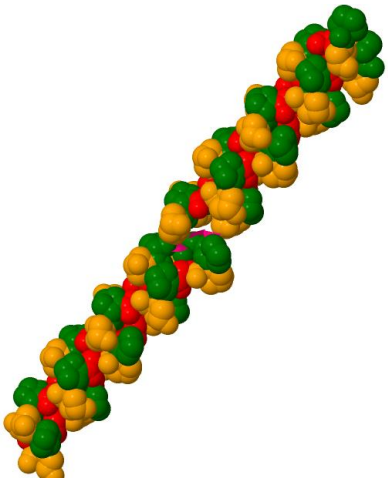

Figure 1.3 The tertiary structure of collagen protein (generated by Jmol [50]). Green residues show proline, red and orange residues are glycine and hydroxyproline, respectively [57].

This protein is versatile for processing; it can be cross-linked with several synthetic and biological polymers and can be modified as desired [56,58]. These unique properties make collagen protein favorable for tissue engineering applications. However, there are some limitations for the use of collagen. It is costly to obtain pure collagen type I and there is batchwise difference in terms of crosslinking density and fiber size. The amino acid content of collagen determines the helix conformation of the protein. Therefore, the isolation step is crucial to isolate pure protein. Moreover, the enzymatic degradation profile of collagen differs.

Based on its advantages, a wide variety of collagen based scaffolds were fabricated for tissue engineering applications. In one of the recent studies, collagen was blended with calcium phosphates and this mixture was 3D printed in order to prepare constructs for bone tissue enginerring [59]. The construct was implanted to rats and osteoconductivity of scaffolds was confirmed by new bone formation observations after 9 weeks.

1.2.2.2.3. Citrus Pectin

Pectin is natural carbohydrate, which is found in cell wall of plants. Citrus pectin is extracted from citrus fruits. It has a high gelling effect because of anionic nature of its backbone; therefore it is used in food industry as a gelling agent [60]. As a polymer, citrus pectin is an anionic polysaccharide, poly (α 1,4-galactronic acid) (Figure 1.4). Pectin polymer is found as esterified with ethanol on carboxyl groups. They are classified as high methoxyl (HM) or low methoxyl (LM) pectin. Pectin conjugate with proteins or polysaccharides and form chemically stable, physically strong extracellular matrix of plants [61]. Pectin in cell wall provides rigidity to cells, control of porosity and water holding capacity [62].

The biological origin and chemical carbohydrate structure of pectin favor cell to cell and cell to matrix interactions, which makes pectin suitable biomaterial for tissue engineering and regenerative medicine applications. Since pectin has plant origin, there is no ethical concern for its use. It is easily obtained from not expensive material. As a biomaterial pectin has been used as delivery systems for bioactive agents (i.e., anticancer drug, doxorubicin, etc.)[63].The polyanionic nature of pectin provides the binding of positively charged cell surface proteins to negatively charged extracellular

matrix and even cell to cell binding. By this high level cellular interaction potential pectin was used as metal implant surface coatings which showed higher binding efficiency [64].

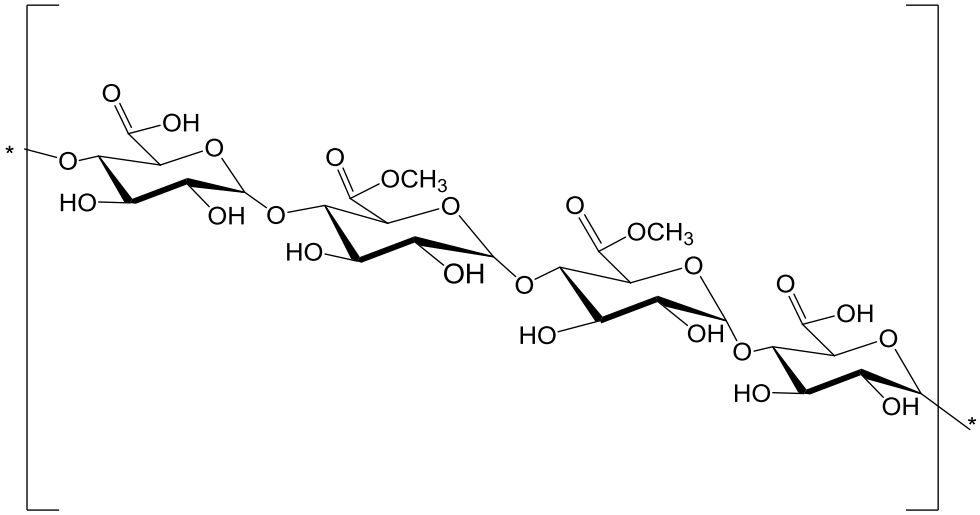

Figure 1.4 Chemical structure of high methoxyl citrus pectin polysaccharide

Pectin also carries a great potential for engineering of bone. Microspheres of pectin blended with RGD (Arg-Gly-Asp) containing oligopeptide were prepared as an injectable microcarrier system for the first time [62]. The viability, metabolic activity, morphology and differentiation of preosteoblasts on this delivery system were investigated in this study. The cell viability was sustained for 29 days in pectin microcarriers. The histological analyses were performed with Alizarin Red and Von Kossa stainings. Mineralization of scaffolds was observed in the histological sections of cell seeded microcarriers [62]. In another study, pectin was mixed with alginate and electrospinned to stabilize folic acid in alginate-pectin based fibers for food industry applications. By stabilizing micronutrients, innovative carrier packages were aimed to produce [65]. Pectin was also used with poly(lactic-co-glycolic acid) (PLGA) for fabrication of 3D scaffolds [61]. Hydrophobic porous PLGA was linked with pectin matrix in the presence of calcium chloride. The mineralization effect of pectin was also studied. The negatively charged nature of pectin triggers the Ca^{2+} physical binding which enhances mineralization process further [66].

1.2.2.2.4. Alginate

Alginate is one of naturally derived biomaterials which is extracted from brown seaweed and bacteria [67]. It is composed of 1-4-linked β-d-mannuronic acid (M) and α-l-guluronic acid (G) residues and it has anionic hydrophilic nature (Figure 1.5). In the presence of divalent atoms such as Ca^{2+} and Mg^{2+} they form coordinate complexes and stable hydrogels are formed by this ionic interaction.

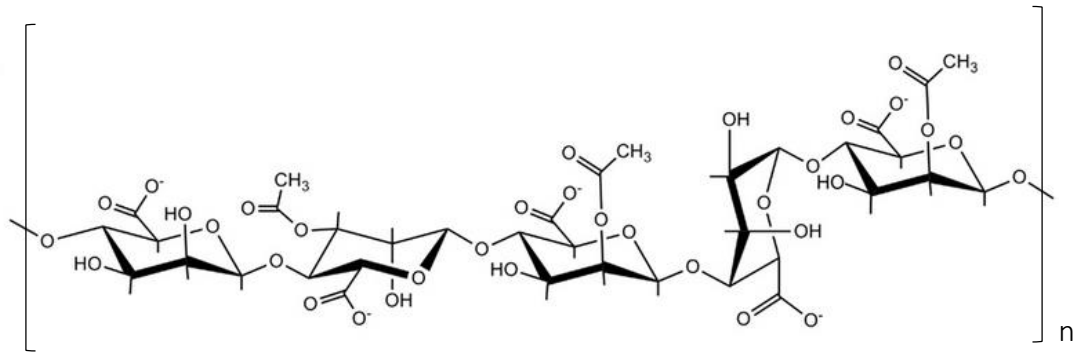

Figure 1.5 The chemical structure of alginate [68].

Alginate is also one of the mostly used materials for drug delivery and tissue engineering applications due to its outstanding properties. It is a biocompatible and biodegradable polysaccharide which can be easily fabricated and functionalized [42]. The stable hydrogel forming ability of polymer with dicationic species is favored for bone tissue engineering applications. There are several studies on alginate based [67,69] and alginate polymer composite based carrier systems [65,70] and alginate incorporated with calcium phosphates [71,72].

1.2.2.2.5. Calcium Phosphate Ceramics for Bone Tissue Engineering

Calcium phosphate materials carry a great potential to be used as implants or as surface coatings of the implants. They also find wide applications in drug or gene delivery and hard tissue engineering applications [73].

In bone tissue engineering, calcium phosphates are preferred since they resemble to natural bone minerals. Bone is a dynamic tissue. Calcium phosphate minerals play vital role in cellular interaction in case of resorption and desorption of bone tissue. The

natural mineralization process occurs in solid-liquid interface; by ionic exchange from solid to liquid and liquid to solid. The collagen protein is involved with this ionic exchange dynamics. Since collagen protein is firmly attached to these mineral crystals osteoblasts or osteoprogenitor cells can directly interact with the mineral phase either in solid or ionic form. In osteogenic differentiation the process takes place as cellular proliferation, maturation and mineralization. The migratory osteoprogenitor cells migrate towards the defect site and the environmental mineral deposit directly affects their proliferation, maturation and mineralization process [8].

In literature, there are numerous studies on calcium phosphate ceramics with different synthesis and fabrication methods for bone tissue engineering applications and other biomedical applications. In one of the studies, the calcium phosphate dissolution rate dependent osteogenic differentiation of progenitor cells was studied and the results revealed that early dissolving calcium phosphate, the release of inorganic ions was found directly related with early bone formation *in vivo* and osteogenic differentiation of progenitor cells [74]. In another study, implants composed of poly (lactic-co-glycolic acid) (PLGA) and calcium phosphate particles were prepared for clinically used bone screws. In order to enhance bone bonding to implant, amorphous calcium phosphate particles were incorporated [75]. With respect to results, the mechanically and biochemically optimal ratio of polymer and nanomaterial blend was decided. Scaffolds without calcium phosphate, showed higher mechanical strength and higher bioactivity potential by surface hydroxyapatite layer formation in simulated body fluid (SBF). In another study, nano sized hydroxyapatite particles were blended with collagen, and scaffolds were examined for cellular activation. After 7 days of culture, pre-osteoblast cells showed 1.5 times higher proliferation [76].

1.2.2.2.5.1. Synthesis of Calcium Phosphate Nanoparticles

Calcium phosphates are obtained by various methods that are classified as high temperature process, wet and dry-based methods [5]. Wet based methods are chemical precipitation, sol-gel, and hydrolysis methods. Dry based methods are solid state method and mechanochemical synthesis. Among these three methods, wet based chemical precipitation is widely preferred due to obtained product is relatively more than other methods. Since precursors are dissolved in aqueous environment, organic

solvent is not used so this method is cost effective [77]. Wet based synthesis method is advantageous in terms of the control of morphology and mean size of obtained calcium phosphate powders. However, low temperature during process leads to impurity of starting materials and results with low crystalline particles [78]. Also for wet based methods pH and temperature synthesis parameters must be strictly controlled [79]. Dry based solid state synthesis method involves mixing of precursor powder. The powder is sintered so the specific surface area decreases. However, the disadvantage of this method is low purity of obtained powder [5]. When these powders are used for biomedical applications, they show reduced contact to body fluid hindering resorption [79].

For nearly three decades, micron and nano sized bioceramics are synthesized by above techniques. The improvements in nanotechnology arouse the interest on bioceramic synthesis in nano sizes. Nano sized materials possess distinct properties compared to micron sized materials. The morphology and interfacial characteristics of nanomaterials determine the specific properties of materials. The physical, chemical and biological properties of nanomaterials differ from the properties of bulk materials [80,81]. The color, melting point, conductivity, dissolution rate, surface charge capacity are some of these specific properties. Nanoparticles have high surface to volume ratios. The larger surface area increases the interaction rate of nanomaterial with its environment. Moreover, the smaller the size of materials their mobility in media and the diffusion rate of materials increase [82]. These properties promote the chemical reactivity of particles. In biological systems, many of processes operate at nanoscales. The properties of nanomaterials can be easily customized to biological systems compared to bulk materials. Cells are in micron sizes, thereby all their biological activities such as signaling, surface adhesion, ion channels; cell to cell contact are all nanoscale phenomena. It is possible to induce cells positively or in adverse manner by cell to nanomaterial interaction. The biological activity of nanoparticles is studied by many research groups [35,81–85]. The studies are mostly conducted on bone tissue specific applications since natural bone tissue has nanostructured organization. The nanosized calcium phosphates are found as dispersed in collagen matrix by which bone tissue gains mechanical strength. Meanwhile, this surface topography of natural bone provides protein adsorption and bone regeneration

[75,86]. The calcium phosphates synthesized at nanosize mimic the natural bone minerals and enhance the binding affinity of cells and proteins to grafts. This recognition activates cellular cascades and induces regeneration. The interface properties of nanoparticles determine the dissolution rate of materials. The dissolved free ions diffuse into cells and activate cellular differentiation towards bone cells, proliferation or recruitment of cells as stated above. Indeed it is proved that free Ca ions in extracellular matrix play an important role in bone modelling process. They diffuse and activate directly intracellular mechanisms such as IGF expression level and so proliferation increases. Phosphate ions also carry important roles in body, they stimulate the expression of matrix protein named "Gla" protein, which is required for bone tissue formation [87].

Flame Spray Pyrolysis method is newly emerged method to synthesize nanostructured materials. This system is highly promising and versatile method that enables nano-particle design and fabrication [88,89]. By precursor chemistry preference and reactor system engineering, FSP system is practical to study several desired particles. Previously, a variety of ceramic powders has been produced by FSP system [90]. It has been also studied to synthesize calcium phosphate bioceramics for biomedical applications [5,79,83,86,91,92]. FSP system is scalable on particle formation, morphology and size when compared to wet and dry based synthesis methods. The choice of solvents or liquid precursors effects the combustion reaction. This provides direct control on primary particle size and phase of materials. The local temperature and residence time of particles while in process determines the crystallinity and nanoscale feature of materials [88,92]. On the other hand, in conventional methods, milling step is required to scale the particle size and gradual calcination and sintering processes are performed for phase transition [73,93–95]. Moreover, FSP system is time effective synthesis method. Conventional systems as sol gel synthesis and precipitation synthesis methods take nearly 12-15 hours to perform and several other drying step and heat treatment cycles are required [96] . These features of FSP system prove the advantages and applicability of system in this field. In fact, thermal quenching in FSP reactor system while collecting particles results with thermally metastable particles [88]. This metastable form on calcium phosphate particle synthesis provides an opportunity for biomedical applications. In natural biomineralization process, the bone

minerals locate on collagen fibers and pose a site for further nucleation. Ion movement and localization induce osteoblast (bone forming cells) for regeneration [97]. In previous studies, this osteoinductive property was mimicked by coating carriers with amorphous metastable form of calcium phosphate particles. The histological studies showed that amorphous form has high resorbability and bioactivity by higher bonding affinity [98]. In the light of these advantages, in this study, we aimed to synthesize calcium phosphate nano-particles by Flame Spray Synthesis method and to test the bioactivity property of particles on undifferentiated urine derived stem cells.

1.2.2.3. Scaffold Fabrication Techniques

The field of scaffold based tissue engineering is open to innovations and new fabrication methods emerge or are manipulated to tissue engineering applications. In Table 1.4 some of these scaffold fabrication techniques are summarized.

Table 1.4 Scaffold fabrication techniques

Techniques	Description	References
Freeze-drying	Polymer solution is casted, frozen and freeze dried	[99]
Electrospinning	Fibers are collected as a nonwoven scaffold in electrical field	[65] [85]
Porogen leaching	Porogen is leached out from polymeric matrix after molding and a porous scaffold is obtained (porogen: salt, gas etc.)	[100]
Phase separation	Polymer-rich phase is formed by temperature change or addition of a non-solvent. With the solvent removal solidification of polymer-rich phase occurs resulting with a porous fibrous scaffold.	[100,101]
Rapid prototyping	Computer aided fabrication of scaffolds by laser sintering, 3D printing and stereolithography	[102–105]
In situ polymerization	Polymerized materials takes a form after implantation	[106]
Self-assembly	Designed peptides are assembled in desired shape as fibers or spheres.	[107]

1.2.2.3.1. Electrospinning

Electrospinning is one of the mostly preferred versatile scaffold fabrication techniques, which produces nanofibers through electrically charged polymer blend using electrostatic force [108,109]. Electrospining has simple setup which consists of syringe to pump polymer solution, two electrodes for electric field, stage to collect the produced fibers and voltage supply. However, the logic behind this setup is not so simple. There are various parameters to be optimized. In order to operate the system in high yields, firstly electrostatics should be grasped. Afterwards, the viscosity of

solution and the properties of polymers and solvents (conductivity) are critical. The external parameters such as applied voltage, ambient temperature and humidity need to be adjusted while in process [13,108]. When the conditions are optimized, the yield of fibrous construct increases. The woven fibers can be collected on stage whether in two dimensional or three dimensional structures and in micro or nano sizes, which is adjusted by changing the parameters of system.

Electrospining is a promising technique for tissue engineering applications by which soft tissue or hard tissue specific scaffolds can be fabricated. There are several studies on electrospun carriers for bone tissue engineering applications. In one of the studies, the self-assembly peptide based scaffolds were prepared by electrospining. This method was performed due to its advantage on modulating the topography of scaffolds. The in vitro characterizations were performed and scaffolds were reported to be cytocompatible. The engineering in electrospinning setup has developed. The oriented electrospun fibers were produced by mixing polymer solution with superparamagnetic iron oxides and magnetic field was applied [110]. Afterwards three dimensional structures were seeded with myoblasts. The results revealed that elongation of fibers induced the myoblastic differentiation.

1.2.2.3.2. Phase Separation -Freeze-drying

Phase separation is one of the scaffold fabrication techniques that is used to mold three dimensional porous biodegradable scaffolds. In principle, there are successive processes in this technique. First the polymer is dissolved and phase separation is induced by gelation followed by solvent removal by sublimation. The construct is frozen from -20^{o}C to -80^{o}C with respect to solvent type [101,111]. The morphology of microstructure of scaffolds is related with the polymer structure, concentration, and solvent selection. By optimizing these parameters the porosity and crystallinity of scaffolds can be manipulated. Since the foam is obtained by precipitating the polymers in solvent, the mechanically strong constructs are obtained. This method is convenient to fabricate large range of polymers.

There are several studies on scaffolds prepared by phase separation-freeze drying technique. [101]. In one of the studies, injectable microcarriers were synthesized from star shaped PLLA by phase separation-freeze drying method for cartilage regeneration

treatments [112]. Nanofibrous structure of star shaped PLLA was obtained and seeded with chondrocytes. The scaffolds were implanted into rabbit; there was higher cartilage regeneration in injected microspheres with chondrocytes relative than only chondrocytes injected group. Gelatin is one of the polymers used to obtain three dimensional nanofibrous structure for bone tissue engineering studies using this fabrication technique. In this work, porogen leaching process was combined with phase separation freeze drying method. By controlling the macroporous structure and overall shape of constructs, the desired scaffold form was obtained [113]. Nanofibrous gelatin based scaffolds showed better stability in *in vitro* studies.

1.2.2.3.3. Crosslinking of Scaffolds

1.2.2.3.3.1. Mechanisms of Crosslinking

There are several criteria that a scaffold should fulfill for tissue engineering applications. They should be biocompatible, highly porous and provide maximized cell attachment and proliferation. They should fulfill structural stability to withstand tissue specific mechanical stresses, but at the same time it should degrade at a rate that matches the tissue regeneration rate. Polymeric scaffolds are mostly preferred in tissue engineering applications; however the main fallback of these carriers is their mechanical properties. Most of these scaffolds are crosslinked and/or reinforced with other biomaterials like hydroxyapatite.

Most of the polymers need to be chemically modified for obtaining mechanically and structurally stable carriers. There are various chemical and physical crosslinking methods used.

1.2.2.3.3.2. Crosslinking with Chemical Crosslinkers

For crosslinking, strong interaction between molecules is desired. Thereby chemical crosslinking methods are mostly preferred over physical methods. The chemical crosslinking methods are categorized by reaction types, as addition reactions, condensation reactions, crosslinking with aldehydes and with high energy irradiation (Table 1.5)). Crosslinking with addition reaction is one type of polymerization in which no by product is formed. Two polymers are conjugated as they are. The readily reactive groups should be on polymer chains. The polymers could be modified or

functional entities can be conjugated on polymer chains. In one of the studies PEG-diacrylamide was designed by acrylamide group integration for tissue engineering applications. Acrylamide groups readily conjugate with thiol groups. By this modification thiol containing peptides were ligated to acrylamide containing PEG molecules directly [114]. The results showed stable conjugation. Click chemistry reaction are also in addition polymerization. Since the final conjugate between azido and alkyne groups forms a cyclic triazole ring, it is named as cycloaddition reactions.

Table 1.5 Different crosslinking methods used for preparation of scaffolds (modified from reference [115])

Methods	Details	Example	References
Physical methods	Ionic interaction, divalent ion interaction	Alginate, Dextran	[69]
	Crystallization by hydrogen bond interaction	PVA	[116]
	Self-assembly	PEG, PLGA	[115]
Chemical methods	Addition reactions	Acrylamide addition	[114]
	Condensation reaction	Carbodiimide; EDC, DCC	[117]
	By aldehydes	Glutaraldehyde	[118]
	By high energy irradiation, photooxidation,	UV& gamma rays	[119]

Second type of polymerization is condensation reactions. If there is a byproduct after polymerization these reactions are classified as condensation. Carbodiimide crosslinking reactions are the most remarkable examples of this polymerization. Carbodiimides link carboxylate and amine functional groups to form amide bonds between the polymers. There are two commonly used carbodiimide reagents, EDC and DCC; EDC dissolves in water due to its salt form, while DCC is soluble only in organic solvents. The solubility parameter affects the choice of reagent used. Since EDC dissolves in aqueous media, it is the mostly preferred carbodiimide crosslinking agent.

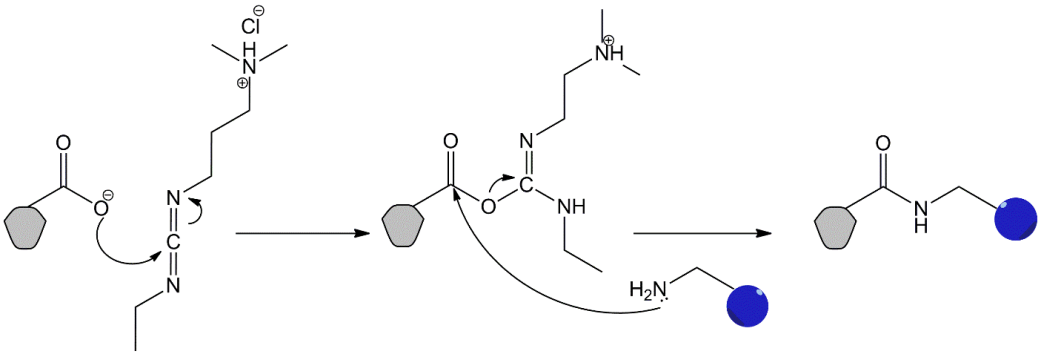

Figure 1.6 The reaction mechanism of carbodiimide crosslinking between primary amine and carboxylic acid.

Third type of chemical crosslinking is the conjugation of complementary groups. The best example for this type of reactions is Schiff base (imine) formation [120]. The carbonyl group reacts with primary amine containing group and imine bond forms. As a result of these reactions strong hydrogels are obtained by strong covalent bonds [121]. Glutaraldehyde is the most remarkable example of this group of reactions; two reactive aldehyde moieties of glutaraldehyde could react with amino containing polymers via imine formation. This connects the two polymers through two imine groups. However, it is less preferred in tissue engineering applications due to its toxicity of unreacted glutaraldehyde [122]. Borate buffer can be used in this reaction to enhance the crosslinking process. Borate buffer is basic and it accepts protons in environment. In this case the proton atoms of primary amine are attacked by sodium tetraborate. Then reactive nitrogen atom attacks to oxygen and chemically stable imine bond forms between them (Figure 1.7).

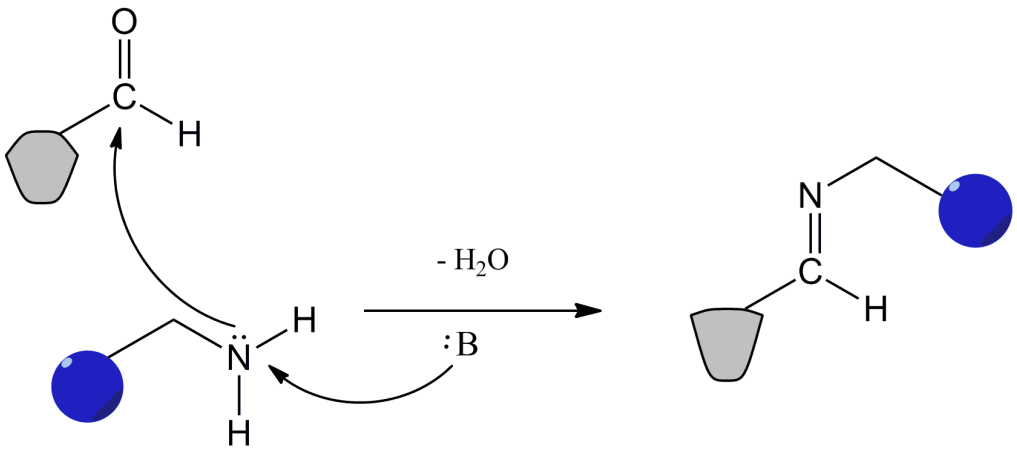

Figure 1.7 The reaction mechanism of Schiff base formation between primary amine and aldehyde groups.

Another chemical crosslinking type is the radical polymerization. In this type of polymerization, UV exposure forms a free radical in the polymer chain and this free radical ion initiates the polymerization and then this polymerization reaction propagates. In one of the studies, UV crosslinking method was applied to crosslink gelatin with phenylazide conjugated poly(acrylic acids) [119]. It was shown that these electrospun fibers were strengthened. L929 cells were loaded on these scaffolds and cell proliferation was higher than gelatin scaffolds crosslinked with glutaraldehyde.

1.3. Click Chemistry in Tissue Engineering Applications

Reactions with rapid rate and high fidelity (no side product formation) with little effort are called click reactions in both chemistry and biology literature. For these reactions two orthogonal functional groups are used (*vide infra*). These functional groups are usually inert to other functional groups except for themselves. Therefore, these reactions find great applications in biomedical applications.

1.3.1. Common Click Reactions Used for Biomaterials

In previous sections, the chemical and physical crosslinking methods and agents were reviewed. However rapid development in tissue engineering and regenerative medicine field favors studies of new methodologies for scaffold design and fabrication, and material functionalization. The biomimetic reactions or new materials are investigated and adapted to biological applications. Click chemistry is one of these reactions which are recently favored in biomedical studies such as drug delivery, chemical signaling and tissue engineering due to its advantages and applicability. The term click chemistry was first used in 2001 to define a class of chemical reactions which link molecules quickly and accurately [123]. In click chemistry reactions azido and alkyne containing entities react and form a 5 membered triazole ring as cycloaddition product. This type of reactions were already studied in organic syntheses [124]. It is revealed that this reaction can take place at ambient temperature and pressure, and in aqueous environment; thereby these reactions become biologically applicable. The advantages of click chemistry reactions for bioconjugation of molecules and scaffold formation are that the functional groups of reactions form irreversible, stable covalent pair and they are chemoselective. They do not react with any other molecules even there are lots of nucleophiles and electrophiles in biological systems. This property of molecules is defined as bioorthogonality. Moreover, the rate and efficiency of the reaction is high [123,125]. There are various click chemistry reactions for chemical conjugation and polymer synthesis; some of which are given in Figure 1.8. Copper catalyzed azide alkyne cycloaddition, Michael additions, Thiol-ene coupling, Diels-Alder click reactions are some of them.

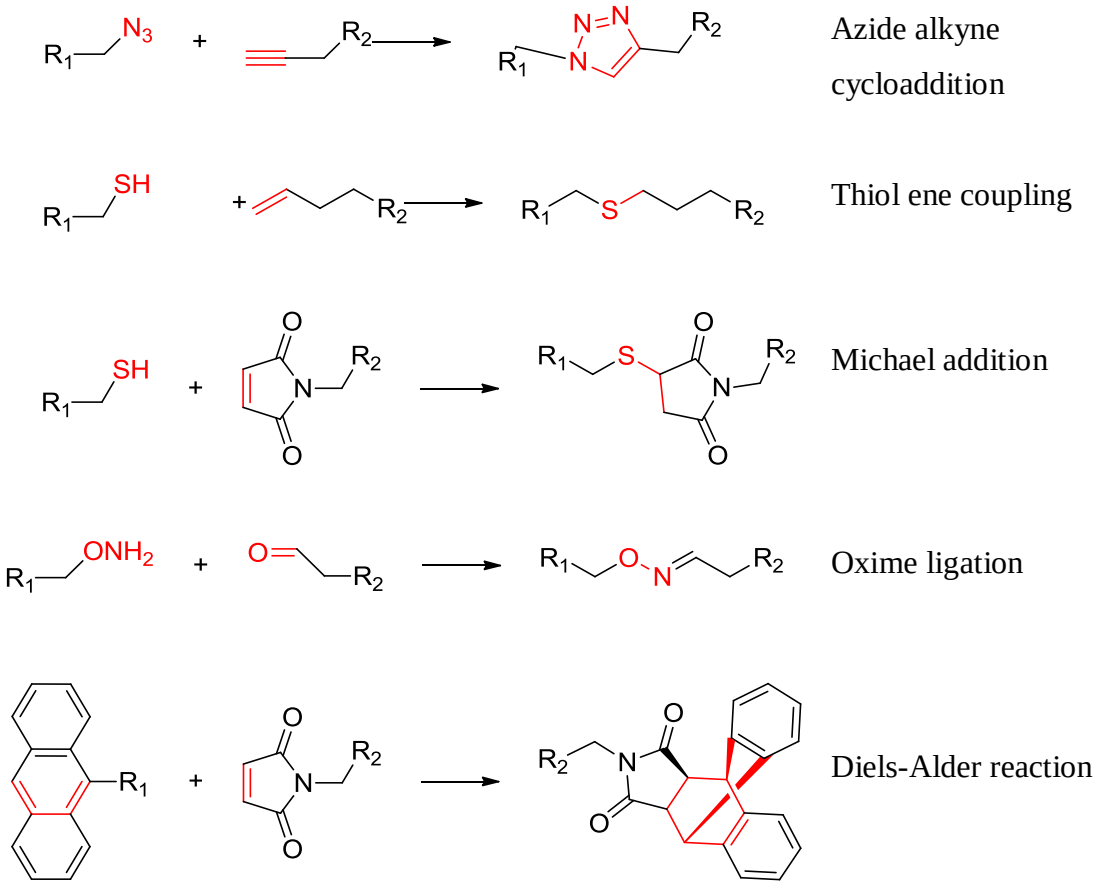

Figure 1.8 Common click chemistry reactions used for polymer synthesis and biomaterial designs [126,127].

In this thesis, azide alkyne cycloaddition click chemistry reactions were examined in detail (Figure 1.9). There are two types of click chemistry reactions; one catalyzed with Cu (I) termed as Cu-catalyzed azide-alkyne cycloaddition (CuAAC) and the other type differing in catalyst used. CuAAC reactions were developed by Sharpless and coworkers from Huisgen cycloaddition. The yield and efficiency of reaction were enhanced by copper. In this reaction, copper coordinates with alkyne entities and forms an intermediate. Meanwhile other copper atom activates azide group by coordinating with electrons on nitrogen atom. At the end of metal centered weak coordination, cycloaddition is generated [123]. The other version of azide and alkyne cycloaddition was first developed by Bertozzi and collaborators which varies in catalyst. In this version the strain of cyclooctyne promotes azide activation and cycloaddition (SPAAC) [128,129]. This version of click chemistry was developed especially for *in*

situ polymerization reactions, biochemical labeling, and chemical signaling and drug delivery studies.

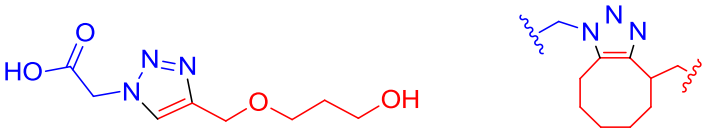

(a) (b)

Figure 1.9 The final scheme of copper catalyzed (a) and copper free (b) azide alkyne cycloaddition

1.3.2. Applications of Click Chemistry in Tissue Engineering

In literature, various synthetic and natural polymers were used in click chemistry reactions. To best of our knowledge, click chemistry reaction types are mostly studied with poly (ethylene glycol) PEG for fabrication of two- and three-dimensional scaffolds or micro and nanohydrogels. The chemical nature of PEG provides makes it possible to analyze click chemistry ligation with ease. Recently, natural polymers; silk fibroin [130], chitosan [131], hyaluronic acid [132] or their composites with PEG [133,134] were examined for biomedical applications.

Chemical modifications on natural polymers pose a risk of natural structure distraction of polymers, which might cause proteins or polysaccharides to lose their functionality. It requires control of parameters like pH, temperature and concentration. When the conditions are satisfied, natural polymers are the best to functionalize and mold. For instance, several chemical modifications were experimented on silk fibroin without any protein structure damage [48,135]. Silk fibroin is one of the mostly studied natural polymers for tissue engineered constructs due to its remarkable properties. Chemical modifications such as carbodiimide or glutaraldehyde mediated crosslinkings have minimal harmful effect on silk fibroin protein structure, in case strict control over experimental parameters are satisfied. However, there is a risk of fibroin conjugation onto itself. This leads to fibroin aggregates in scaffold and inhomogeneous polymer concentration. In the case of tailoring biologically active agents on fibroin-based

scaffolds, inhomogeneity may lead to problems such as different local densities in the scaffold. Therefore, the studies on click chemistry based conjugation of silk fibroin have been advanced. Click chemistry reactions provide chemoselectivity and prevent fibroin to fibroin conjugation. In one of the click chemistry based studies, surface modification of silk fibroin was examined by click-grafted PEG molecules [134]. In this study, azido group was ligated to via serine or tyrosine to silk fibroin and PEG was modified with alkyne groups. CuAAC was done and the reaction mixture was casted as thin film for tissue engineering applications [133,136]. In another previous study silk fibroin was clicked with glycopolypeptides to enhance the molecular recognition of scaffold in order to mimic the extracellular matrix for engineering functional tissues [137]. In here, the cycloaddition crosslinking was characterized and demonstrated by ligating fluorescent dyes with functional entities. In another study, fibroin was clicked with dye by both azido and alkyne group addition on protein for biomedical applications [130]. In this study the crosslinking efficiency was compared between click reaction and carbodiimide crosslinking reactions by measuring stability of ligated dye to protein unit. UV-Vis and FTIR results confirmed that the dye conjugated with click reactions was more stable on silk protein amino acid residues than EDC/NHS crosslinking. This shows that the clicked silk fibroin or poly (ethylene glycol) would be more long standing material in body which will enable enough time for regeneration of the damaged tissue.

Other than silk fibroin, click chemistry is studied on sugar molecules like chitosan, dextran and alginate for regenerative medicine. The linear polysaccharide chain gives opportunity to functionalize the free groups on chain without harming structure. In one of these studies, azido chitosan was synthesized and clicked with acetylene terminated poly (ethylene glycol) for development of injectable biomaterials. Copper free click chemistry reactions were performed; however in this case, reaction took place at higher temperatures. The blend was used for microcarrier design and microcarriers were seeded with mesenchymal stem cells. No toxic effect of matrix on cells was observed [138]. Alginate was also functionalized with azide or linear alkyne group and clicked to form gel capsules to carry cells. These capsules were compared with calcium-mediated crosslinking of alginate based capsules in terms of water swelling, stability and permeability. The physicochemical properties of clicked alginate showed better

results [139]. Dextran was modified with click chemistry reactions and conjugated with polyethylene glycol. Dextran was modified with azide entities and clicked with alkyne functionalized dextran in the presence of copper catalyst. The degree of substitution was analyzed with ^{1}H-NMR and FTIR analyses [140].

1.4. Aim of Thesis

Bone tissue engineering is a rapidly evolving field of study since there are still several challenges encountered by researchers to produce promising clinically applicable ideal bone tissue constructs. An ideal scaffold designed for bone tissue engineering applications should fulfill the requirements such as being three-dimensional, highly porous but still be able to withstand mechanical stresses in bone. Additionally, it should closely mimic the extracellular matrix of bone, which will ensure the regeneration of bone tissue.

With this in mind the objective of this thesis was to develop three-dimensional porous scaffolds using two natural polymers silk fibroin and citrus pectin for bone tissue engineering applications. Silk fibroin was selected since it has remarkable mechanical properties besides that it has slow biodegradation rate, low immunogenicity and versatility in processing. Citrus pectin was studied in order to enhance the cellular adhesion and proliferation on three dimensional matrix by virtue of polysaccharide's anionic structure. Additionally, we aimed to synthesize nano calcium phosphates with different Ca/P ratios using Flame Spray Pyrolysis method for preparing polymer/bioceramic composite scaffolds for future studies. Human urine derived stem cells were used for testing the in vitro biocompatibility of synthesized particles.

The thesis is composed of three parts. In the first part of the thesis the objective was to prepare three dimensional scaffolds with crosslinking biopolymers by click chemistry. The organic synthesis route and characterizations were emphasized in this chapter. Second chapter of the thesis covers the preparation of 3D porous scaffolds by freeze drying of modified pectin and fibroin blends at different ratios and comparison of EDC/NHS and borax mediated crosslinking on the morphology, stability of the fibroin and pectin based scaffolds. Third chapter focuses on the synthesis of nano sized calcium phosphate (CaP) particles by industrially applied aerosol derived Flame Spray Pyrolysis which could be used for reinforcement of the mechanical properties of fibroin and pectin based scaffolds prepared for bone tissue engineering applications. The biocompatibility of synthesized nanoparticles was tested using human urine derived stem cells. The isolation and characterization of these stem cells have been discussed in detail in this chapter.

CHAPTER 2

MATERIALS & METHODS

2.1. Materials

For scaffold fabrication; silk fibroin was purchased from Akman İpek Company (Bursa, Turkey) and high methoxyl citrus pectin was obtained from Prof. Dr. Yakup Sedat Velioğlu, Department of Food Engineering of Ankara University. All commercially available chemicals used in organic syntheses were received from Sigma-Aldrich (Germany), unless stated otherwise. NMR solvents; $CDCl_3$, D_2O and DMSO-D6 were purchased from Merck (Germany). Silica gel 60 (0.040-0.063 mm) purchased from Merck (Germany) was used for the column chromatography.

For in vitro studies; Keratinocyte serum free medium (KSFM Invitrogen, USA), DMEM low glucose (1 g/l) with L-glutamine, DMEM high glucose (4.5 g/l) with L-glutamine, heat inactivated fetal bovine serum (FBS), trypsin EDTA and penicillin/streptomycin were purchased from Biochrom (Germany). Dimethyl sulfoxide (DMSO) (molecular biology grade) and Triton X-100 were obtained from AppliChem (Germany). Trypan blue solution (0.4%) and non-essential amino acid solution were purchased from Sigma-Aldrich (Germany). Alamar Blue and Presto Blue were obtained from Invitrogen (USA). Bovine serum albumin (BSA), copper sulfate pentahydrate solution ($CuSO_4\,5H_2O$), sodium azide, bicinchoninic acid (BCA) reagent were the products of Sigma (Germany) Anti-CD73 and Anti-CD90 were purchased from Abcam (USA).

For calcium phosphate nanoparticle synthesis; calcium acetate hydrate and tributyl phosphate was obtained from Sigma-Aldrich (Germany) and propionic acid was purchased from Merck, (Germany). GF/B glass microfiber filter (1.0 μm) was the product of Whatman, GE Life Sciences (UK). The methane, oxygen and dry air gases were obtained from Habaş (Kocaeli, Turkey).

2.2. Methods

PART I

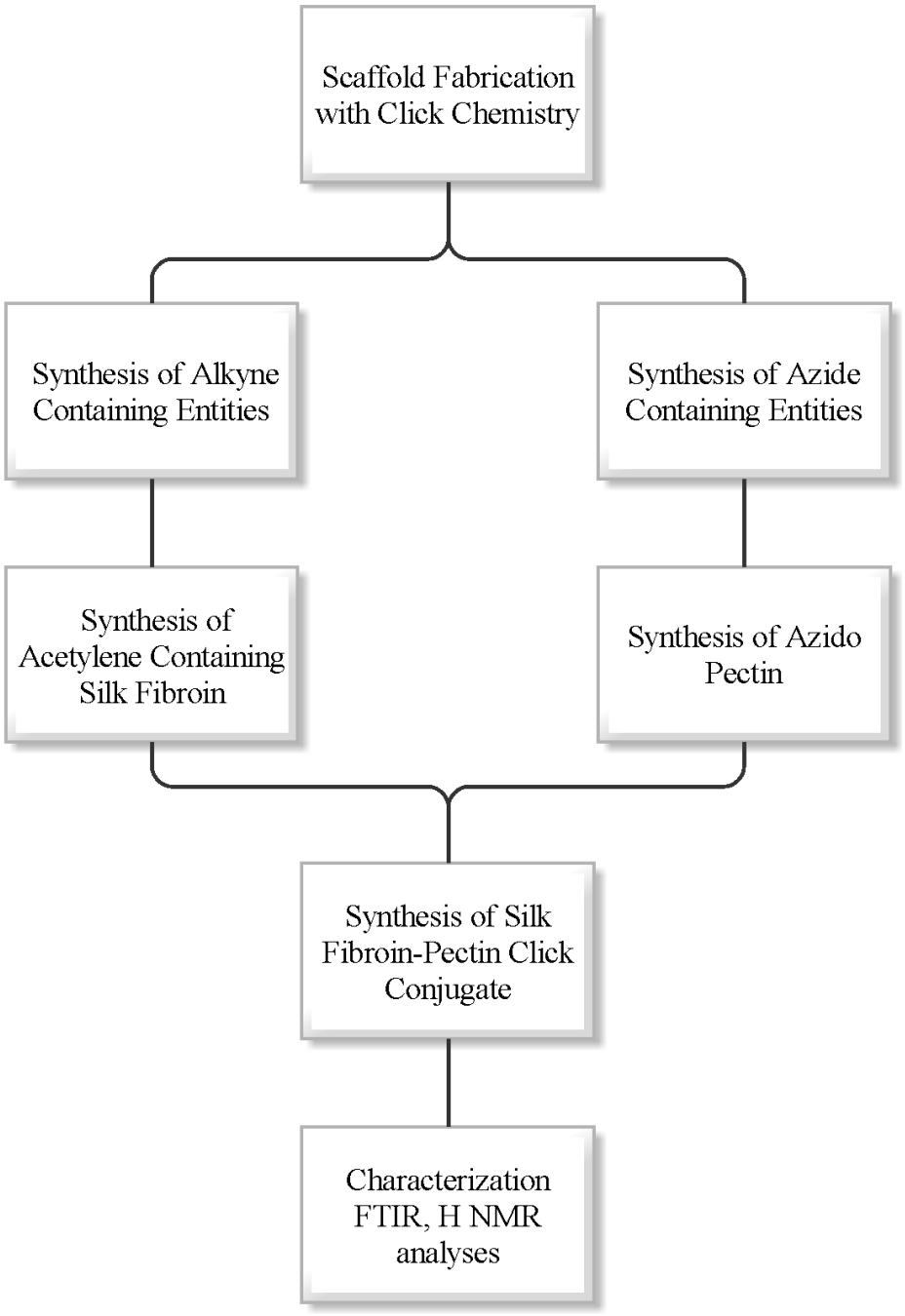

Figure 2.1 The shematic presentation of steps of scaffold fabrication with click chemistry

.

2.2.1. Scaffold Fabrication with Click Chemistry

The organic syntheses of functional group containing linker compounds were conducted, then characterized by NMR spectra (400 MHz Bruker Spectrospin Advance DPX NMR spectrometer, Germany) and IR spectra (Bruker Platinium ATR-IR spectrometer, Germany) analyses. ^{1}H, ^{13}C NMR and IR spectra of products are given in Appendix B (Spectral data). Chemical shifts were recorded in parts per million (ppm) relative to the internal standard tetramethylsilane. In interpretation of NMR spectra, spin multiplicities were specified as singlet (s), doublet (d), doublet of doublets (dd), triplet (t) and multiplet (m) and coupling constants (J) were reported in Hertz (Hz). In thin layer chromatography analysis, UV-lamp and iodine were used for visualization of the spots. All calculations were performed with Gaussian 09, A.02.i. Compounds given below were drawn by using ChemBioDraw Ultra 12.0 (CambridgeSoft).

2.2.1.1. Synthesis of Alkyne Containing Entities

2.2.1.1.1. Synthesis of 8,8-Dibromocyclooctyne [141]

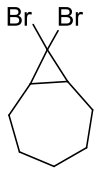

1

Potassium *tert*-butoxide (1.08 g, 96 mmol) suspended in *n*-hexane (10 ml) at room temperature and was stirred for 20 minutes. Cycloheptene (0.71 g, 74 mmol) was added and mixture was cooled to -10°C. Bromoform (1 ml, 111 mmol) was added to the reaction mixture dropwise. The mixture was turned brown. Then the reaction was allowed to reach room temperature and stirred overnight. H_2O (10 ml) was added to quench reaction. The mixture was acidified by addition of HCl (3 ml, 2M). The product was extracted with n-hexane and organic layers were washed with H_2O, dried over $MgSO_4$, filtered and concentrated *in vacuo*.

^{1}H NMR ($CDCl_3$, 400 MHz) δ 1.14-1.27 (m, 3H); 1.34-1.45 (m, 2H); 1.69-1.77 (m, 2H); 1.82-1.93 (m, 3H); 2.25-2.31 (m, 2H)

^{13}C NMR ($CDCl_3$, 100 MHz): δ 28.04, 28.92, 32.25, 34.67, 40.70.

2.2.1.1.2. Synthesis of *(E)*-4-(2-bromocyclooct-2-enyloxy)propan-1-ol [142]

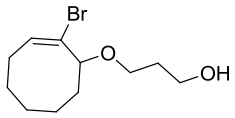

2

To a stirred suspension of 1,3-propanediol (1 ml, 14 mmol) and silver perchlorate (0.40 g, 1.93 mmol) in toluene (1 ml) were added to a solution mixture of 8,8-dibromocyclooctyne (0,10 g 0.52 mmol) in a mixture toluene (1 ml) and pyridine (1.5 ml). The resulting mixture was heated to reflux for 4 h in dark. Then insoluble silver salts were filtered. Brine (20 ml) was added and then HCl (50 ml, 1M) was added to mixture. Extraction was done with diethyl ether. The combined organic layers were washed with dH_2O and dried over Na_2SO_4 and concentrated in vacuum.

^{1}H NMR ($CDCl_3$, 400 MHz) δ 6.15-6.20 (m,1H), 3.84-3.89 (m, 1H), 3.55-3.71 (m, 3H), 3.28-3.35 (m, 1H), 2.67-2.80 (m, 1H,) 2.25-2.31 (m, 2H), 1.90-2.05 (m, 4H), 1.70- 1.72 (m, 5H), 1.41-1.56 (m, 1H), 1.23-1.34 (m, 1H), 0.74-0.85 (m, 1H)

2.2.1.1.3. Synthesis of 4-(cyclooct-2-yn-1-yloxy)propan-1-ol [142]

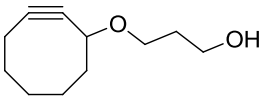

3

The bromocycloalkyne (450 mg, 1.08 mmol) was dissolved in DMF:THF (1:1) solution mixture and NaH (260 mg, 10.80 mmol) was added. The resulting mixture was stirred at room temperature for 5 h. Then mixture was cooled to 0°C. By addition of 1M HCl (50 ml), mixture was neutralized. Extraction was done with ethyl acetate and organic layers were washed with dH_2O, dried over Na_2SO_4, filtered and concentrated.

^{1}H NMR ($CDCl_3$, 400 MHz) δ 4.15-4.19 (m, 1H), 3.60-3.66 (m, 3H), 3.31-3.38 (m, 1H), 2.41 (br s, 1H), 2.07-2.32 (m, 3H), 1.78-2.00 (m, 4H,) 1.62-1.70 (m, 6H), 1.45-1.51 (m, 1H)

2.2.1.1.4. Synthesis of 3-(prop-2-ynyloxy)propan-1-ol [143]

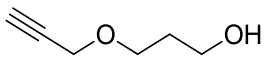

4

A solution of 1, 3-propanediol (6.10 g, 0.08 mol) in DMF (7 ml) was dropwise added into a suspension of sodium hydride (60 wt. %) (3.20g, 0.08 mol) in DMF (15 ml) at 0°C. After 30 minutes of stirring at 0°C, a solution of propargyl bromide (80 wt %) (3 g, 0.02 mol) in DMF (7 ml) was added. The mixture was then stirred for 24 h at room temperature. The product was extracted with ether, washed with water, dried over $MgSO_4$, and evaporated. The crude product was purified with column chromatography (SiO_2, 1:30 EtOAc:Hexanes).

^{1}H NMR (400 MHz, $CDCl_3$): δ 1.63–1.75 (m, 4H), 1.91 (s, 1H), 2.44 (m, 1H), 3.57 (m, 2H), 3.67 (m, 2H), 4.16 (m, 2H);

^{13}C NMR (100 MHz, $CDCl_3$): δ 32.06, 58.13, 60.28, 67.94, 74.55, 79.62;

IR (ATR cm^{-1}): 3285.31, 2928.31, 2122.45

HRMS: Calcd.for $C_6H_{10}O_2$: 114.0759 Found: 115.1424 (H^+ -1)

2.2.1.1.5. Synthesis of 3-((3-(prop-2-ynyloxy)propoxy)carbonyl)propanoic acid

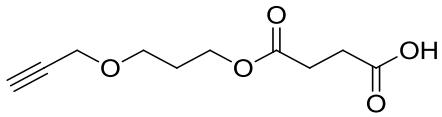

5

The acylation of 3-(prop-2-ynyloxy)propan-1-ol was performed with succinic anhydride. To a stirring solution of 3-(prop-2-ynyloxy)propan-1-ol (0.38 g, 3.33 mmol) in dimethylformamide (20 ml) solid succinic anhydride (0.38 g, 3.30 mmol) was added. The reaction mixture was stirred for 2 h at room temperature. TLC analysis was performed to control final product conversion. The solvent was evaporated

IR (ATR cm^{-1}): 3289.40, 2921.24, 2851.86, 2114.11,1457.08

HRMS: Calcd.for $C_{10}H_{14}O_5$: 214.2151 Found: 237.0739 (Na^+ -22.998)

2.2.1.1.6. Synthesis of 3-(prop-2-ynyloxy)prop-1-ene [144]

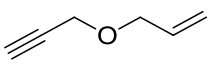

6

A solution of allyl alcohol (0.58g, 10mmol) in DMF (7 ml) was dropwise added into a suspension of sodium hydride (60 wt. %) (0.99 g, 25 mmol) in diethyl ether/DMF (7 ml) at 0°C. After being stirred for 2 h under N_2 at 0°C, a solution of propargyl bromide (80wt %) (1.50 g, 10 mmol) in diethyl ether/DMF (7 ml) was added. The mixture was then stirred for 24 h at room temperature. The product was quenched with brine and extracted with diethyl ether, washed with water, dried over $MgSO_4$, and evaporated.

2.2.1.2. Synthesis of Azide Containing Entities

2.2.1.2.1. Formation of Benzyl Azide From Benzyl Bromide [145]

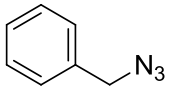

7

Benzyl bromide (2 ml, 16.84 mmol, 1.0 eq.) was dissolved in DMSO (40 ml). Sodium azide (1.64 g, 25.26 mmol, 1.5 eq.) was added and the reaction was stirred overnight at room temperature. Water was added slowly to quench reaction. The product was extracted with diethyl ether. The combined organic layers were washed with brine dried over $MgSO_4$ and evaporated.

IR (ATR cm^{-1}): 2088.62 (-N_3)

2.2.1.2.2. Synthesis of α-Azidoacetic Acid [146]

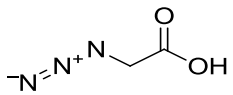

8

Sodium azide (0.57 g, 8.8 mmol) was dissolved in deionized water (15 ml) and mixture was cooled to 0°C. Bromoacetic acid (1 g, 7.2 mmol) was added to reaction mixture and left to reach room temperature by stirring for 24 h. The reaction mixture was acidified with HCl addition (1:1, HCl: H_2O; 4 ml). The product was extracted with

diethyl ether. Organic layers were collected, dried over $MgSO_4$, and evaporated to obtain product as colorless liquid.

^{1}H NMR (400 MHz, $CDCl_3$): δ 3.90 (s, 2H), 11.40 (s, 1H)

^{13}C NMR (100 MHz, $CDCl_3$): δ 49.6, 174.4

IR (ATR cm^{-1}): 3104.70, 2108.45, 1714.79

2.2.1.2.3. Synthesis of Azidoacetic Anhydride [147]

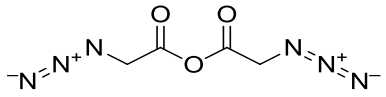

9

To a solution of azidoacetic acid (0.37 g, 3.66 mmol) in anhydrous THF, DCC (N,N'Dicyclohexylcarbodiimide) was added (0.39 g, 1.89 mmol). The rubber septum was placed in the mouth of flask. The reaction mixture was stirred for 5 h at room temperature. After TLC analysis control, reaction mixture was filtered to remove solid DCU (N,N' Dicyclohexylurea). The solvent was evaporated.

IR (ATR cm^{-1}): 3307.81, 2931.15, 2124.02, 1598.68

HRMS: Calcd.for $C_6H_{10}O_2$: 184.1130 Found: 183.1108 (H^+ -1)

2.2.1.2.4. Synthesis of 3-Hydroxypropyl 2-Azidoacetate

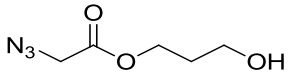

10

To solution of 1-3, propanediol (0.23 g, 3.0 mmol) in chloroform (10 ml) α-azidoacetic acid 8 (0.29 g, 3 mmol) and DMAP (4-Dimethylaminopyridine) (0.36 g, 3 mmol) was added and kept at 0^{o}C. To this reaction mixture, DCC (0.62 g 3 mmol) was added slowly and reaction was stirred for overnight at room temperature. After reaction time, precipitated DCU was filtered. The organic layer was washed with HCl (0.2 ml, 3 mmol, 37%) to protonate remaining DMAP. According to TLC chromatography, column chromatography was performed. FTIR and ^{1}H NMR were performed.

2.2.1.2.5. Synthesis of Allyl 2-Azidoacetate

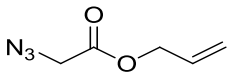

11

For this product, firstly allyl 2-bromoacetate was synthesized via Mitsunobu reaction [148]. In presence of sodium azide, allyl 2-azidoacetate 11 was obtained. Triphenylphoshine (PPh_3) (2.60 g, 9.90 mmol) and diisopropyl azodicarboxylate (DIAD) (2 ml, 14.78 mmol) was mixed in anhydrous THF (50 ml). The mouth of flask was tightly closed with septum. Reaction mixture turned to yellow-white like color and solidified. Then bromoacetic acid (1.20 g, 8.60 mmol) and allyl alcohol (0.6 ml, 8.6 mmol) was added to mixture. The color of solution was disappeared and solid form was gone. The flask was immersed into ice bath at 0°C. After 15 minutes, flask was taken from ice bath and stirred at room temperature for 3 h. After this time period, with respect to spots on TLC paper, column chromatography was performed. ^{1}H NMR analyses of each spot were done. Then as explained in azidoacetic acid synthesis, sodium azide (0.07 g, 1.03 mmol) was dissolved in in deionized water (15 ml) and mixture was cooled to 0°C. Allyl 2-bromoacetate (0.15 g, 0.84 mmol) was added to reaction mixture and stirred at room temperature for 24 h. The reaction mixture was acidified with HCl addition (1:1, HCl: H_2O; 4 ml). The product was extracted with dichloromethane (DCM). Organic layers were collected, dried over $MgSO_4$, and evaporated. ^{1}H NMR and FTIR analyses were performed.

IR (ATR cm^{-1}): 2925.49, 2108.45, 1736.04, 1108.74

2.2.1.2.6. Synthesis of (Oxiran-2-yl) methyl 2-azidoacetate (Epoxidation)

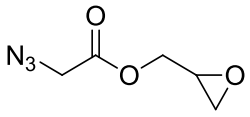

12

To a solution of allyl 2-azidoacetate 11 (0.15 g, 1 mmol) in dry dichloromethane solution, meta-chloroperoxybenzoic acid (*m*-CPBA) (0.51 g, 3 mmol) was added dropwise at 0°C. The flask was tightly closed and N_2 was given. After 1 h later, the ice bath was removed and the mixture was left to reach room temperature for 24 h. The

reaction mixture was washed with $NaHCO_3$ then with brine to remove *m*-CPBA. After TLC analysis confirmation, solvent was evaporated.

2.2.1.3. Copper Catalyzed Click Chemistry Reactions

2.2.1.3.1. Synthesis of Azido Pectin

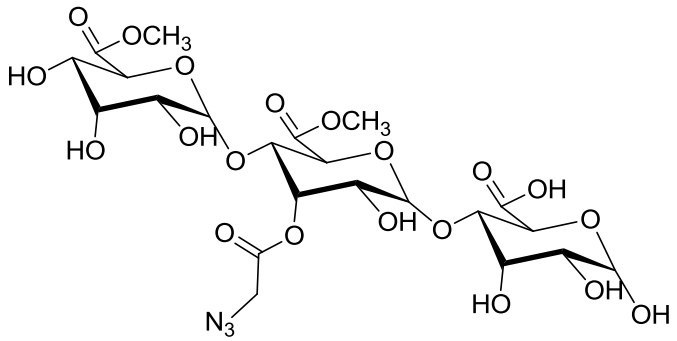

13

High methoxyl citrus pectin (0.1 g) was dissolved in deionized water (5 ml). Then $NaHCO_3$ (0.04 g, 0.4 mmol) was added to deprotonate hydroxyl groups on sugar chain. To reaction mixture, azidoacetic anhydride 9 (0.04 g, 0.2 mmol) was added and stirred overnight. The reaction was confirmed with presence of azide specific peak in FTIR analysis.

2.2.1.3.2. Synthesis of Acetylene Containing Pectin

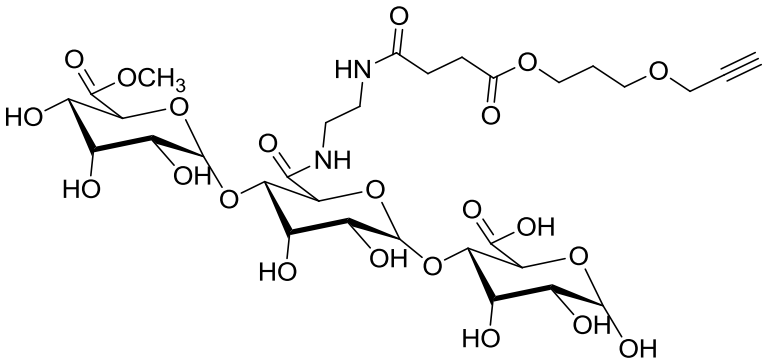

14

Citrus pectin was premodified to conjugate alkyne containing entity on sugar chains. Citrus pectin (0.3 g) was dissolved in deionized water. Then ethylenediamine (6 ml, 0.09 mmol) was added to pectin solution and stirred for 24 h. The mixture was dialyzed

against deionized water for a day. 3-((3-(prop-2-ynyloxy)propoxy)carbonyl)propanoic acid 5 (0.015 g, 0.075 mmol) was dissolved in DMF/deionized water (5 ml). 1-Ethyl-3-(3-dimethylaminopropyl)carbodiimide (EDC) (0.013 g, 0.08 mmol) was then added and stirred for 20 minutes at room temperature. Amidated pectin (0.1 g in 3 ml) was added to reaction mixture and stirred for 2 h. The solvent was evaporated. To confirm the alkyne group conjugation on sugar residues, FTIR analysis was performed. The alkyne specific IR peaks were checked.

2.2.1.3.3. Synthesis of Azido Silk Fibroin

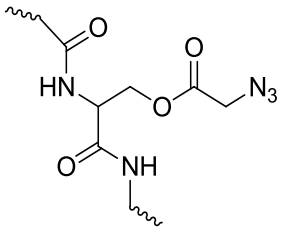

15

To silk fibroin (0.5 g) solution in deionized water, $NaHCO_3$ (0.25 g, 2.9 mmol) was added to deprotonate hydroxyl groups on serine residues. To reaction mixture, azidoacetic anhydride 9 (0.05 g, 0.27 mmol) was added and stirred overnight. The reaction was confirmed by FTIR analysis with the presence of azide specific peak.

2.2.1.3.4. Synthesis of Acetylene Containing Silk Fibroin

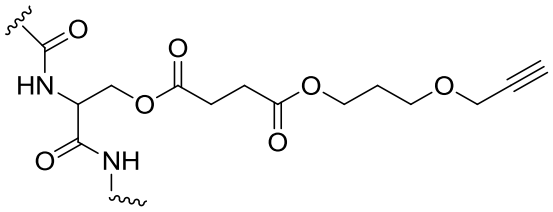

16

3-((3-(prop-2-ynyloxy)propoxy)carbonyl)propanoic acid 5 (0.02 g, 0.1 mmol) was dissolved in DMF/deionized water (5 ml). Then 1-Ethyl-3-(3-dimethylaminopropyl)carbodiimide (EDC) (0.02 g, 0.13 mmol) was added and stirred for 20 minutes at room temperature. Silk fibroin (0.1 g in 10 ml) was added to the reaction mixture and stirred for 2 h. To confirm the alkyne group conjugation on silk

fibroin residues, FTIR analysis was performed. The alkyne specific IR peaks were checked.

2.2.1.3.5. Synthesis of Silk Fibroin-Pectin Conjugate

$CuSO_4.5H_2O$ (7 mg, 0.03 mmol) and ascorbic acid (35 mg, 0.19 mmol) were dissolved in *t*-BuOH/dH_2O mixture (1:1, 10 ml). Acetylene containing silk fibroin 16 (0.1 g) and azide containing citrus pectin 13 (0.1 g) was added to the reaction mixture. The reaction was stirred for 72 h at room temperature under N_2 gas. After time period, the mixture was analyzed by FTIR to control the azide and alkyne specific IR peaks presence in spectrum.

2.2.1.3.6. Click Reaction of Linker Molecules

$CuSO_4.5H_2O$ (1.7 g, 7 mmol) and ascorbic acid (6.16 g, 35 mmol) were dissolved in *t*-BuOH/dH_2O mixture (1:1, 15 ml). 3-(prop-2-ynyloxy) propan-1-ol 4 (0.08 g, 0.7 mmol) and α-azido acetic 8 (0.065 g, 0.6 mmol) were added to the reaction mixture. The reaction was stirred for 72 h at room temperature under N_2 gas. After incubation, the mixture was analyzed by FTIR to control the azide and alkyne specific IR peaks presence in spectrum.

PART II

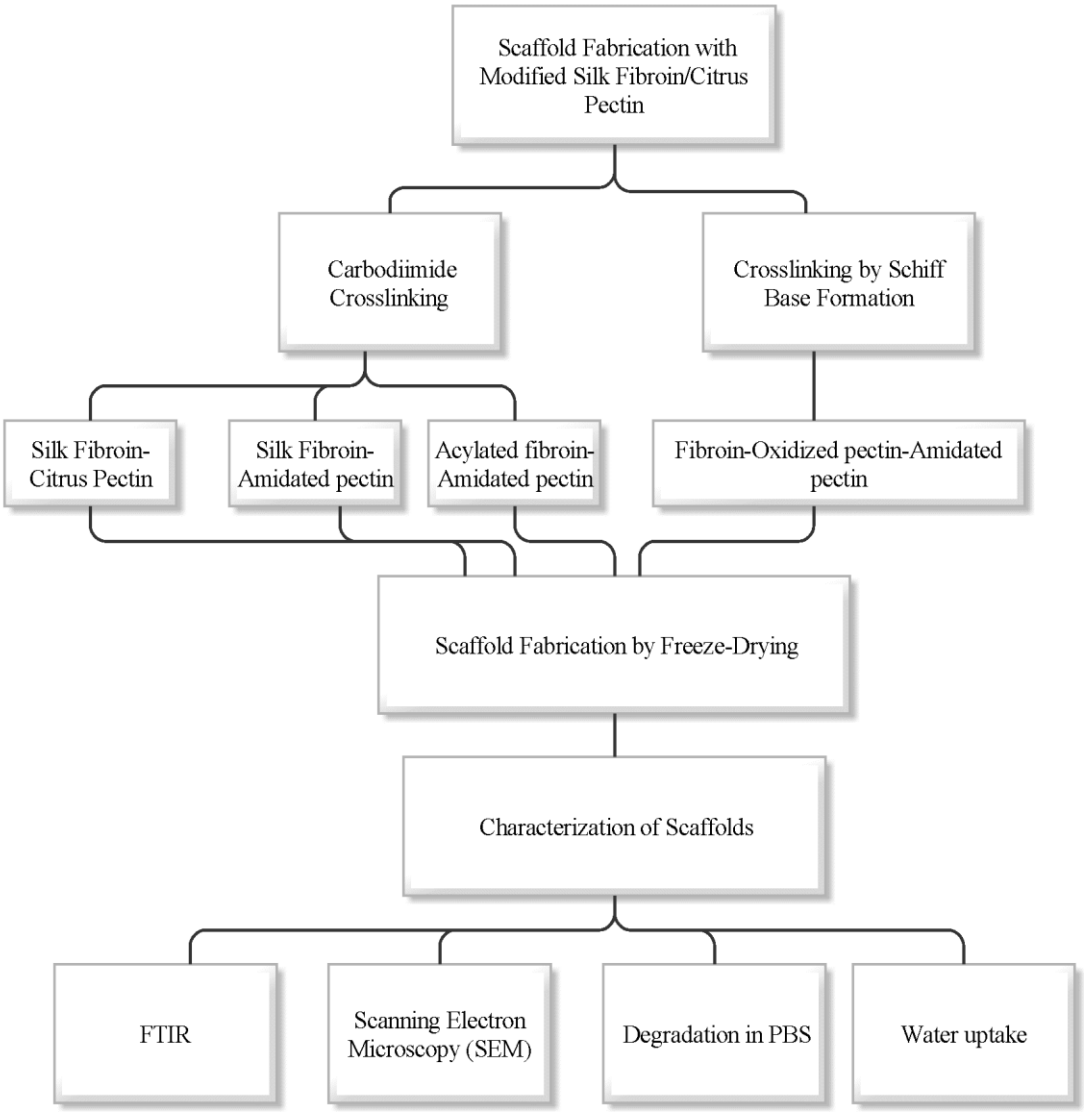

Figure 2.2 The shematic presentation of steps of scaffold fabrication with modified silk fibroin/citrus pectin

2.2.2. Scaffold Fabrication with Modified Silk Fibroin/Citrus Pectin

For scaffolding silk fibroin and pectin were used. Silk fibroin and citrus pectin were firstly modified chemically to enhance crosslinking. Carbodiimide crosslinking and imine formation by borax presence were performed to form biologically inert conjugation of biopolymers.

2.2.2.1. The Purification of Silk Fibroin from Silkworm Cocoons

The silk fibroin isolation from cocoons of *Bombyx mori* was performed as described in the study of Rockwood et al.[47]. Briefly, cocoons were cut into small pieces and boiled with 0.02 M Na_2CO_3 for 30 min and washed with deionized water several times for 60 min to remove the glue-like sericin proteins from the silk fibers. The degummed silk fibers were then dried overnight at 37°C. Dried fibers were dissolved in 9.3 M LiBr at 60°C for 4 h and the solution was centrifuged at 9000 rpm for 20 min at 4°C in order to remove undissolved fibers or debris. The regenerated silk fibroin solution was dialyzed against deionized water for 48 h with several changes of water to remove the lithium bromide. The final concentration of the fibroin solution was found to be about 8-9% (w/v), which was determined gravimetrically after drying fibroin solution at 60°C.

2.2.2.2. The Chemical Modification of Silk Fibroin

Silk fibroin was isolated from cocoons of *Bombyx mori* as described above. The acylation of silk fibroin was performed according to the protocol in the study of Li et al [149]. Mainly serine residues aimed to be attacked but tyrosine and lysine residues are also attacked at excess amount of succinic anhydride (Figure 2.3). The silk fibroin solution was diluted to 2% (wt/wt) by adding deionized water. Succinic anhydride was weighed as 4% (wt/wt; 0.08g) of silk fibroin and dissolved in dimethylformamide (DMF). Silk fibroin solution was stirred in ice bath and succinic anhydride in DMF was gradually added. The pH was checked and adjusted to 8 by adding $NaHCO_3$. The solution was stirred for 2 hours. The reaction mixture was dialyzed against deionized water at 4°C for 24 hours. The reaction was confirmed by IR analysis.

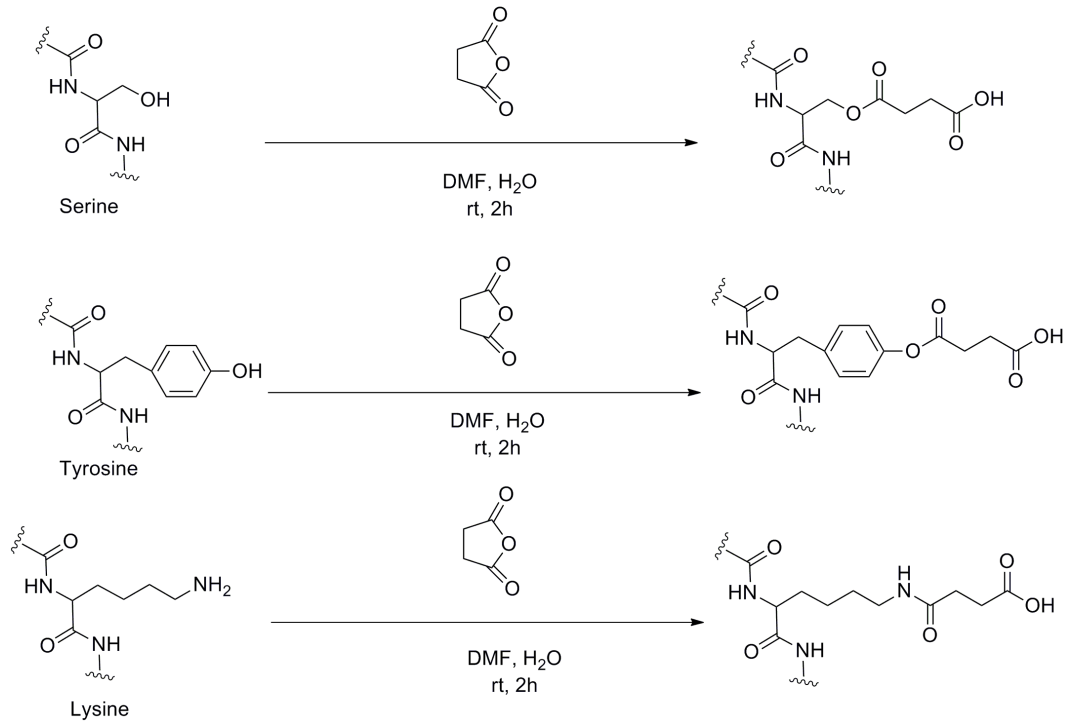

Figure 2.3 The chemical modification scheme of silk fibroin in the presence of excess succinic anhydride. Small amount of lysine residues also react with succinic anhydride.

2.2.2.3. The Chemical Modification of Citrus Pectin

2.2.2.3.1. Oxidation of Citrus Pectin

High methoxyl citrus pectin was oxidized as described previously [150] (Figure 2.4). Citrus pectin (0.4g) was dissolved in deionized water- ethanol mixture (12.5 ml, 4:1 volume ratio). Sodium periodate (0,117g, 0.5 M) was added. The reaction mixture was stirred at 40^{o}C and pH was adjusted to 3.5 for 2 hours. The reaction mixture was wrapped with aluminum foil. After 2 hours, the mixture was precipitated with isopropanol.

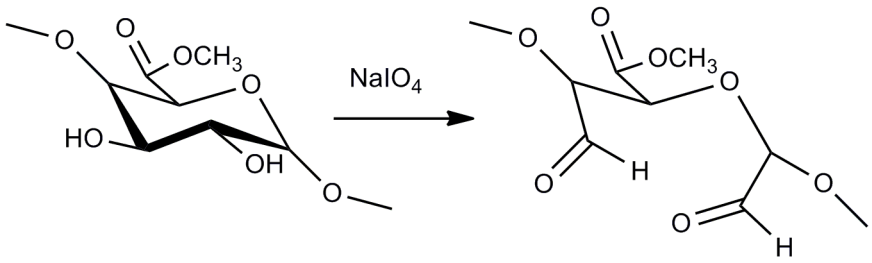

Figure 2.4 The oxidation of citrus pectin with 0.5 M sodium periodate

Aldehyde amount on citrus pectin chain was quantified by reacting oxidized pectin with dinitrophenylhydrazine (DNPH) [150]. Hydrazines react with aldehyde and form hydrazones (Appendix C, Figure C.2). In this reaction, dinitrophenylhydrazine is converted to dinitrophenylhydrazone by reacting with formed aldehyde groups on citrus pectin. The amount of aldehyde is correlated with amount of converted DNPH. The calibration curve was executed by reacting DNPH with benzaldeyde (in range of 5-20 µg/ml). DNPH solution (0.06 M) was prepared by dissolving 100 mg DNPH in 0.5 ml H_2SO_4. 7.7 ml ethanol:water mixture (10:1) was then added and the mixture was stirred for 15 min. Concisely, 0.3 mg oxidized pectin was dissolved in 10 ml DNPH solution and mixture was reacted for 1 h. The reaction mixture was centrifuged and the absorbance of the supernatant was measured at 326.5 nm. The amount of aldehyde was calculated with the equation below;

$$Aldehyde\ content\ \left(\frac{mmol}{g}\right) = \frac{\frac{Reacted\ DNPH(mg)}{Molar\ mass\ of DNPH}}{3x10^{-4}}$$

2.2.2.3.2. Amidation of Citrus Pectin Methoxyl Group

The amidation was executed from methyl ester units of citrus pectin chain (Figure 2.5). High methoxyl citrus pectin (0.3 g) was dissolved in deionized water (10 ml). Ethylenediamine (5 ml) was added into pectin solution. The mixture was stirred for 24 hours. The solution was dialyzed against deionized water to remove unbound ethylenediamine. The solution was evaporated. The amidation reaction was verified by amide I and amide II vibrations in IR spectra.

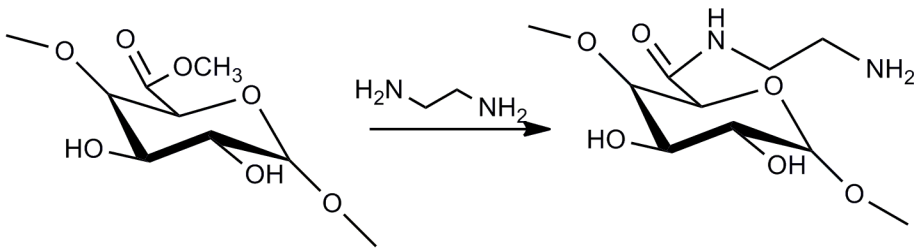

Figure 2.5 The amidation reaction of citrus pectin through methyl ester groups

2.2.2.4. Scaffold Fabrication by Freeze-Drying

Scaffolds were prepared by crosslinking modified pectin and modified fibroin with two different chemical crosslinking methods followed by treatment with 0.1 mM $CaCl_2$ in methanol for 30 min and final immersion in methanol:water (1:1) solution for 30 min. After final immersion, the casted and gelled solutions were frozen at -20 ^oC and freeze-dried for 48 h with a freeze-dryer (FreeZone 18, Labconco Co.,USA).

2.2.2.4.1. Carbodiimide Crosslinking of Modified Citrus Pectin and Modified Silk Fibroin

Carbodiimide crosslinking was used to form an amide bond between reactive carboxyl groups (COOH) and primary amine groups (NH_2). To accomplish this reaction, acylation of fibroin and amidation of pectin were performed. To compare the efficiency of modified polymers for carbodiimide crosslinking, the reaction was conducted with control groups as given in Table 2.1. Mainly, carbodiimide crosslinking of COOH groups on silk fibroin and NH_2 groups on amidated pectin was aimed. Since carbodiimide reaction also occurs between carboxyl and hydroxyl groups, unmodified silk fibroin and citrus pectin was included into experimental groups.

Each solution was prepared as 4% (w/v) by dissolving in deionized water. To activate carboxyl groups N-hydroxysuccinimide (NHS) (10% wt of final polymer weight) was added into fibroin-amidated pectin mixture and stirred for 15 minutes. Then 1-ethyl-3-(3-dimethylaminopropyl)-carbodiimide (EDC) (20% wt of final polymer weight) was added into solution. The pH of mixture adjusted to 6.0-6.5. The solution was

stirred for 2 hours at room temperature. The mixture was casted into 6 cm^2 molds and frozen at -80 ^oC overnight. After 12 hours initial evaporation at -80 ^oC, the scaffolds were immersed in 0.1 mM $CaCl_2$ solution in methanol for 30 min. Then solvent was removed and scaffolds were immersed into methanol:water (1:1) mixture for 30 min. The solvent was removed and scaffolds were frozen at -80 ^oC for overnight again. The scaffolds were further lyophilized for 12 hours. This step was done to enhance the intramolecular interaction of pectin and silk fibroin. The reaction was confirmed by FTIR analysis.

2.2.2.4.2. Crosslinking of Modified Citrus Pectin and Modified Silk Fibroin by Schiff Base Formation

In Schiff base formation reactions, carbonyl (C=O) reacts with primary amines (NH_2) and forms an imine (C=N) and stable covalent bond. To crosslink carbonyl group on oxidized pectin with amine group on silk fibroin and amidated pectin, borax mediated crosslinking was performed (
Figure **2.6**). The experimental groups are given in Table 2.1. Each polymers solution was prepared as 4% (w/v) in deionized water. Amidated pectin and silk fibroin were mixed previously and added onto oxidized pectin. Borax was added to the mixture at different concentrations and the solution was vigorously stirred to facilitate the crosslinking between fibroin and pectin residues. The reaction mixture was stirred and casted into a mold at room temperature. As stated above, the same methanol and $CaCl_2$ crosslinking step was implemented on these scaffolds. To verify the crosslinking of blend, FTIR analyses were performed to observe imine bond (C=N) specific IR peaks.

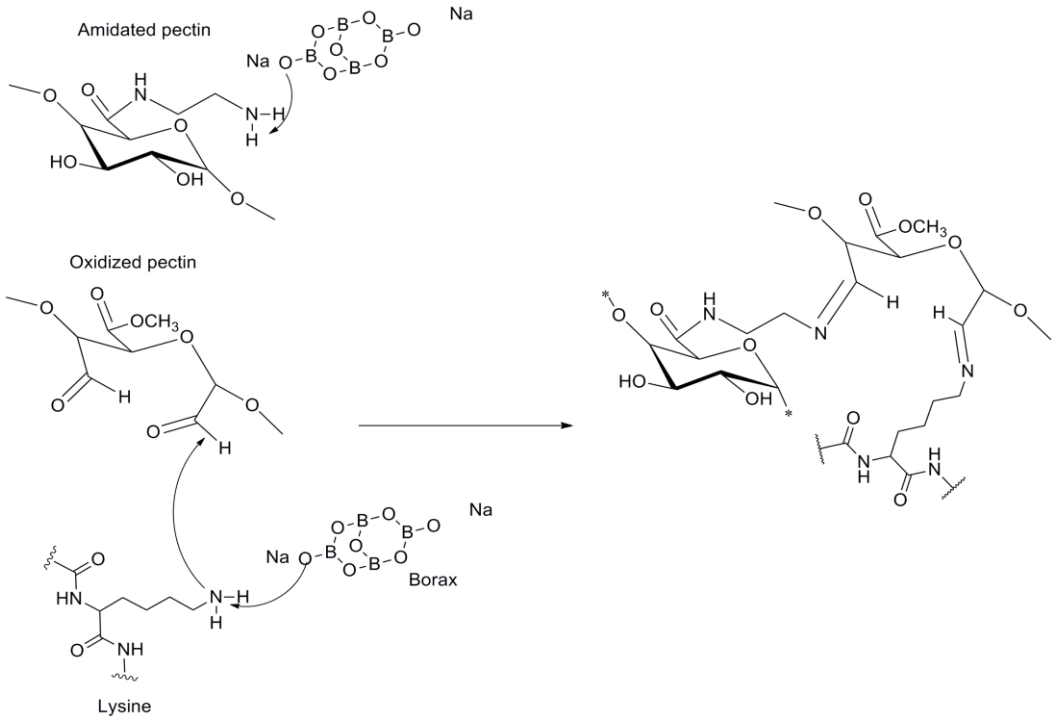

Figure 2.6 The imine bond formation between amidated pectin and oxidized pectin or silk fibroin lysine residues and oxidized pectin

Table 2.1 The chemical crosslinking methods, chemical modifications and blend ratios

Carbodiimide, EDC				Schiff base formation, Borax	
Polymer	Volume ratio	Polymer	Volume ratio	Polymer	Volume ratio
Silk fibroin(SF)	3	Citrus Pectin (CP)	1	Silk fibroin(SF)	3
Silk Fibroin (SF)	3	Amidated Citrus Pectin (A-CP)	1	Amidated Citrus Pectin (A-CP)	0.5
Acylated Fibroin(A-SF)	3	Amidated Citrus Pectin (A-CP)	1	Oxidized Citrus Pectin (O-CP)	0.5

2.2.2.5. Characterization of Scaffolds

2.2.2.5.1. Fourier Transform Infrared Radiation- Attenuated Total Reflectance

All chemical modifications and conjufation reactions were confirmed by FTIR ATR analyses (Bruker Platinium ATR-IR spectrometer, Germany) at the spectral region 400-4000 cm^{-1} as stated in part I title.

2.2.2.5.2. Scanning Electron Microscopy (SEM)

The morphology of scaffolds was investigated by scanning electron microscopy (SEM). Scaffolds were coated with ultrafine (10 nm) gold layer by precision etching coating system (682 PECS, Gatan, Inc., USA) and then imaged via Scanning Electron Microscopy (FEI, Nova Nano SEM 430, USA).

2.2.2.5.3. Degradation in PBS

The degradation profile of scaffolds (n=3) was studied in PBS (10 mM, pH 7.2) at 37ºC in water bath (Nüve Bath NB5, Turkey) for a week. After 1st and 7th days of incubation, preweighed samples were removed from PBS, wet weights of the scaffolds were recorded after removing excess water by blotting with filter paper. The scaffolds were then lyophilized and weighed. The pH of PBS was recorded. The water uptake and weight percent loss of the scaffolds were determined by the following formulas [151].

$$Weight\ loss(\%) = \frac{Wi - Wd}{Wi} * 100$$

W_i: Initial weight of sample

W_d: Remaining weight of sample at defined time point

$$\boldsymbol{Water\ uptake}\ (\%) = \frac{\boldsymbol{Wwet - Wdry}}{\boldsymbol{Wdry}} * \mathbf{100}$$

Wwet: Wet weight of sample at defined time point

Wdry: Dry weight of sample

2.2.2.5.4. Cell Culture Studies

Cell culture studies were conducted with urine derived human mesenchymal stem cells. The characterization of cells was accomplished, and they were used for in vitro cytotoxicity tests of flame spray synthesized CaP particles.

2.2.2.5.4.1. Urine Derived Stem Cell (USCs) Culture

Urine derived stem cells were isolated from spontaneously voided healthy human urine (male, 24 years) with the consent of Middle East Technical University Human Subjects Ethic Committee (see Appendix A). The isolation procedure followed was the same as in literature [27,28,30]. Briefly, sterile mid-stream urine samples were centrifuged at 2000 rpm for 5 min. Afterwards, cells were rinsed with PBS and they were cultivated in 6 well plates in a mixture of Keratinocyte serum free medium (KSFM) and Embryonic fibroblast medium (EFM) (1:1 ratio). Embryonic fibroblast medium consists of Dulbecco's modified Eagle's medium (DMEM), heat inactivated fetal bovine serum (HI-FBS, 10%v/v), and 1% non-essential amino acids. This growth medium was supplemented with penicillin/streptomycin (100 units/ml), 5 ng/ml epidermal growth factor (EGF) and 50 ng/ml bovine pituitary extract (BPE). Urine derived stem cells were cultured at 37^{o}C in 5% CO_2 under humidified atmosphere (5215, Shel Lab, USA). The first appearance of cells was controlled every day, after that medium was changed regularly every third day of appearance on plate. When cells reached to 80% confluency, they were passaged at a ratio of 3:1 using 0.1% trypsin-EDTA.

2.2.2.5.4.2. Characterization of Urine Derived Stem Cells

2.2.2.5.4.2.1. Immunophenotyping of USCs

Immunophenotypic characterization of USCs were done by using a Flow Cytometry (BD Accuri C6, USA). The positive markers were CD73, CD90, CD105, CD44 and negative markers were CD31, CD45, and CD34. After cells reached confluency, they were trypsinized and centrifuged at 3000 rpm for 5 min. The pellet was washed with PBS containing 1/100 BSA and 1/1000 sodium azide. Afterwards, cells were centrifuged. The cells were fixed with 4% (w/v) formaldehyde addition and vortexed. After 15 minutes incubation for fixation, cells were centrifuged and pellet was

resuspended in PBS. Aliquots of cells (100 µL) were transferred to eppendorf tubes. To each tube 2 µL of primary antibodies (1 µg/mL) was added. After 30 min incubation at room temperature, cells were washed three times with PBS, and centrifuged (3000 rpm, 5 min). The cells were then incubated in green fluorescent dye labeled secondary antibody solutions (1 µg/mL), anti-Rabbit IgG H&L (DyLight®488) and the tubes were kept in dark for 30 min. After staining, cells were washed with 1 mL of PBS, centrifuged, and resuspended in 400 µL of PBS. The fluorescent responses were studied under a flow cytometer through three channels: forward scatter channel (FSC), side scatter channel (SSC) and fluorescence channel (FL1 filter, laser 488 nm). All data were analyzed with CFlow®Plus software (BD Biosciences, USA) and the forward and side scatter profiles were gated on live cells. An isotype control was used in each experiment to calculate specific staining.

2.2.2.5.4.2.2. Proliferation Capacity of USCs

The proliferation capacity and clonogenicity of USCs was studied by determining cell viability with Alamar Blue staining at specific time points after 1st passage. Alamar Blue is one of the mostly referenced redox indicator. The active reagent of assay; resazurin acts as electron acceptor and interferes electron transfer chain of healthy cell metabolism. The oxidized form of active reagent turns into fluorescent red like color. The assay was conducted by adding 10% Alamar Blue solution (10 % Alamar Blue & 90 % DMEM) to each well and incubating scaffolds at dark for 4 hours. The optical densities of reduced solutions were obtained at wavelengths 570 nm and 600 nm via microplate spectrophotometer (µOuantTM, Biotek Instruments Inc., USA).

The percent reduction was interpreted on following equation;

$$\%Reduction = \frac{\varepsilon ox\lambda 2A\lambda 1 - \varepsilon ox\lambda 1A\lambda 2}{\varepsilon red\lambda 1A'\lambda 2 - \varepsilon red\lambda 2A'\lambda 1}$$

ε_{ox}; Molar extinction coefficient of Alamar Blue oxidized form (blue),

ε_{red}; Molar extinction coefficient of Alamar Blue reduced form (red),

A; Absorbance of test wells,

A'; Absorbance of negative control well (no cells)

λ_1; 570nm

λ_2; 600nm.

In interpretation of percent cell viability, the media and dye without cells were defined as negative control.

2.2.2.5.4.2.3. Multi-lineage Differentiation Potential of USCs

The potency of urine derived stem cells were evaluated on osteogenic, chondrogenic and adipogenic differentiation. For these differentiation routes, cells were seeded as 30,000 cells/cm^2 into 24 well plates. After reaching 70% confluency, cells were incubated with differentiation media specific for each cell lineage. For osteogenic differentiation; medium was prepared as DMEM (1.5g/L glucose) supplemented with 10% FBS, 100 units/ml penicillin/streptomycin, 50 µg/ml ascorbic acid, 10 mM β-glycerophosphate and 10^{-8}M dexamethasone. Cells were cultured in osteogenic medium for 14 days. The medium was refreshed two times a week. Chondrogenic medium was consisted of DMEM (4.5g/L glucose) supplemented with ITS+1 supplement (1.0 mg/ml bovine insulin, 0.55 mg/ml human transferrin (substantially iron-free), and 0.5 µg/ml sodium selenite), 100 nM dexamethasone, 0.17 mM L-ascorbic acid-2-phosphate, 1 mM sodium pyruvate, 0.35 mM L-prolin, 10 ng/mL TGFβ3. Medium was changed three times a week. For adipogenic differentiation, used medium consisted of DMEM supplemented with 10% FBS, 100 units/ml penicillin/streptomycin, IBMX solution (1:100), insulin (1:1000), dexamethasone (1:1000). The medium was changed in every two days.

2.2.2.5.4.2.3.1. Alkaline Phosphatase Enzyme Activity of USCs

To characterize the osteogenic differentiation of urine derived stem cells, alkaline phosphatase enzyme activity (ALP) of the cells at two different time period was studied. After 3rd passage, cells were seeded at an initial seeding density of 30.000 cells/cm^2 into 24 well plates. The intracellular ALP activity of cells was measured by colorimetric methods in which p-nitrophenyl phosphate (p-NPP) conversion to p-nitrophenol was measured by absorbance readings at 405 nm. In reaction mechanism, ALP hydrolyses the phosphate group on p-nitrophenyl phosphate and converts to 4-nitrophenol.

The protocol of ALP activity assay was performed as follows. After 7 and 14 days of culture, cells were rinsed with PBS and lysed with lysis buffer (0.1% Triton-X-100, 0.1% w/v sodium azide, 1% protease inhibitor in PBS) upon freezing for 30 minutes at -20 ^{o}C and thawing. 100 µl pNPP substrate solution was added into 20 µl aliquots of each cell lysate. After 30 minutes incubation at 37^{o}C, the absorbance of each sample was measured at 405 nm using µOuantTM microplate spectrophotometer (Biotek Instruments, USA). The calibration curve was constructed with 4-nitrophenol in a concentration range of 25-250 µM. The protein amounts in the cell lysates were determined by BCA assay. The specific ALP activity was expressed as nmol/mg protein/min.

Bicinchoninic acid (BCA) assay was performed according to manufacturer guideline. BCA working solution was prepared as 50 parts BCA reagent and 1 part 4% copper sulfate pentahydrate solution. 20 µL sample aliquot was incubated with 250 µL BCA working solution at 60^{o}C for 15 minutes. After reaction mixture reaching to room temperature, the protein amount was determined by measuring the absorbance at 562 nm using µOuantTM microplate spectrophotometer (Biotek Instruments, USA). In principle, Cu (I) was converted to Cu (II) and it reacts with BCA. The reaction resulted with purple like color. The protein amount of lysates were defined by comparing with bovine serum albumin (BSA) standards prepared in the range of 0-1.2 mg/ml (Appendix C, Figure C.3)

2.2.2.5.4.2.3.2. Alizarin Red S Staining

For further characterization of osteogenic differentiation, to detect calcium in monolayer cells Alizarin Red S staining was performed. The monolayer cells were washed with PBS. The cells were fixed with 4% paraformaldehyde for 30 minutes, washed with PBS several times. Alizarin Red solution (2 % (w/v)) was prepared in water and pH was adjusted to 4.2. Cells in 24 well plate were incubated with 500 µl of this solution for 15 minutes. Afterwards, cells were rinsed with water. Nuclei were counterstained with hematoxylin for a minute and washed thoroughly in distilled water before examining under microscope.

2.2.2.5.4.2.3.3. Oil Red O (Sudan IV) Staining

For adipogenic differentiation characterization, the accumulated intracellular triglycerides were stained with Oil Red O [152]. The monolayer cells were washed with PBS. The cells were fixed with 4%paraformaldehyde for 30 minutes, washed with PBS several times and covered with 0.5% (w/v) oil red O solution in 60% isopropanol. After 45 minutes, cells were rinsed in 60% isopropanol and washed thoroughly in distilled water. Nuclei were counterstained with hematoxylin for a minute and washed thoroughly in distilled water.

2.2.2.6. Statistical Analyses

All data are presented as the mean±standard deviation (SD). One-way ANOVA analysis of variance was used to determine statistically significant differences among groups and pair wised comparisons were also performed with two sample t-test with unequal variances. Statistical significance was considered for $p<0.05$.

PART III

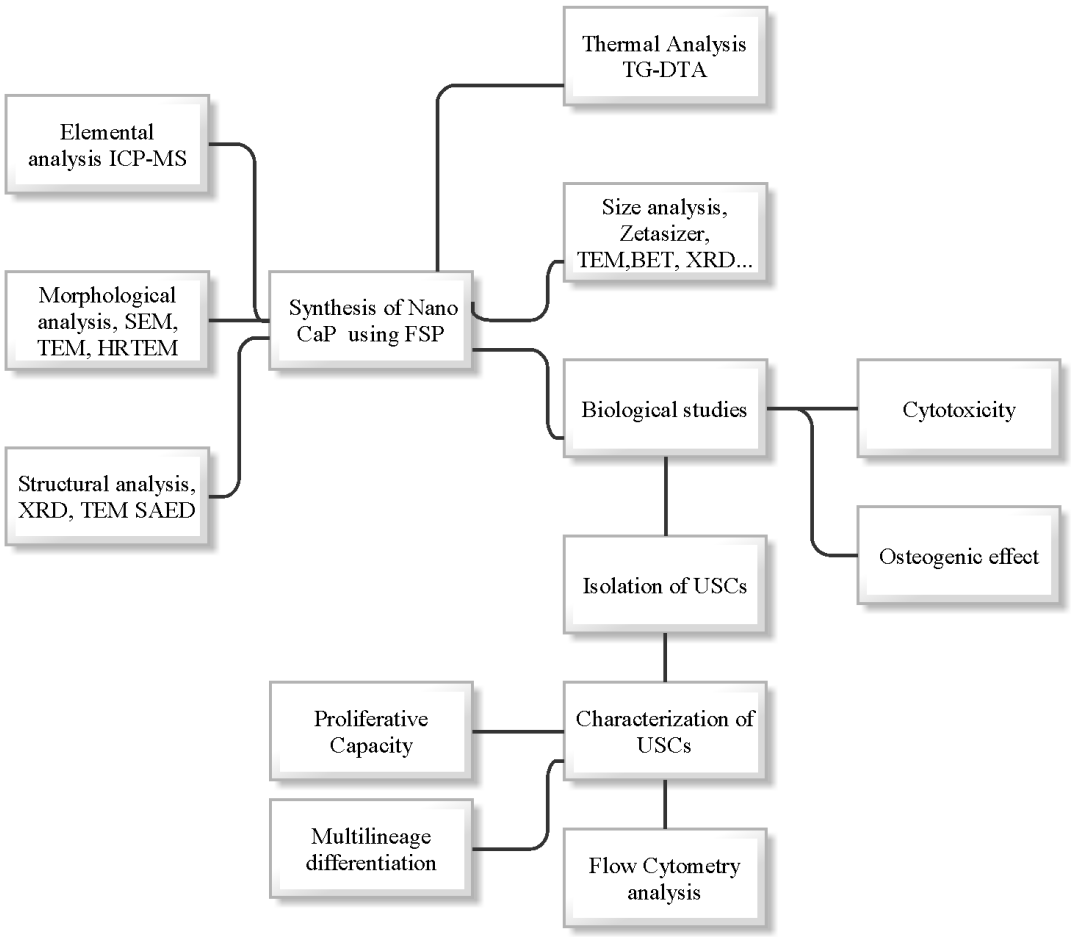

Figure 2.7 The schematic representation of steps in nano sized calcium phosphate synthesis by FSP

2.2.3. Synthesis of Nano Sized Calcium Phosphate Particles Using Flame Spray and Characterization Studies

In order to fabricate biologically active scaffolds for bone tissue engineering, calcium phosphates were synthesized. Nano calcium phosphates at different Ca/P ratios (1.20, 1.31, 1.54, 1.91, and 2.19) were synthesized by Flame Spray Pyrolysis process and characterized. Due to time limitation not enough CaP nanoparticles were produced for preparing polymer-nanohydroxyapatite composite scaffolds. Therefore, we conducted only dose and composition dependent cytotoxicity and osteogenic effect of particles on human urine derived stem cells.

2.2.3.1. The Preparation of Calcium and Phosphate Precursor Solutions

In flame spray pyrolysis system, metal precursor type, its chemical solubility, solvent type, decomposition temperature of metal precursors as well as the flame operating parameters should all be considered to obtain particles with desired properties. Precursor and the solvent type in this study were selected considering these critical points and relevant previous studies [77,79,91]. The acetate form of Ca precursor (calcium acetate), and propionic acid as the solvent, of Ca precursor provided high enough combustion enthalpy to decompose the precursors, to sustain the flame and to produce nanoparticles in our experimental Ca/P precursor ratio range.

Calcium and phosphate precursors were prepared by using calcium acetate hydrate (99. 99% Sigma-Aldrich) dissolved in propionic acid (for synthesis ≥ 99%, Merck) at 60^{o}C for 1 hour, and tributyl phosphate precursor in liquid form (assay ≥ 99%, Sigma-Aldrich) was added after clear solution was observed (0.4 M precursor solution). A range of different Ca/P ratios from low to high (1.20, 1.31, 1.54, 1.91, 2.19) was synthesized and characterized. The liquid precursors were pumped through nozzle with the aid of a syringe pump (Watson, 323 S/D) at 7 rpm (2.4 ml/min), dispersed by oxygen (9 L/min) gas and ignited with methane (2 L/min) and oxygen (2 L/min) premixed gases. The formed nanoparticles were collected on GF/B glass microfiber filter (1.0 μm, Whatman) above the flame with the aid of a vacuum pump.

2.2.3.2. Synthesis of Nanosized Calcium Phosphate Particles by FSP Method

Metal precursors, which were dissolved in propionic acid solvent, were fed into the premixed burner by using a liquid pump and a two-phase nozzle with a capillary insertion, which was located in the center of the burner. Precursor solution was then sprayed into the flame by an oxygen dispersion gas, and ignited by 25 premixed methane/oxygen flamelets creating a stable main flame in which the particles were formed. Particles produced in the flame were collected on a vacuum applied glass fiber filter (GF/B) simultaneously. The burner and the chamber where the GF/B filter was placed were cooled to prevent overheating.

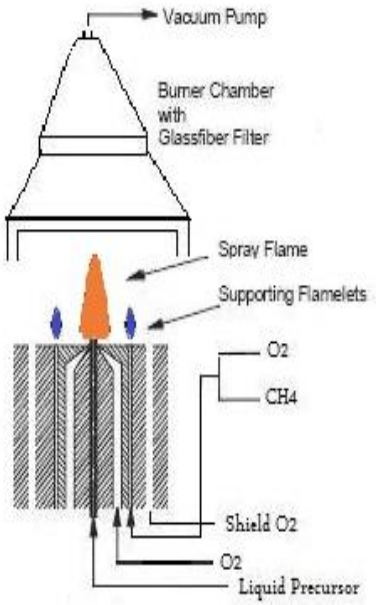

Figure 2.8 Schematic presentation of flame spray pyrolysis (FSP) system [153].

2.2.3.3. Characterization of Synthesized CaP Particles

X-ray diffraction (XRD), scanning electron microscopy (SEM), transmission electron microscopy-energy dispersive spectrometry (TEM-EDS), selected area electron diffraction (SAED) and high resolution transmission electron microscopy (HRTEM) techniques were used for structural and morphological characterization of the nanoparticles. Prior to each analyses, as prepared samples were dried in vacuum oven

at 65°C. XRD (X-Ray Diffractometer, D/MAX2200/PC, Rigaku Co., Japan) was used to determine the phases in the samples. Powder form of particles were spread on glass stage smoothly in order to expose radiation throughout of sample. The general morphology of particles was studied by SEM analyses. Samples were prepared by mounting on carbon tapes to enhance the electron conductivity and then coated with gold-palladium. The powder calcium phosphate samples were investigated by scanning electron microscopy using JEOL JSM-6335F FEG/SEM operating at 20 kV equipped with an Oxford Instruments X-Max80 (AZtec software)

TEM and HRTEM were used for more detailed analyses: for atomic lattice imaging, nanoparticle size, crystal structure and morphology of the particles. TEM was equipped with energy dispersive X-ray spectroscopy (EDS) to determine the surface elemental distribution. Transmission electron microscopy investigations were performed using JEOL-2100 HRTEM operating at 200 kV (LaB6 filament) equipped with an Oxford Instruments INCA X-Sight 6498 EDS system (30 mm^2 ATW2 window, Oxford Inca Suite 4.05 software). Images were taken by Gatan Model 694 Slow Scan CCD Camera. SEM and TEM analyses were conducted at TÜBİTAK-MAM Institute of Metalurgical Sciences, Laboratory of Electron Microscopies and Atomic Force Microscopy.

Elemental analysis of precursors and the prepared nanoparticles were performed by inductively coupled plasma mass spectrometry (ICP-MS, Elmer DRC II model ICP-MS, USA). The samples were prepared as dissolving particles in 2% NO_3 solution. Brunauer-Emmett-Teller specific surface area (S_{BET}) measurements were used to determine the surface area of the particles produced by using Micromeritics Gemini 2365 Automated Physisorption Analyzer (USA). Samples were degassed at 250°C for 2 h under N_2 gas atmosphere prior to the analysis. The mean particle size was determined by counting more than 500 particles and measuring from HRTEM images. To examine the crystallization behavior of prepared nanoparticles, thermogravimetric and differential thermal analyses (DTA) (Setaram Labsys, France) were performed. The temperature was programmed from room temperature to 900°C at a heating rate of 10°C/min.

2.2.3.4. Cell Culture Studies

For bioactivity and cytotoxicity studies, nanoparticles were sterilized at 200°C for 30 min. $3x10^5$ urine derived cells were seeded per well in 24-well plates in osteogenic medium. Amorphous CaP nanoparticles in DMEM were added to each well at different final concentrations of particles (5, 10, 25 and 50 μg/ml). Urine derived stem cell cultured in osteogenic medium without nanoparticles served as control. The cell viability assay was performed by PrestoBlue assay (Invitrogen, USA) at days 1, 3, 5 and 7 according to the manufacturer's guidelines. At days 7 and 14, ALP activity of cells in all groups was determined as described in detail in previous part. Four replicates were used for all groups.

CHAPTER 3

RESULTS & DISCUSSION

PART I

3.1. Scaffold Fabrication with Click Chemistry

Among click chemistry reactions as stated in the introduction part, azide-alkyne cycloaddition (AAC) was examined. We, firstly, wanted to perform copper free azide alkyne cycloaddition click reactions. However, we were not able to proceed further this reaction due to the high reactivity of the reagents. With these results in hand, copper catalyzed version was experimented. The azide and alkyne containing entities were synthesized and their addition reactions were assessed both in polymer conjugated and unconjugated molecules. The results were discussed through synthesis route.

3.1.1. Synthesis of Alkyne Containing Entities

In this thesis, copper free version of click chemistry reactions were performed as Bertozzi et al. proposed to conjugate silk fibroin and citrus pectin [128]. The reason we started with this copper free click chemistry was that copper could coordinate with many functional groups present on our biomacromolecules. The second reason was that copper is a cytotoxic element. This click reaction was driven forward with the help of the high strain on cyclooctyne. With this in mind, we started with the synthesis of 4-(cyclooct-2-yn-1-yloxy)propan-1-ol (**3)** by following the Bertozzi's work. A carbene addition reaction to cycloheptene furnished 8,8-dibromobicyclo[5.1.0]octane (**1)**. The addition product was then treated with 1,3-propanediol in the presence of silver perchlorate to yield (E)-3-((2-bromocyclooct-2-en-1-yl)oxy)propan-1-ol **(2)**. Despite many attempts to convert the monobromo specie into the alkyne product **3**, the desired product formation was not observed. (Figure 3.1). Although the tendency

of bromide is high as a leaving group in the presence of sodium hydride through E_2 reaction mechanism, we could not obtain the cycloalkyne structure.

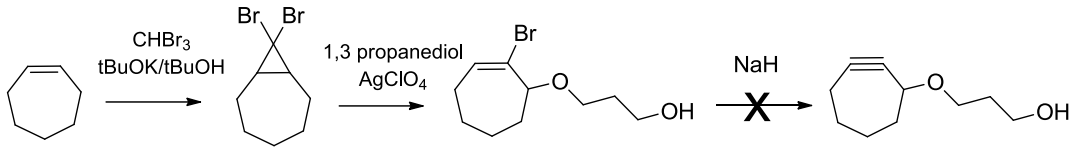

1 **2** **3**

Figure 3.1 Attempted synthesis of 4-(cyclooct-2-yn-1-yloxy)propan-1-ol (**3**) (**1**; 8,8-dibromobicyclo[5.1.0]octane, **2**; (E)-3-((2-bromocyclooct-2-en-1-yl)oxy)propan-1-ol))

In the second strategy, we conducted click chemistry reactions in the presence of copper catalyst to synthesize linear alkyne containing linker molecules and conjugate these linker molecules either on silk fibroin or citrus pectin for functionalization of these biomacromolecules. The alkyne was successfully synthesized in high yields, (83.3%) and characterized with ^{1}H NMR, ^{13}C NMR, FTIR and HRMS analyses (Appendix B Figures B.5, B.6, B.7). Due to the success of linear alkyne synthesis and ease of the procedure, we conducted click chemistry in the presence of copper. For the functionalization of this hydroxyl terminated end of alkyne containing compound, the alcohol was treated with succinic anhydride to convert hydroxyl groups into an ester resulting with one carboxylic acid group hanging at end position of the alkyne. The carboxylic acid was later used to covalently bond the alkyne to the biomacromolecules. The alcohol **4** was treated with succinic anhydride to get the carboxylic acid **5** in DMF. While characterizing **5** with the spectroscopic methods, DMF was always present in spectra due to the high boiling point of DMF. FTIR-ATR, ^{1}H NMR ^{13}C NMR and HRMS analyses were used to confirm the structure. Acetylenic specific IR peaks were apparent in the spectrum (see Appendix B. Figure B.8). Due to the low solubility of compound **5** in common NMR solvents ($CDCl_3$) we could not record ^{1}H and ^{13}C NMR spectra. With HRMS (ESI-TOF-MS) analysis the structure of compound **5** was confirmed. After characterization of 3-((3-(prop-2-ynyloxy) propoxy) carbonyl) propanoic acid (**5**), this compound was treated with both citrus pectin and silk fibroin

by carbodiimide crosslinking. (Scheme 3.2) The final conjugated biopolymers were characterized by FTIR spectroscopy.

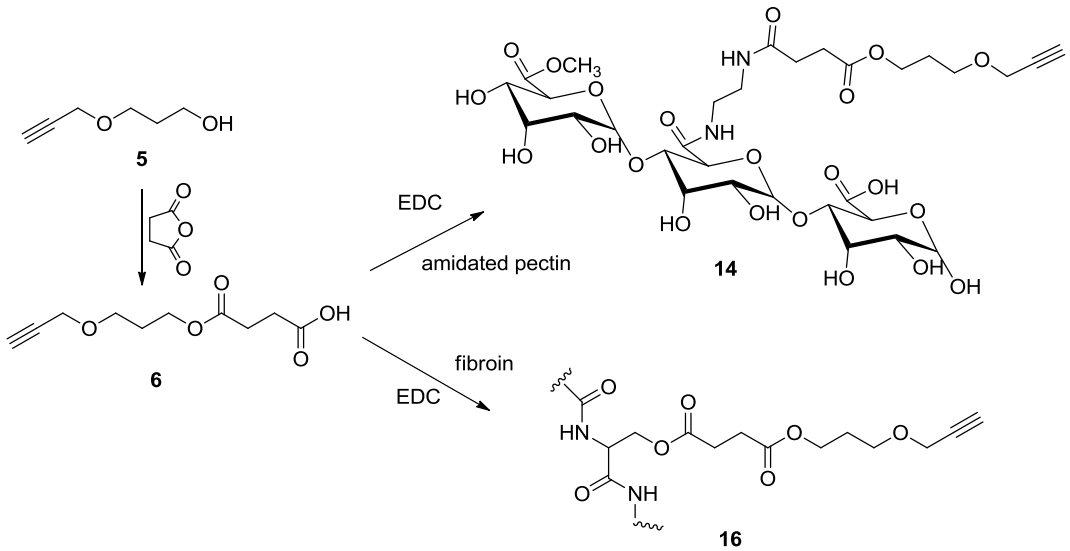

Figure 3.2 The synthesis route of alkyne containing silk fibroin and citrus pectin. (**4;** 3-(prop-2-ynyloxy) propan-1-ol **5;** 3-((3-(prop-2-nyloxy)propoxy)carbonyl) propanoic acid **14;** acetylene containing pectin **16;** acetylene containing silk fibroin

The spectral analyses of polymers verified the acetylene group ligation with the appearance of specific peaks at *circa* 2200 cm^{-1} (C≡C) and at *circa* 3300 cm^{-1} (C≡C-H) (Figure 3.3) Since single bond stretching, like O-H or N-H is generally observed at around 3500 cm^{-1} . There are numerous skeletal atoms like O-H or N-H on our polymers, the peak of C to H bond stretching on triple bond was not accurate on spectrum. Moreover, the stretching below 1500 cm^{-1} are admitted as fingerprints. The vibrations and bending of skeletal atoms mainly appear at this region of spectrum. Therefore, to characterize the ligation on polymers, especially the triple bond stretching was controlled in spectrum which appears at around 2500-2200 cm^{-1} as a weak peak. The absorption peak of triple bond on IR spectrum was less than other bond stretching. Nevertheless, we could characterize the existence of alkyne on the biopolymers with peaks around 2200 and 3300 cm^{-1} (Figure 3.3).

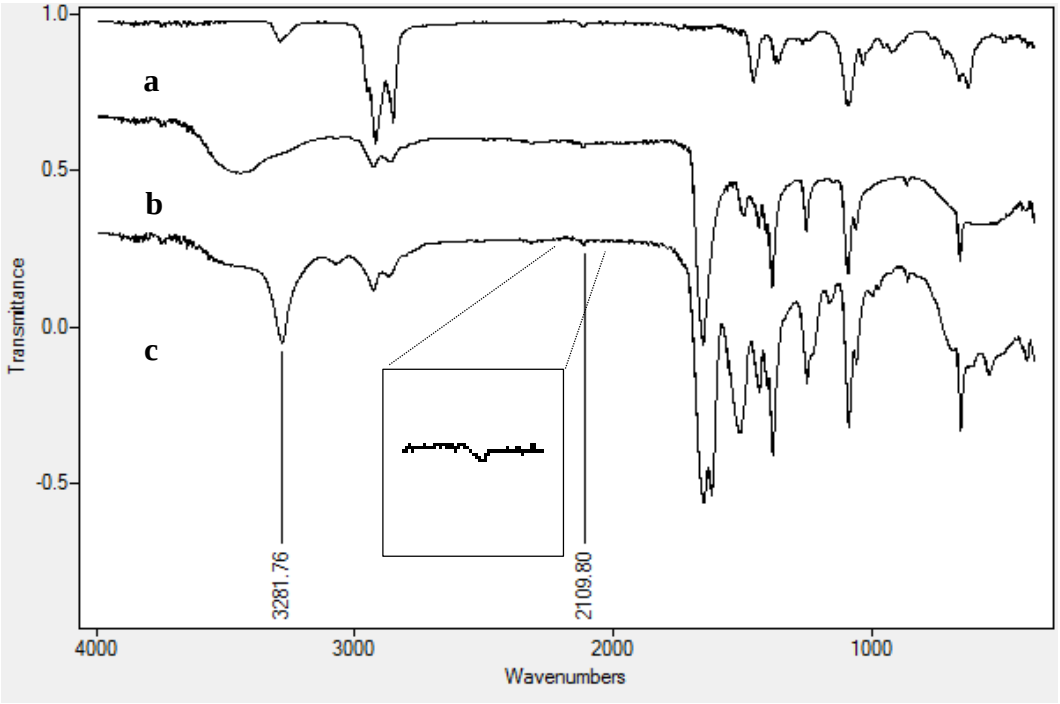

Figure 3.3 FTIR ATR spectra of (a) alkyne linker molecule, (b) alkyne conjugated pectin, (c) alkyne conjugated fibroin. The inset demonstrates alkyne specific peaks on silk fibroin spectra.

In order to increase the conjugation efficiency of linker molecules which contain click reaction entities, another method was employed; instead of carboxylic acids as a linking group, an epoxide was foreseen to be a linker. To synthesize this epoxide propargyl bromide was treated with allyl alcohol in presence of a base to yield allyl propargyl ether. Then, this ether was treated with *meta*-chloroperbenzoic acid to convert the alkyne part into an epoxide. Although a new compound formation was observed on thin layer chromatography, during the workup of the reaction an inseparable reaction mixture was obtained. Even though we repeated this reaction couple of times, we obtained same result each time. Therefore, we abandoned this route.

3.1.2. Synthesis of Azide Containing Entities

Azide containing functional groups were synthesized by a simple S_N2 reaction. The bromide atom on bromoacetic acid was substituted by an azide nucleophile. These

reactions were monitored by NMR. However, we found that the easiest way to characterize the azide containing compound was FTIR-ATR spectroscopy due to the characteristic $–N_3$ stretching frequency at *circa* 2100 cm^{-1}. Firstly, 2-azidoacetic acid (**8**) was synthesized from a reaction of sodium azide with 2-bromoacetic acid in water with the yield of 63.2%. ^1H NMR showed a single singlet peak at 3.90 ppm which corresponds to methylene protons on azido acetic acid (see Appendix B, Figure B.11). Besides ^1H NMR spectral analyses, FTIR showed a strong peak at around 2109 cm^{-1}. All modifications on azido acetic acid, *e.g* esterification, did not alter the azide structure which was also confirmed by FTIR.

As planned in alkyne group ligation to the biomacromolecules, azide containing entities were experimented to ligate on biopolymer chains. 3-hydroxypropyl 2-azidoacetate **(10),** allyl 2-azidoacetate **(11),** and azidoacetic anhydride **(9)** were synthesized as described in materials and methods part. The compound **11** was synthesized to convert later the alkene end group into an epoxide by the action of *meta*-chloroperbenzoic acid. This epoxidation reaction was monitored by TLC. After TLC showed no starting material left, the crude products were analyzed by FTIR. It was revealed that azido group was not intact. Despite many efforts to characterize the compounds resulted from this reaction, we failed to do so. The compound **10** was synthesized, however the azido group was not observed on FTIR spectrum after purification attempts by column chromatography on silica gel (SiO_2). Among synthesized azido containing linker molecules, azidoacetic anhydride was purified and characterized. Moreover, the binding mechanism of this molecule was simple compared to the other planned ones. The anhydride form of the azide entities was synthesized by treating azidoacetic acid with dicyclohexylcarbodiimide and reacted with alcohol (hydroxyl groups on sugar chain) to form an ester. This reaction is common in organic syntheses. Anhydride is the second most reactive acid derivative towards nucleophiles. It is stated that anhydrides may react with carbohydrate hydroxyls even in aqueous environment [125]. Similar reactions in living organisms, phosphate ester synthesis reactions occur. For instance, ATP molecule has similar structure with anhydride, and it binds to glucose backbone through hydroxyl groups [125]. In this reaction azido acetic anhydride dissociates and binds to hydroxyl groups

on sugar or hydroxyl groups on serine residues of fibroin (Figure 3.4). The remaining azido acetic acid can be easily removed from the reaction mixture by converting to salt form and transferring to water phase.

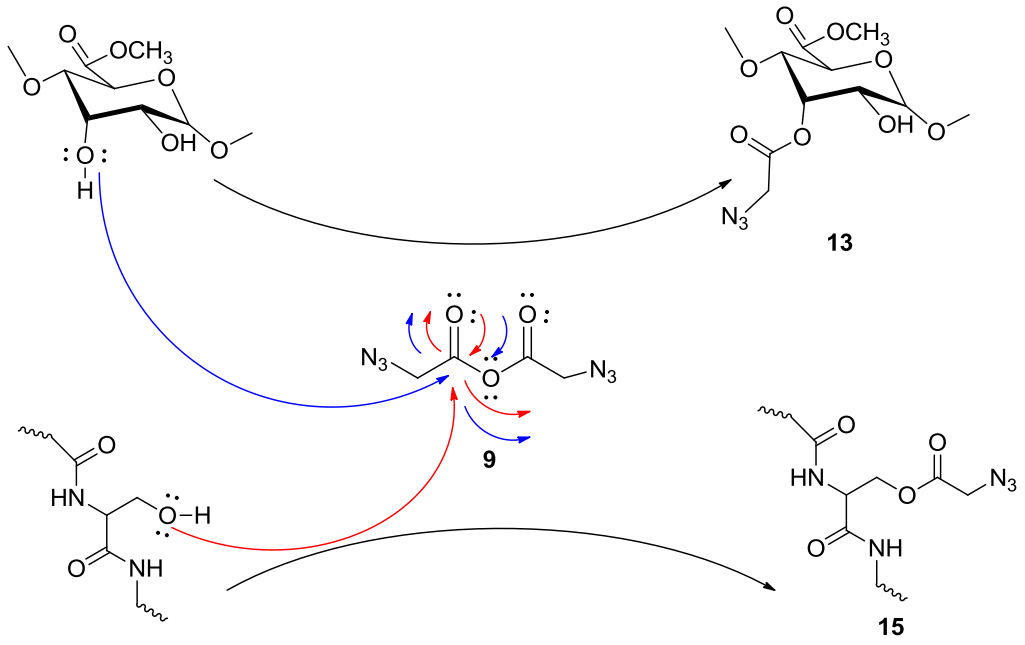

Figure 3.4 The reaction mechanism of azido acetic anhydride with silk fibroin and citrus pectin

The end products of azido group addition reactions were confirmed by FTIR ATR spectroscopy. The characteristic $-N_3$ stretching frequency at *ca* 2100 cm^{-1} (at 2114 cm^{-1}) was observed at conjugated biopolymer analyses (Figure 3.5). As stated above, the peaks below from 1500 cm^{-1} were considered as fingerprints. The peaks at around 3500 cm^{-1} were interpreted as single bond stretching as O-H or N-H vibrations. The peaks observed at around 3000 cm^{-1} were belong to C-H stretching. The location of specific peaks were identified with respect to the characteristic IR absorption list defined by University of Colorado, Chemistry and Biochemistry Department [154]. The previous studies showed similar IR profiles with our discussed bands [150,155].

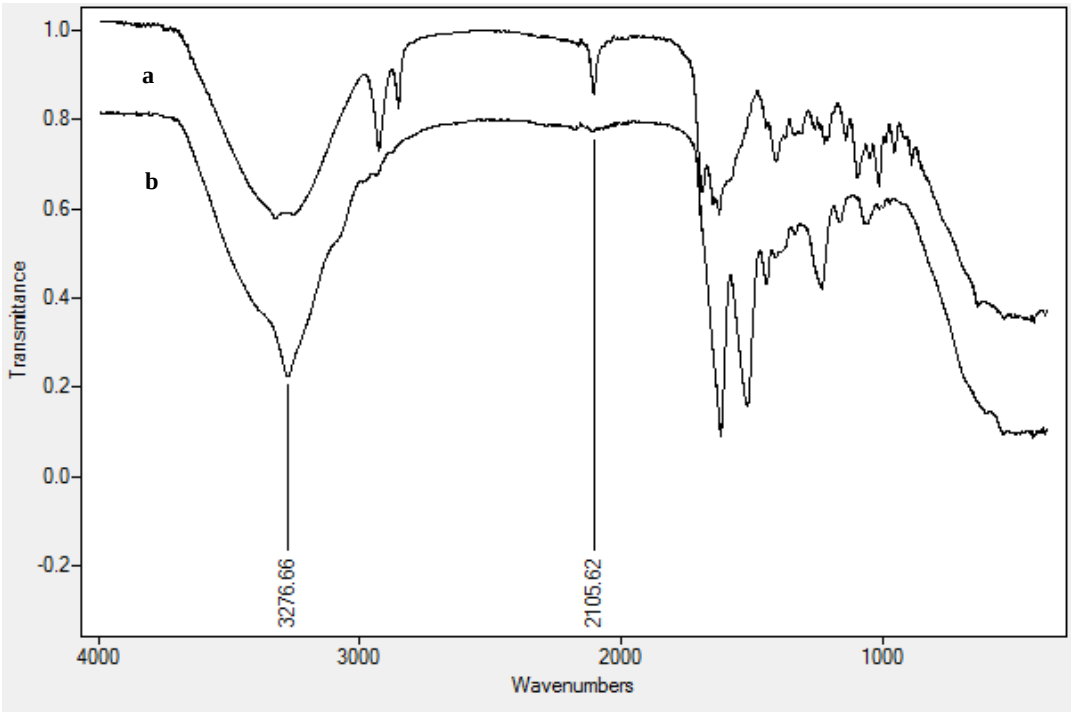

Figure 3.5 FTIR ATR spectra of azidoacetic anhydride ligated, (a) citrus pectin and (b) silk fibroin. The peak at 3276.66 cm^{-1} belongs to C-H stretching, 2105.62 cm^{-1} belongs to $-N_3$ stretching [138].

3.1.3 Copper Catalyzed Azide Alkyne Cycloaddition Models

To find the optimal conditions for copper catalyzed click reactions, azide containing compound **8** and alkyne containing compound **4** were reacted with each other in the presence of excess amounts $CuSO_4.5H_2O$ and ascorbic acid (ascorbic acid reduces Cu(II) to Cu(I), which catalyzes the 1,3-dipolar cycloaddition reactions). The mixture was stirred for 72 hours at room temperature and under N_2 gas [156]. The click reaction between linker molecules was studied by comparing the IR spectra of molecules and the mixture. The specific IR peaks at around 2200-2100 cm^{-1} which belongs to azide and alkyne characteristic bands were disappeared (Figure 3.6). This result indicates that azide and alkyne functional entities reacted with each other and formed 1,2,3 triazole ring. In literature, the characteristic 1,2,3 triazole IR absorption was stated as weak band at 3139 cm^{-1} [157]. However, this weak band was hard to observe in compounds' IR spectra. Therefore, we concluded the ligation reaction by observing

disappearance at 2200-2100 cm^{-1}. Best results were obtained when reaction mixture was left to react for 72 hours. In 24 hours, we still observed the azide and alkyne functionalities by FTIR analyses.

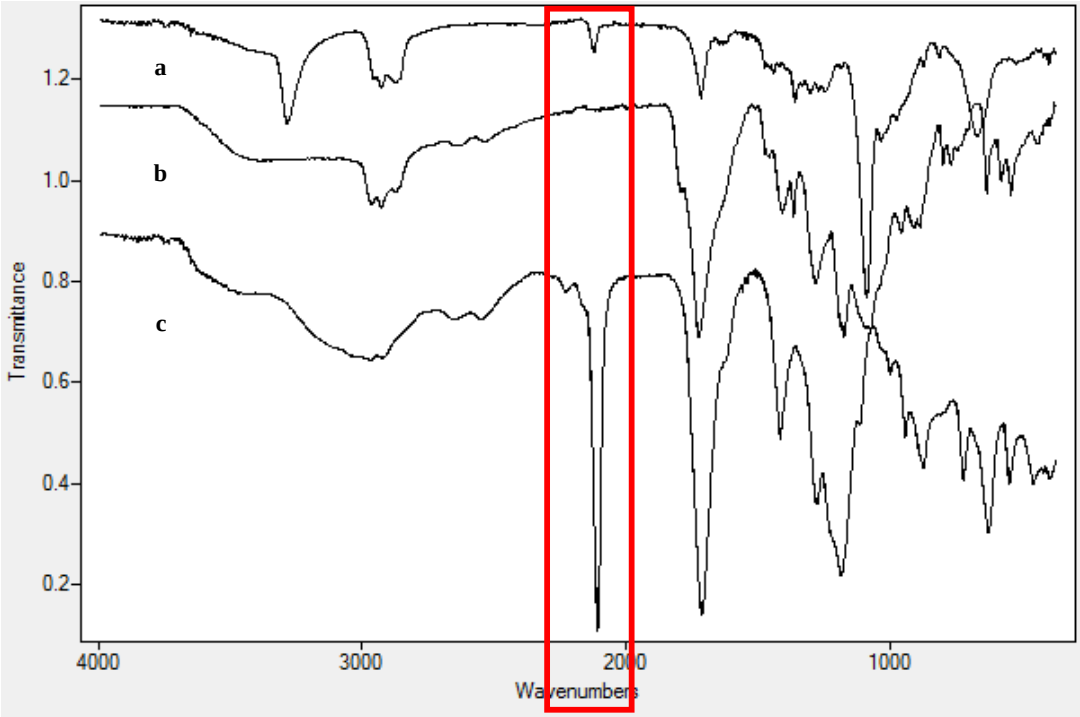

Figure 3.6 IR ATR spectra of (a) 3-(prop-2-ynyloxy)propan-1-ol; (b) product of click reaction; (c) azido acetic acid. The peak at 2200-2100 cm^{-1} (belonging to alkyne (a) and azide (c) functional entities) in spectra of the product of click reaction disappeared as shown in border (b).

After the observation that the linker molecules combined with each other via click chemistry, the linker compounds were incorporated to either hydroxyl groups on serine residues of silk fibroin or hydroxyl groups on citrus pectin chain. The click reaction was performed on the modified functional biomacromolecules as described in materials and methods section (Figure 3.7). To judge whether the click reaction occurred between linker molecules on biopolymers, IR spectra of the reaction mixture were analyzed (Figure 3.8). The analysis showed that 24 hours was not enough for

completing reaction. Therefore the reaction was extended to 72 hours for complete conversion (Figure 3.9).

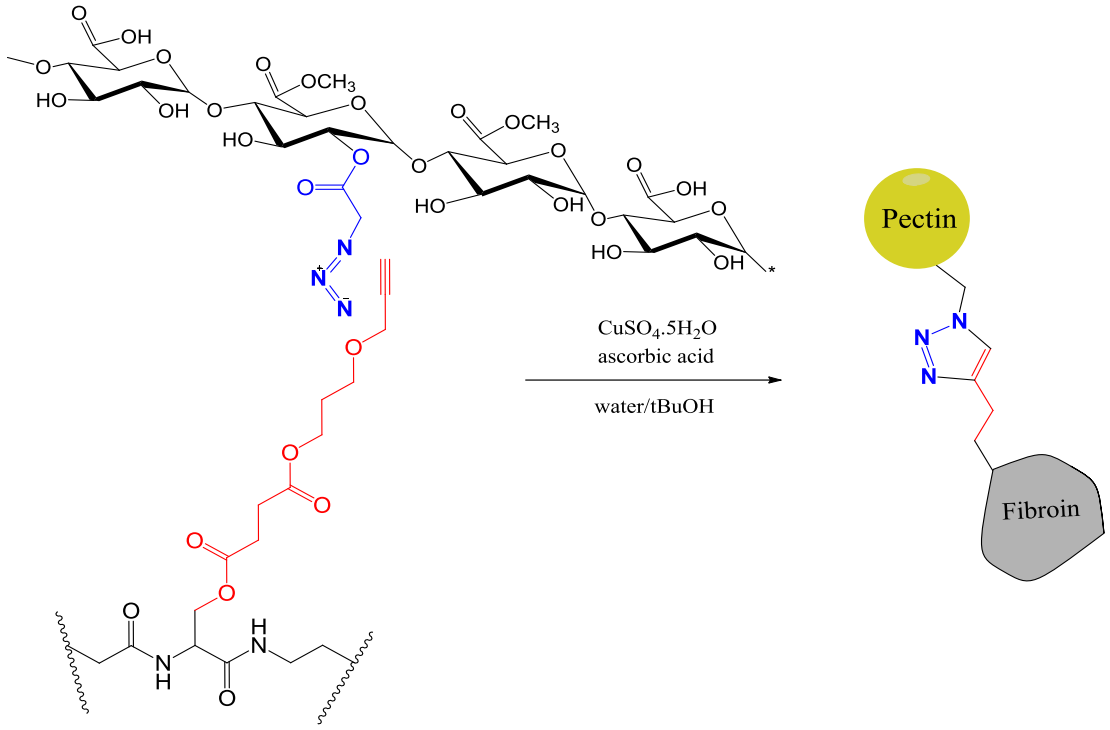

Figure 3.7 Model for click conjugation of serine residues on silk fibroin and high methoxyl citrus pectin chain

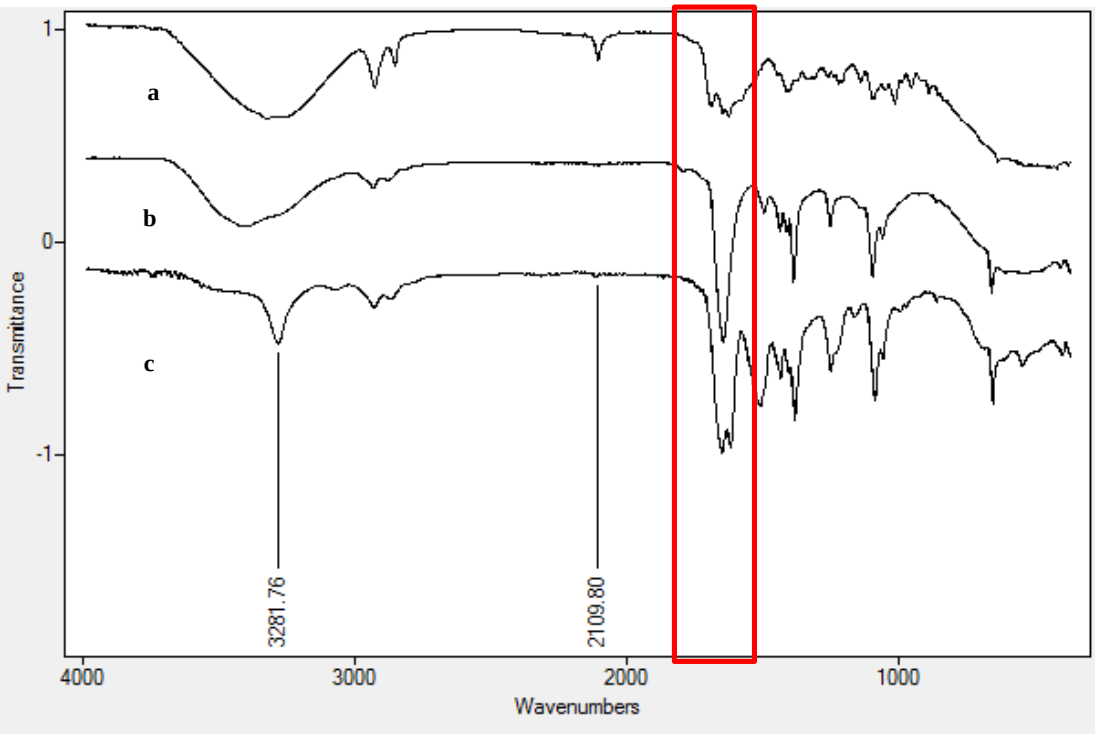

Figure 3.8 IR ATR spectra of (a) azido pectin, (b) product of click reaction, (c) acetylene terminated fibroin. The peak at 3281.76 cm^{-1} belongs to C-H stretching on both biopolymers, 2109.80 cm^{-1} comprises $-N_3$ stretching from pectin (a) and band at ~2100 cm^{-1} belongs to C≡C stretching from fibroin (c).

After characterization of silk fibroin and citrus pectin chemical conjugation, the mixture was casted in mold, frozen and vacuumed at -80°C. The methanol immersion was performed to induce conformational change from random coil to β-pleated sheets in fibroin resulting an increase in the crystallinity in the polymeric matrix of the scaffold [158]. The orthogonality of functional groups on biopolymers provides one to one interaction of reactive molecules. By virtue of their position on fibroin β-sheets, in particular, the hydroxyl groups of tyrosine and serine in silk fibroin are expected to be the most reactive toward chemical modification with reactive groups bearing alkyne or azido functional groups (Figure 3.6). Serine and tyrosine residues are found at the end groups of β-sheets [51]. Since citrus pectin has linear sugar chain, the conjugation through free end groups of silk fibroin could be accomplished. The patterned like conjugation of two polymers would be obtained.

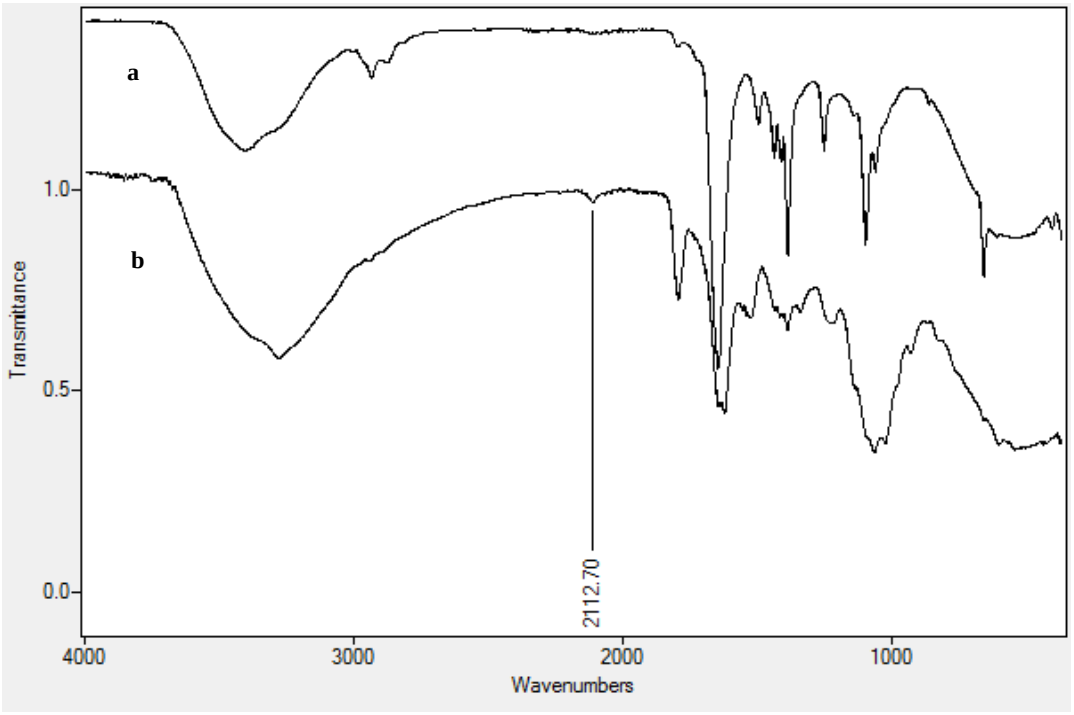

Figure 3.9 IR ATR spectra of pectin and silk fibroin clicked reaction products after (a) 72h, (b) 24h, the band at 2112.70 cm^{-1} corresponds to either alkyne or azide vibrations in mixture

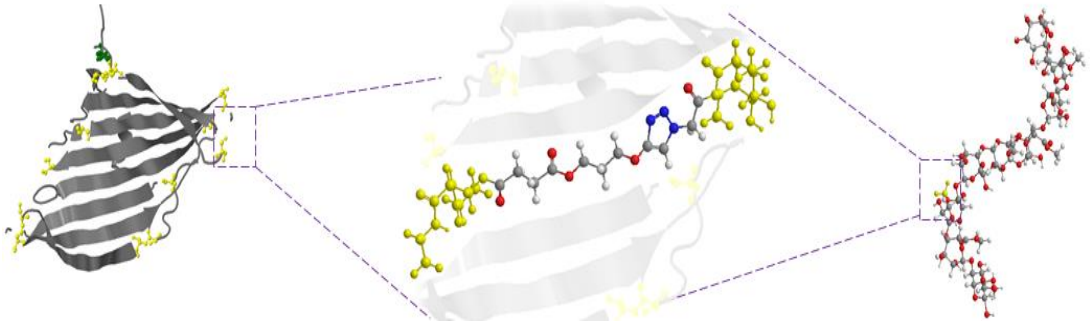

Figure 3.10 The cycloaddition conjugation model between azido-pectin and alkyne mediated silk fibroin (configured by Jmol [50])

The reaction mixture was casted in 10 cm^2 mold, frozen at -80°C and lyophilized to form porous structure. The foam was in green like color due to copper presence. To remove copper, in previous studies, foams were immersed into water for 7 days [159,160]. After lyophilization, the foam was immersed into pure methanol previous

to water immersion to induce the crystallinity of fibroin. Afterwards, foam was frozen and lyophilized to remove methanol. The foams became more fragile. When immersed into water it spliced into several pieces and dissolved in water. The scaffold fabrication will be repeated to form stable structure.

PART II.

3.2. Scaffold Fabrication with Modified Silk Fibroin and Citrus Pectin

Collateral to click chemistry reactions, silk fibroin and citrus pectin were attempted to be conjugated by already used methods as carbodiimide crosslinking (EDC) and imine (Schiff base) formation (Borax). For the efficiency of crosslinking silk fibroin and citrus pectin were modified by the addition of functional groups or creating functional groups on biopolymer chain.

3.2.1. Chemical Modification of Silk Fibroin

The primary sequence of silk fibroin provides a processability of the protein besides providing its mechanical strength via intra- and intermolecular interactions. There are several reactive amino acid residues in protein structure which can be functionalized in desired manner. In biomedical applications, silk fibroin protein has already profiled for its tunable chemical structure. The surface modification of silk fibroin based matrix systems have already been designed for tissue engineering applications [48,135,161–163].

In this thesis, silk fibroin was functionalized by treating with succinic anhydride in order to increase the carbodiimide crosslinking efficiency. By this modification free hydroxyl groups from serine (12.2 mol%) and tyrosine (0.2 mol%) and even free primary amine groups from lysine (0.2 mol%) residues were converted into esters by nucleophilic addition of succinic anhydride with one carboxylic acid group at the end [48]. In the case of excess succinic anhydride presence in reaction, lysine residues tend to form an ester bond [149]. This added carboxylic acid was used to covalently bond silk fibroin to amine group containing citrus pectin (*vice supra*) via EDC/NHS carbodiimide coupling. This reaction was confirmed by FTIR spectroscopy (Figure 3.11). In discretely different from the unmodified silk fibroin spectrum (N-H stretching at 3269 cm^{-1}, amide I (C=O) stretching at 1621 cm^{-1}, and amide II (N-H) stretching at 1525 cm^{-1}), additional peaks at *circa* 3445 cm^{-1} (O-H stretching), 1651 cm^{-1} (C-H bending from added chain length) and 1414 cm^{-1} (C=O stretching from added carboxylic acids) were observed proving the succinic acid ligation to fibroin chain.

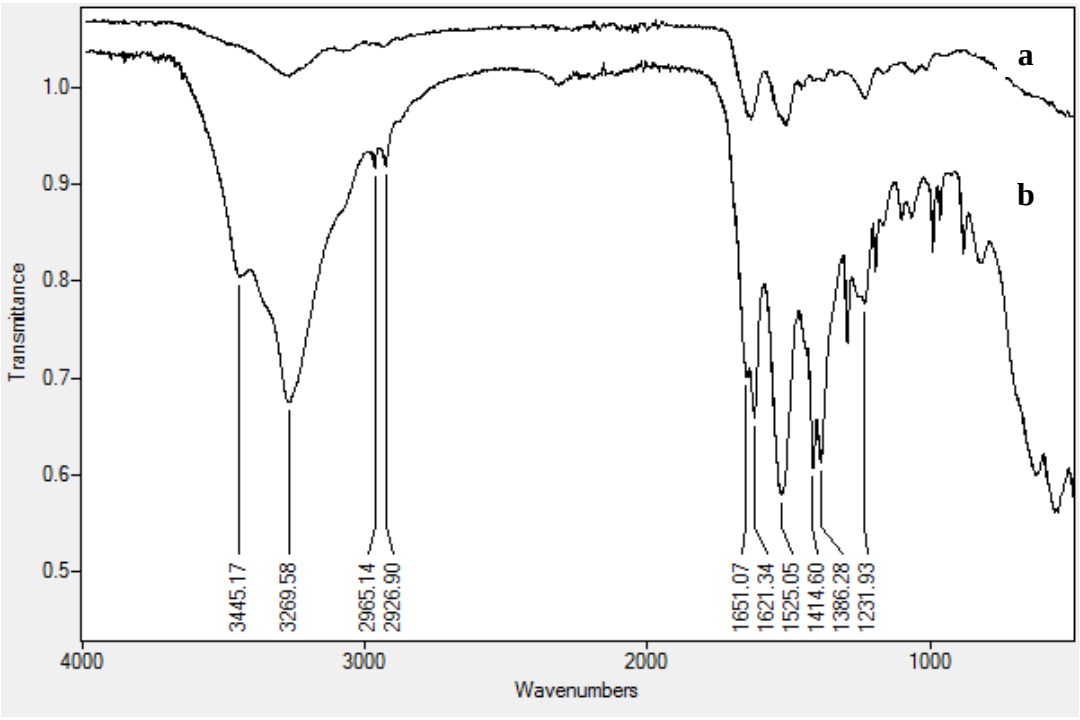

Figure 3.11 IR spectra of (a) unmodified fibroin, (b) acylated fibroin. The stretching at 1621 and 1525 cm^{-1} are amide I and amide II bonds, specifically. The shoulder at 1651cm^{-1} and broad peak at 3445 cm^{-1} shows carboxyl group addition

In case for silk fibroin EDC coupling crosslinking, self-crosslinking of protein presents a challenge. Silk fibroin contains 0.5 mol% aspartic acid, 0.6 mol% glutamic acid and 0.2 mol% lysine residues in its structure [48]. Aspartic acid and glutamic acid hold reactive carboxylic acid end groups and lysine includes free amine group. These residues may covalently bind and hinder other reactive amino acids in protein structure and cause protein aggregates. By this further chemical modification of silk fibroin, we aimed to prevent self-crosslinking of protein in EDC presence.

3.2.2. Chemical Modification of Citrus Pectin

Polysaccharides are naturally synthesized in metabolic pathways of living organisms and they undergo further biosynthetic modifications. Their structure is so convenient for modifications. Therefore, they have huge application areas in biotechnology. Citrus pectin is one of the polysaccharides that can be easily manipulated like alginate, pullulan, dextran, and chitosan [164].

3.2.2.1. Amidation of Citrus Pectin

The highly methylated citrus pectin chain enhances chemical modifications by providing an attack site on methyl ester groups [165–167]. Previously, amidation of citrus pectin were conducted by reacting with hydrazines, hydroxamic acids, ammonia in methanol and alkylamines [165,166]. In this thesis, we employed amidation of citrus pectin by reacting with ethylenediamine (alkylamines). FTIR spectra was analyzed to confirm the primary amine addition to citrus pectin (Figure 3.12). In analysis, appearance of the amide I (C=O) and amide II (N-H) stretching in spectrum at 1603 cm^{-1} and 1505 cm^{-1} respectively showed that primary amine addition was succeeded. C=O vibration from either methyl ester or free carboxyl acids at around 1731 cm^{-1} was clearly observed in unmodified pectin spectrum. In amidated pectin spectrum this vibration was observed as shoulder at around 1700 cm^{-1}. The conversion into amidated form lowered the carbonyl frequency because of strong sharp peak of amide I. The peaks in amidated pectin spectrum at around 2930-2850 cm^{-1} were interpreted as methylene vibrations by covalent binding of ethylenediamine to citrus pectin chain.

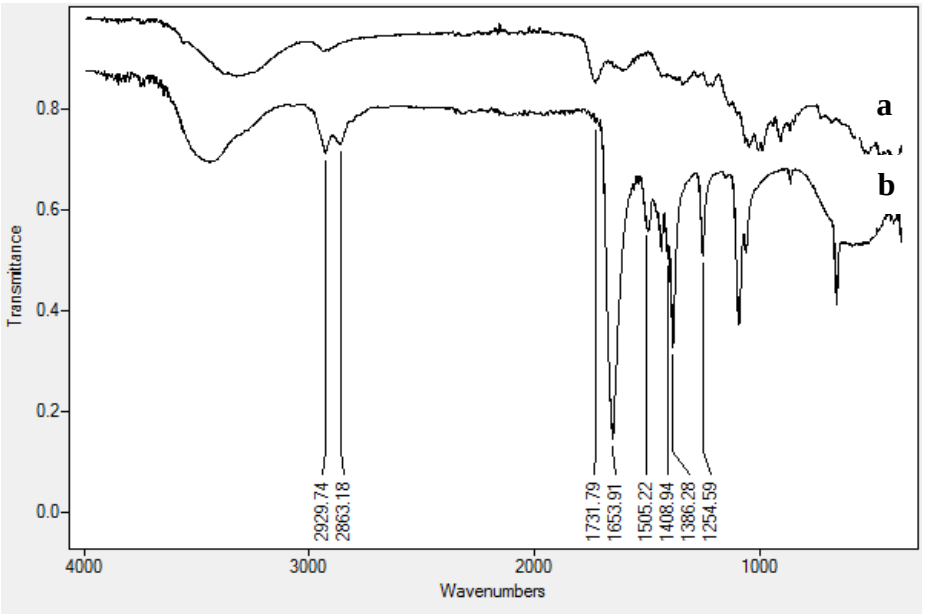

Figure 3.12 IR spectra of (a) unmodified citrus pectin, (b) amidated citrus pectin. The stretchings at 1653 and 1505 cm^{-1} are amide I and amide II bonds, specifically. The band at 1731 cm^{-1} belongs to ester bond vibrations, this band disappeared in modified pectin and amide characteristic band was observed.

3.2.2.2. Oxidation of Citrus Pectin

In native structure of proteins, amino acids, oligonucleotides or polysaccharides, aldehyde group is not found [125]. Introducing a reactive aldehyde group on biomacromolecules provides an opportunity to selectively modify biopolymer structure through these residues in specific locations. Aldehyde groups can be generated within biopolymers by periodate oxidation. In this thesis, we oxidized citrus pectin in order to introduce aldehyde groups on hydroxyl groups of carbons 2 and 3 of the sugar backbone. These aldehydes were formed to ligate with primary amines either on amidated pectin or silk fibroin. The oxidation of citrus pectin was confirmed by colorimetric measurements and FTIR analysis. The aldehyde content of oxidized pectin was determined by reacting oxidized sample with DNPH solution (as stated in Materials and Methods section). The aldehyde amount was defined as 3.05 mmol/g of pectin. It is reported that the full aldehyde formation was impossible since the neighboring hydroxyl groups donate proton atom to aldehyde structure and forms

hemiacetals [150]. The obtained aldehyde amount was in correlation with literature and found 3.25 mmol/g in the same conditions [150].

The FTIR spectra of neat citrus pectin and oxidized pectin are given in Figure 3.9. The native citrus pectin specific methyl ester or free carboxylic acid C=O stretching was observed at around 1730 cm^{-1}. It is reported that the aldehyde specific vibration was observed in 1732-1734 cm^{-1} range in oxidized pectin [150]. In our FTIR results, the broad signal appeared at 1733 cm^{-1}. This was interpreted as aldehyde specific signal. It was also reported that the free COO^- groups were assigned at around 1614 cm^{-1}. In our data this vibration was observed at 1600 cm^{-1}. After oxidation, the specific peak intensity increased in the spectrum.

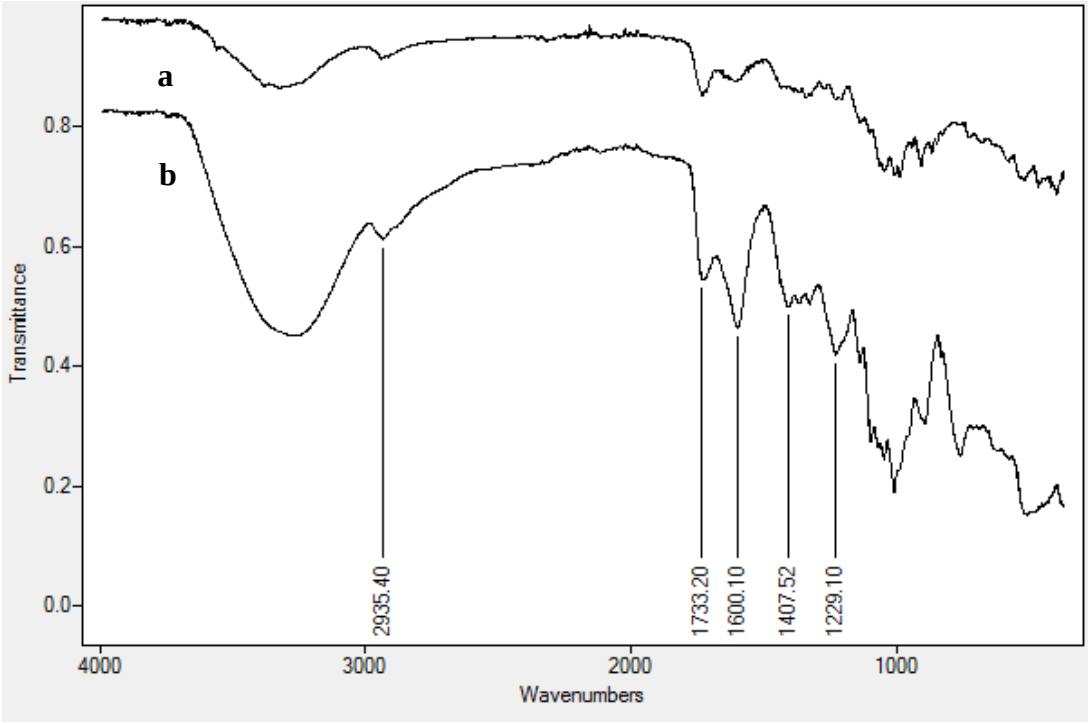

Figure 3.13 IR spectra of (a) unmodified citrus pectin, (b) oxidized pectin. The intensity at 1733 cm^{-1} increased in oxidized pectin by the increase of C=O stretching from aldehyde group.

3.2.3. Characterization of Citrus Pectin and Silk Fibroin based 3D Scaffolds

After crosslinking reactions with EDC and Borax, the 3D and porous structures of fibroin and pectin based scaffolds were prepared by casting and freeze-drying. The properties of scaffolds were examined.

3.2.3.1. Fourier Transform Infrared Spectroscopy Attenuated Total Reflectance (FTIR-ATR) Analyses

This tool is used to define the functional groups by specific vibrations in infrared radiation. We used this method to interpret the crosslinking efficiency of scaffolds. The IR spectra of cross-linked scaffolds were examined and results were discussed. Each crosslinking agent (EDC or borax) is separately discussed as stated in Materials and Methods section.

In EDC mediated crosslinking, covalent amide bond was planned to be formed between carboxyl groups (COOH) of silk fibroin and amine groups (NH_2) of amidated citrus pectin. To improve the efficiency of this reaction, acylation of fibroin (introducing new COOH groups) and amidation of pectin (introducing NH_2 groups) were performed. To compare the carbodiimide crosslinking efficiency of scaffolds with modified polymers, the reaction was conducted with control groups as given at Materials and Methods section (Table 2.1). Since carbodiimide reaction also occurs between carboxyl and hydroxyl groups and forms ester bonds, unmodified silk fibroin (carboxyl groups of aspartic and glutamic acid; 1.2% (mol)) and citrus pectin (hydroxyl groups on carbon 2 and 3) were also considered. After crosslinking, the amide bond specific vibration peaks; C=O and N-H stretching were expected to appear in spectrum. We observed amide I and amide II bonds in wavenumbers at around 1624 and 1549 cm^{-1} since silk fibroin protein contains numerous amide bonds in its primary structure (Figure 3.14). Therefore, the crosslinking efficiency was only assessed from degradation test results.

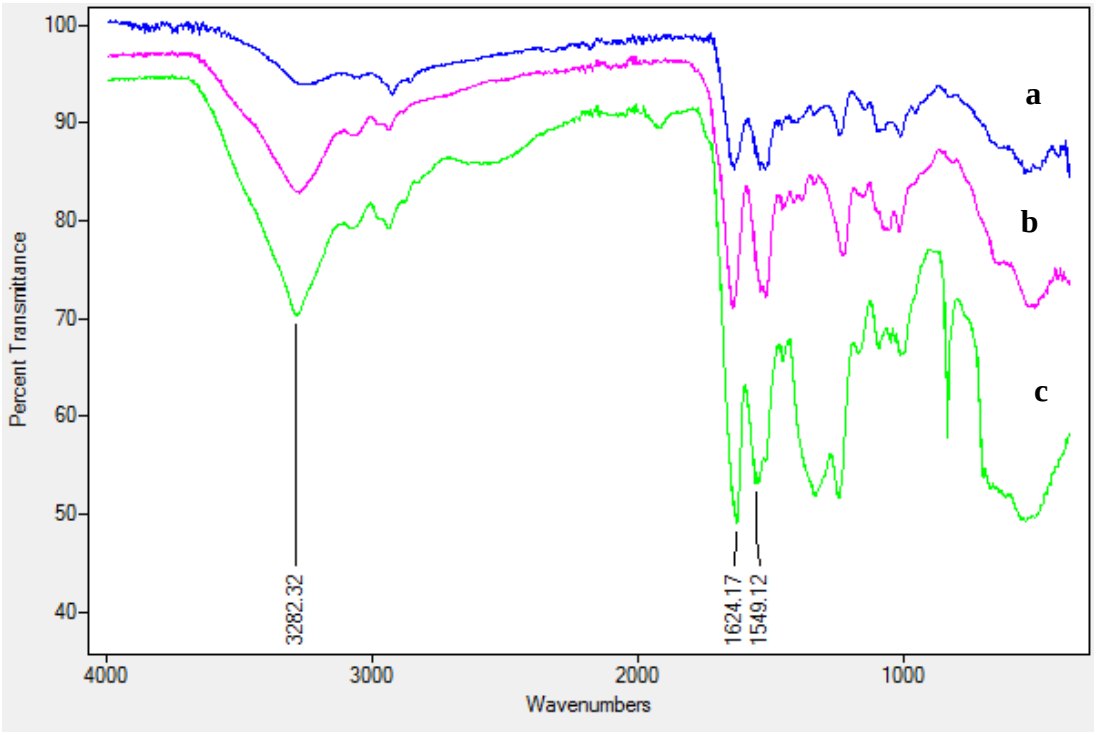

Figure 3.14 IR spectra of EDC mediated crosslinked (a) SF:PEC, (b) SF:A-PEC, (c) A-SF:A-PEC. The broad band at 3282.32 cm^{-1} belongs to O-H stretching, the sharp peaks at 1624 and 1549 cm^{-1} belong to amide I and amide II bonds.

In borax mediated crosslinking, the covalent bond formed after crosslinking was an imine (C=N) bond between aldehyde groups of oxidized pectin (COHR) and primary amines of amidated pectin and silk fibroin (NH_2) in the presence of borax. Borax (sodium tetraborate) consists of four coordinated boron atoms (BO_3 triangles). The electronegativity of oxygen atoms on tetraborate structure causes withdrawal of proton atoms of the primary amines in amidated pectin and fibroin. The free electrons on nitrogen atom attacks to aldehyde group on oxidized pectin and an imine bond forms.

Since imine is not an irreversible covalent bond, there is a risk of hydrolysis in acidic environment. Borax keeps the medium alkaline and supports the covalent bond. On the other hand, alkaline pH might cause breakage of peptide bonds. Although tertiary structure of silk fibroin limits peptide bond damage in acidic environment by folding, the peptide bonds on amidated pectin and some of peptide bonds on fibroin chain are prone to damage by pH rise in the presence of borax. Therefore, to define optimum

reactive concentration of borax, we employed different concentrations of borax from 0.005 M to 0.05 M as final concentration in the polymer solution. Preliminary studies were also conducted with borax with 0.1 M as final concentration. The foam split into pieces which could be due to degradation of the polymers due to elevated pH in the presence of 0.1 M borax concentration. The FTIR spectra revealed that with decreasing Borax concentration ratio, the amide specific bands were observed. This means decreasing borax concentration decreased the hydrolysis of peptide bond**.**

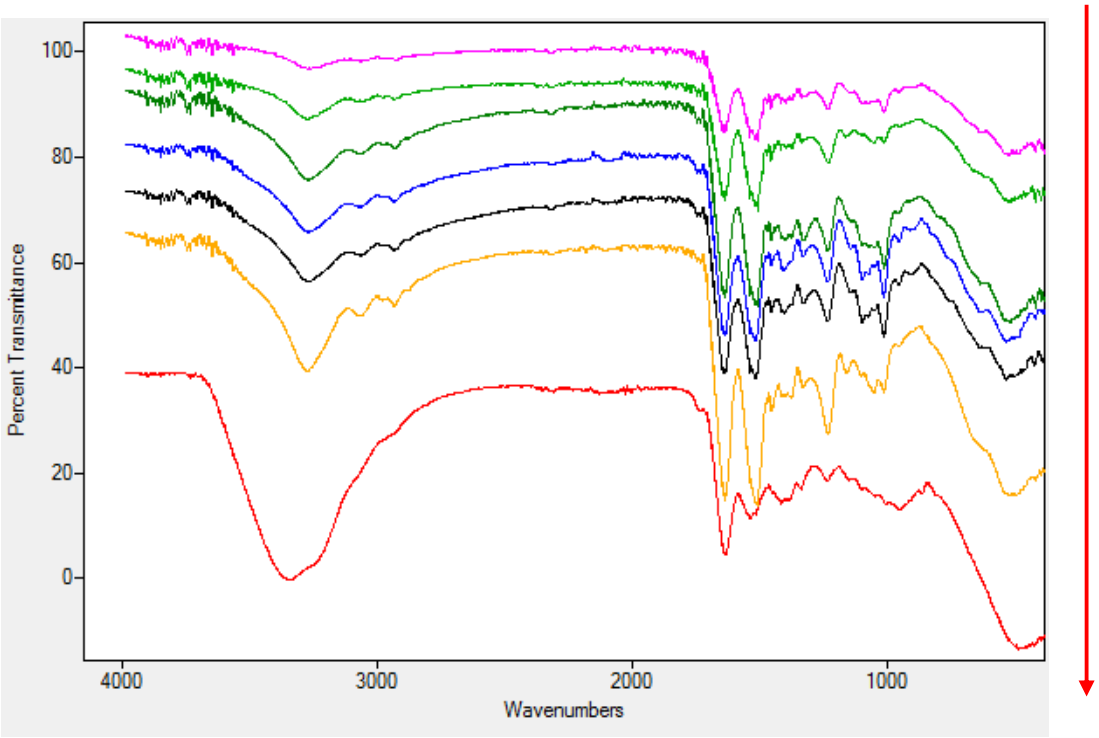

Figure 3.15 IR spectra of borax mediated crosslinked SF: O-PEC: A-PEC scaffolds the borax concentration increases from top to bottom. The red colored spectrum belongs to scaffolds crosslinked with 0.1M borax concentration.

3.2.3.2. Degradation and Water Uptake Profiles

For both crosslinking studies, both polymers were prepared at 4% (w/v) final concentration and they were blended at different volume ratios of 3:1, 2:1 and 1:1 (SF to PEC). In scaffolds prepared by blending SF to PEC ratios of 2:1 and 1:1, citrus pectin tended to dissolve in water resulting with collapse of the scaffolds. Silk fibroin

has a crystalline structure which makes it insoluble in aqueous media and has good mechanical properties [51].

In carbodiimide crosslinking analysis, EDC and NHS amounts were defined as 20% and 10% weight ratios of final polymer amount [130,168]. The working concentration of EDC was 0.25 M. The pH of solution was lowered to 6 to increase the efficiency of EDC. Although it is written in manufacturer's guidelines that lower pH (pH 4.5) would be better for efficiency, this pH resulted with inhomogeneous gelation. So we decided to work with pH 6. The blend was allowed to react for 2 hours at room temperature and it was then frozen at -20^{o}C. The gelation of the reaction mixture was not observed in these crosslinking experiments. After initial lyophilization, foams were immersed into pure methanol or 0.1 mM $CaCl_2$ in methanol. Methanol immersion of silk fibroin changes the physicochemical properties of protein. The studies revealed that in methanol the β-sheets of silk fibroin is induced and crystallinity of protein increases [158]. Calcium ions have a crosslinking effect on polysaccharides by ionic binding to sugar backbone. The calcium crosslinking of citrus pectin was previously studied and hydrogels were produced [61,169,170]. As a result of this immersion step, foams became more fragile and they were split out into parts when incubated in PBS. Therefore, we decided to add further immersion step to scaffolds in methanol: water mixture (1:1). In this treatment, water diffuses into sponge and hydrates the attached fibroin and pectin chains in methanol and provides a flexibility to polymers. This treatment maintained the matrix structure of foams. The degradation profile of foams changed.

The degradation and water uptake ability of scaffolds are crucial features to assess the biomaterial properties of scaffolds for tissue engineering applications [171]. To examine the degradation profile of scaffolds in physiological hydrolysis reaction, samples were incubated in PBS at 37^{o}C and their weight loss was measured at 1st and 7th days. Among EDC crosslinked scaffolds, there was a notable difference in weight loss values between physical crosslinking employed and unemployed scaffolds (Table 3.1). The physical crosslinking employed samples showed lower weight loss values than unemployed samples except group involving unmodified polymers. This higher weight loss might have resulted because of inefficient crosslinking between unmodified polymers. For the scaffolds containing silk fibroin (SF) and pectin (PEC),

some of unbound pectin and fibroin might have left the structure while in methanol+$CaCl_2$ solution. The degradation results at day 1, methanol+$CaCl_2$ solution treatment employed SF:PEC based scaffolds showed weight loss as 53.36±8.32%. The acylated fibroin (A-SF) and amidated pectin (A-PEC) based scaffolds showed lower weight loss (27.92±3.24%) after physical crosslinking step than unemployed scaffolds (65.93±7.33%). The acylated fibroin was highly viscous, therefore the risk of inhomogeneous mixing might be the reason that a lower crosslinking was observed. Among all experimental groups, for 1st and 7th day results the best results were observed in silk fibroin (SF) and amidated pectin (A-PEC) based foams. The methanol and $CaCl_2$ immersion resulted with slight difference in loss values. For all groups, there was numerical difference between day 1 and day 7 weight loss. However, between experimental groups, there was statistically significant difference ($p<0.05$).

The working volume ratio was 3:1 for EDC crosslinking, so 25% of final sample consists of pectin residues. Therefore, weight loss values can be interpreted as unbound pectin chains in PBS. Both day 1 and day 7 weight loss values of SF:A-PEC based scaffolds were lower than 25% (Day 1 20.80± 4.35, 19.70±2.39; Day 7 23.38± 0.64, 24.58± 2.48). We can conclude that silk fibroin (SF) and amidated citrus pectin (A-PEC) based scaffolds constitutes more pectin chain in matrix.

Table 3.1 The weight loss values of EDC crosslinked scaffolds at 1st and 7th days in incubation media (0.1 M PBS)

Groups	Weight loss (%) (day1)	Cum. Weight loss (%) (day 7)
SF:PEC	43.32±6.34	48.53±3.10
SF:PEC (MeOH+$CaCl_2$/MeOH:H_2O)	53.36±8.32	55.92±5.44
SF:A-PEC	20.80±4.35	23.38±0.64
SF:A-PEC (MeOH+$CaCl_2$/MeOH:H_2O)	19.70±2.39	24.58±2.48
A-SF:A-PEC	65.93±7.33	69.52±6.88
A-SF:A-PEC (MeOH+$CaCl_2$/MeOH:H_2O)	27.92±3.24	29.80±5.57

In Schiff base formation reactions, borax concentration was the crucial for crosslinking efficiency. The imine bond is prone to hydrolysis into aldehyde in excess water presence. In order to determine ideal borax concentration for crosslinking, the effect of different concentration on crosslinking and their behavior in PBS were studied (Table 3.2). Scaffolds were frozen and lyophilized after borax mediated gelation. As employed to EDC crosslinked scaffolds, the foams were immersed into 0.1 mM $CaCl_2$ in methanol for 30 minutes and further immersed into methanol: water (1:1) solution for 30 minutes. As an alternative to this crosslinking process, for one borax concentration (0.015 M), $CaCl_2$ was mixed with fibroin solution prior to borax addition. They gelled in few minutes after stirring. The degradation test was executed in PBS. After one day of incubation, physical crosslinking unemployed samples fully degraded. Table 3.2 lists physical crosslinking procedure employed on scaffolds.

Table 3.2 The weight loss values of borax crosslinked scaffolds at 1st and 7th days in incubation media (0.1 M PBS)

Borax Concentration (in terms of molarity)	**Weight loss (%) DAY 1**	**Cum. Weight loss (%) DAY 7**
0.005 M	21.83±3.14	26.66±6.95
0.01 M	20.72±2.27	24.63±1.33
0.015 M	28.88±3.43	38.23±3.33
0.02 M	17.37±3.69	19.76±3.06
0.025 M	13.19±2.01	14.55±1.66
0.05 M	14.08±2.54	38.52±8.66
0.1 M	32.16±4.54	-
0.015 M (pregelation)	11.35±2.12	15.45±1.02

Among 1st day incubation results, in higher borax containing samples (>0.015 M), except 0.1 M borax containing samples, there was acceptable weight loss. However, among the lower loss results, the lowest was observed for scaffolds crosslinked with 0.025 M borax (13.19±2.01%). Among all groups, the pregelation employed scaffolds displayed lowest weight loss value (11.35±2.12%). In 7th day of incubation, the profile changed slightly. As an exception, the samples containing 0.05 M borax gave higher weight loss value. The scaffolds crosslinked with 0.02 M and 0.025 M borax concentration, and pregelation performed scaffolds (0.015 M) resulted with lowest weight loss value and there was numerical difference between day points ($p<0.05$). Among all groups, there was numerical differences between day 1 and day 7 results.

In comparison of EDC and borax crosslinked scaffolds degradation profile, for 1 day incubation, scaffolds crosslinked with borax displayed lower weight loss percentage than EDC crosslinked scaffolds. The rapid gelation of reaction mixture in borax presence provided dimensional stability to scaffolds and resulted with lower weight loss values. In literature, similar to our study, silk fibroin and chitosan based scaffolds

were blended in 2:1 ratio (SF:Chitosan, 2:1) and crosslinked with glutaraldehyde then fabricated as three dimensional porous scaffolds [172]. The degradation profile of scaffolds was studied both enzymatically and hydrolytically. The hydrolytic degradation assay showed that samples with highest silk fibroin amount (2:1, SF:Chitosan) had lower weight loss values (10-15%) at day 7 since silk fibroin has low hydrophilicity. Chitosan amount increase resulted with increase in weight loss of scaffolds. However, in this study, chitosan was incorporated into silk fibroin in order to overcome the low hydrophilicity and small pore structure of silk fibroin based scaffolds.

Swelling behavior and structural stability determine the biocompatible properties of scaffolds and evaluate the possible practical use in tissue engineering. The water uptake ability of scaffolds reflects the hydrophilic property of materials. Increase in hydrophilicity increases the water absorption property [173]. Generally polysaccharides are incorporated into protein or synthetic polymer based scaffolds in order to increase swelling pressure of scaffolds to draw water in matrix and to modulate the pore structure of scaffolds [174–176]. However, swelling behavior influences the dimensional maintenance of scaffolds and therefore microenvironment of cells [177]. Moreover, swelling profile of scaffolds depends on the pH of environment where they implanted [173]. The swelling behavior of fabricated scaffolds was studied by examining water uptake ratio and pH of incubation medium (Table 3.3).

Table 3.3 The pH change and water uptake (%) values of EDC crosslinked scaffolds after 1 and 7 days incubation in PBS (0.1 M, pH 7.4) (n=3)

Groups	Water uptake (%) day1	pH	Water uptake (%) day 7	pH
SF:PEC	403.24±28.97	6.60	351.18± 48.34	7.39
SF:PEC (MeOH+$CaCl_2$/ MeOH:H_2O)	931.09± 35.44	6.77	670.51± 82.05	7.59
SF:A-PEC	470.80± 29.37	6.88	576.12± 50.32	7.43
SF:A-PEC (MeOH+$CaCl_2$/ MeOH:H_2O)	694.09± 26.93	6.84	1025.60±97.56	7.49
A-SF:A-PEC	279.12±23.65	9.11	911.37± 24.55	7.78
A-SF:A-PEC (MeOH+$CaCl_2$/ MeOH:H_2O)	798.48± 38.03	7.45	978.61± 63.52	7.5

After 1 day incubation, the decrease was observed in pH of PBS except acylated fibroin and amidated pectin based scaffolds (A-SF:A-PEC). Pectin solution has pH value range 3-4 [178]. Thus the pH decrease of experimental groups confirmed the pectin (anionic polysaccharide) loss from matrix. The pH of acylated fibroin and amidated pectin based scaffolds were high since acylated fibroin solution pH was kept at around 8 and the incorporated primary amine groups on polymer chains of pectin and fibroin are Lewis bases, they increased the pH of PBS with their release. At day 7 the pH values were recorded closer to incubation medium (pH 7.4).

The water uptake profile of scaffolds crosslinked with EDC, showed significant differences between methanol and $CaCl_2$ employed and unemployed samples. In comparison, A-SF:A-PEC blended scaffolds has lowest water uptake value among day

1 results (279.12±23.65%). These scaffolds showed higher weight loss (65.93±7.33%), lower water uptake percentage. The water penetration to the matrix led to relaxation of fibroin and pectin polymers, in case of low level crosslinking, this relaxation resulted with degradation of scaffolds. Especially the removal of pectin which is one of the hydrophilic polysaccharides resulted with decrease in water absorption capacity. The results correlated with each other. The scaffolds with lower weight loss values showed higher water uptake percentage (Figure 3.16). It shows that hydrophilic polymers were retained in polymeric matrix of scaffolds and adsorbed water. Among EDC crosslinked scaffolds, pectin was retained higher in methanol and $CaCl_2$ treatment employed SF:A-PEC based scaffolds.

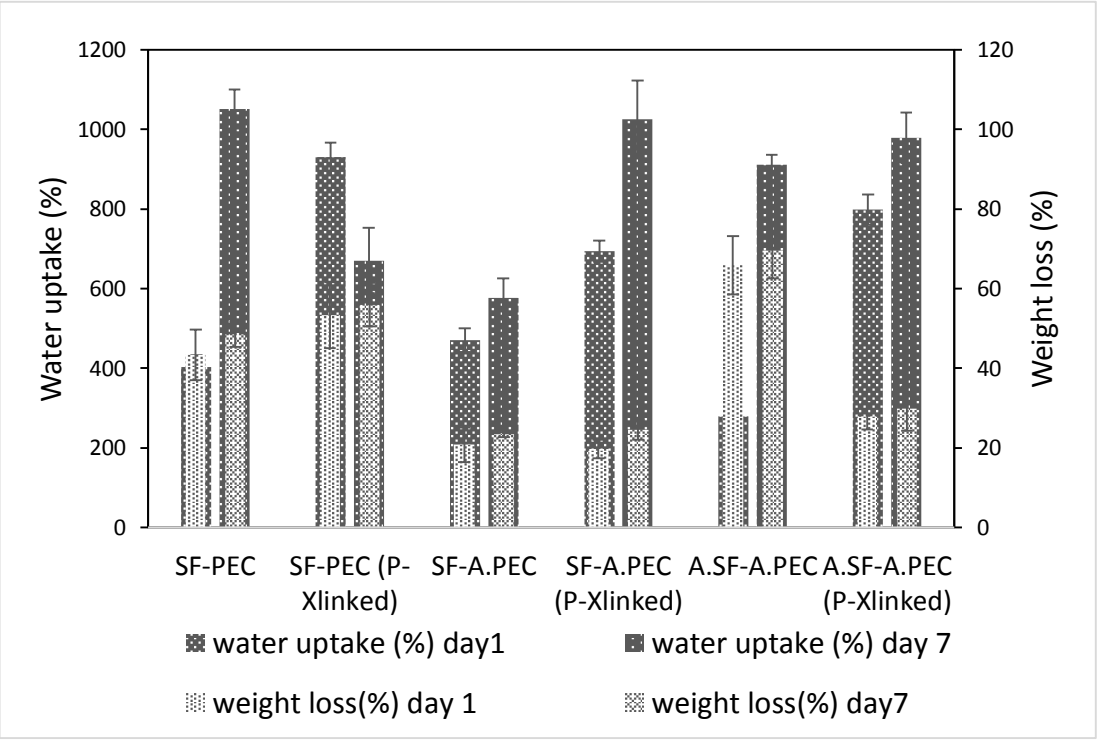

Figure 3.16 The comparison of water uptake (%) and weight loss (%) values of scaffolds crosslinked with EDC.

Unlike from carbodiimide crosslinking, the gelation tendency was higher in borax crosslinked scaffolds. However the gelation profile differed among concentration

groups. With increasing amount of borax in reaction mixture, the gelation time decreased. The gelation process enhances the water retention in structure, the final hydrogel form reaches to equilibrium level of swelling [179]. The water uptake profile and degradation of scaffolds examined Table 3.4.

Table 3.4 The pH change, water uptake (%) values and gelation profile of borax mediated crosslinked scaffolds (SF:O-PEC: A-PEC) (physical crosslinking employed) after 1 and 7 days incubation in PBS (0.1 M, pH 7.4) (n=3)

Borax Conc. (in terms of molarity)	**pH**	**Water uptake day 1 (%)**	**Gelation**	**pH**	**Water uptake day 7 (%)**
0.005 M	7.53	657.04±33.68	Low	7.59	1044.35±24.83
0.01 M	7.63	606.76±18.65	Low	7.51	1050.83± 37.98
0.015 M	7.69	470.14±14.82	Moderate	7.56	441.93±15.48
0.02 M	7.56	597.37±21.95	Moderate	7.5	767.36± 26.95
0.025 M	7.93	601.18±28.62	Moderate	7.53	691.53± 30.54
0.05 M	7 46	718.41±27.55	High	7.48	557.03± 37.03
0.1 M	8.65	785.70±24.53	High	-	-
0.015 M (pregelation)	7.60	586.96±23.65	High	7.49	819.12± 25.68

When the water uptake profiles of scaffolds crosslinked with borax were examined, it was observed that scaffolds crosslinked with 0.015M borax had the lowest water uptake value both for day 1 and day 7 results (Figure 3.17). With increasing borax concentration, the swelling behavior of scaffolds changed. However among them, the scaffolds crosslinked with 0.02 M and 0.025 M borax concentration, and pregelation performed scaffolds (0.015 M) resulted with lowest weight loss values and relatively

higher water uptake values (Table 3.4). The comparison between day points revealed that water uptake value increased for scaffolds with lower weight loss values. This result may be observed by increasing porosity of scaffolds at day 7 which yields with higher swelling propensity.

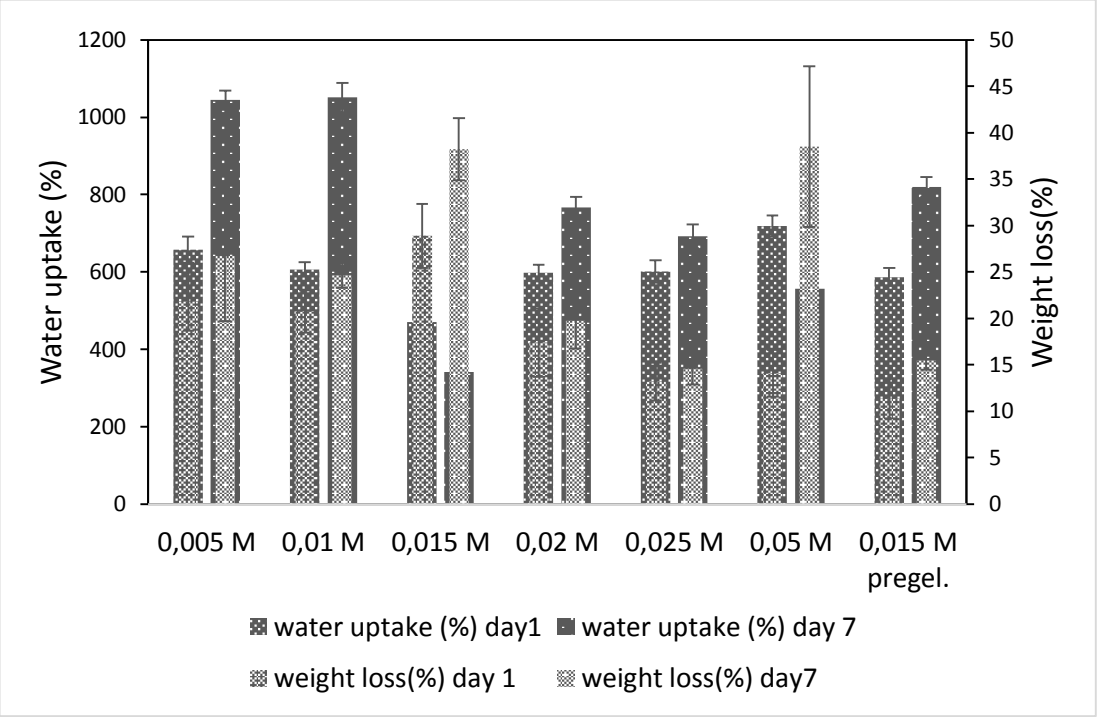

Figure 3.17 The comparison of water uptake (%) and weight loss (%) values of scaffolds crosslinked with different borax concentrations.

Polysaccharides are known by their higher swelling behavior than proteins. By their chemical nature, they tend to be in ionic interaction with water molecules. Water molecule interaction of polysaccharides within scaffolds, increases the swelling of scaffolds [120,180]. Pectin is mostly used for drug delivery systems since its swelling behavior in aqueous medium provides a controlled release of target drug [63,180]. In one of the studies, chitosan, pectin and alginate based scaffolds were crosslinked with formaldehyde and fabricated for tissue engineering applications. Their physicochemical characteristics and biological activities were assessed [181]. The water uptake of scaffolds were recorded for successive 7 hours and found that swelling

ratio (%) increases from 600 to 1200. It was stated that chitosan, alginate and pectin based scaffolds showed weight reduction as 17.90±0.30% in presence of lysozyme after 1 week. The 1200% swelling ratio was concluded as desirable scaffold properties. Our results gave closer values and also correlated with literature. In another study, scaffolds were fabricated from chondroitin sulfate-hyaluronate acid-silk fibroin (CHS) for reconstructing the bone ligament junction [182]. The weight uptake ratio of CHS scaffold was recorded as 635.7±48.3%. This was about four times higher than that of silk fibroin 137±12%.

In comparison of EDC and borax crosslinked scaffolds with lowest weight loss in individual comparisons, water uptake profile showed that borax crosslinked scaffolds reached equilibrium swelling with respect to EDC crosslinked scaffolds. The initial gelation of borax containing samples has role in this profile. In comparison with related studies in literature, the borax containing scaffolds has closer weight loss and water uptake profile with respect to EDC crosslinked scaffolds.

Indeed, the pore morphology and its distribution in scaffolds affect the water absorption and water permeability [183,184]. It was stated that the scaffolds presented a large swelling capability that increased with increasing porosity [185].

The scanning electron microscopy (SEM) analyses were conducted to study the surface morphology of scaffolds as well as pore sizes will be discussed in Section 3.2.3.3.

3.2.3.3. Morphology of Scaffolds

The morphology and size of pores of scaffolds were examined by SEM. Samples analyzed by SEM were selected according to the degradation test results. SEM examinations of the samples were done before and after 1 day incubation in PBS. Among EDC crosslinked scaffolds SF:A-PEC group was chosen. The macroscopic images of SF:A-PEC scaffolds are given in Figure 3.18.

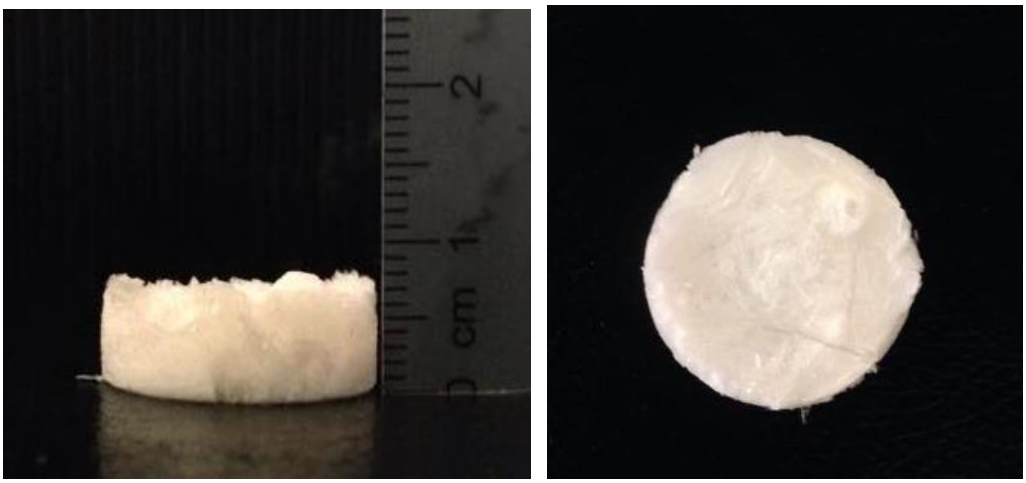

(a) (b)

Figure 3.18 The macroscopic images of silk fibroin and amidated pectin based scaffolds, (a) side view (b) top view.

The effects of methanol immersion on scaffold porosity and degradation properties of scaffolds were examined. The scaffolds that were not immersed in had tubular like porous structure. The parallel lamellar formation was observed (Figure 3.19). It was like the lamellae aligned within three dimensional structure. In literature, there are several studies that scaffolds were casted with lamella morphology. This had been done to construct the lamellae microstructure of natural bone tissue [26,186]. It was stated that by controlling the physics of ice formation, it is possible to obtain scaffolds with lamella morphology [186]. After methanol and $CaCl_2$ immersion, the scaffolds had similar interior structure. Discretely, small calcium ion deposits were observed in methanol immersed scaffolds (data not presented).

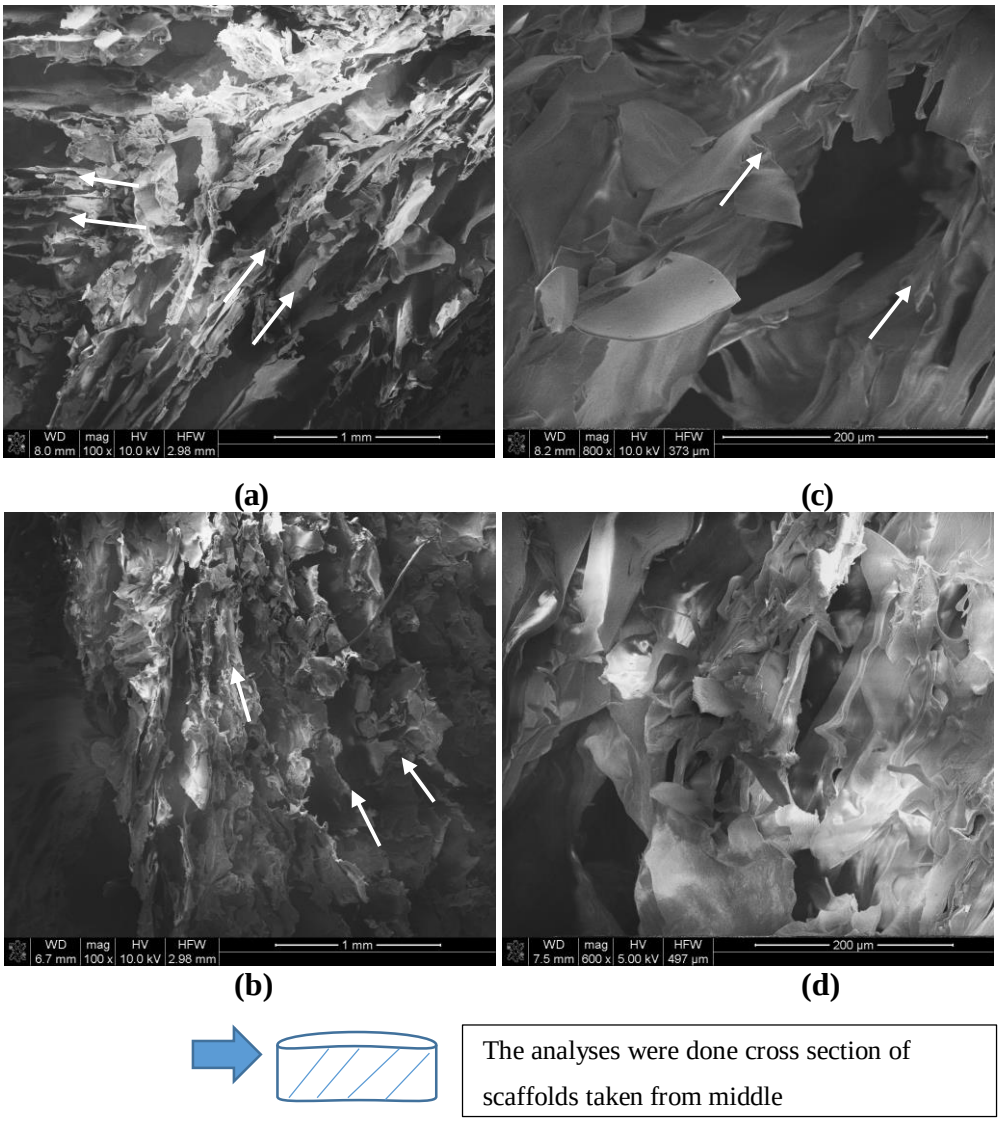

Figure 3.19 SEM images of SF:A.PEC (a) scale bar: 1 mm (c) scale bar: 200 µm, and treated with MeOH+$CaCl_2$, (b) scale bar: 1mm (d) scale bar: 200 µm. White arrows show lamella morphology of scaffolds

SEM images showed that pore size distribution changed in scaffolds incubated in PBS. More homogenous pore size and interconnectivity were observed in these samples. There was skin layer formation on top of scaffolds (data not shown). The freezing-lyophilization process is required to be performed properly to obtain symmetric interior and surface morphology of scaffolds. In case of uncontrolled processing, there is a risk of dense layer formation on top of scaffold due to melting of surface polymer.

However, in literature, the chitosan based scaffolds were casted and by controlling the freezing-lyophilization process, the asymmetric layer was obtained, this bilayer form was studied for skin tissue engineering applications [187]. However, in tissue engineering applications, cells were seeded on top of scaffolds and cells diffuse into matrix, adhere, proliferate and populate through matrix. Therefore scaffolds require a surface porosity for cells to diffuse into matrix. For our scaffolds, further surface modifications or reproduction of scaffolds are needed for further tissue engineering studies.

Among borax crosslinked scaffolds, firstly the gelation profile was studied. Gelation rate was higher for the last two highest borax concentrations; 0.025 M and 0.05 M (Figure 3.21). Their degradation profiles were similar therefore, we examined these two groups by SEM. The macroscopic images of scaffold are given in Figure 3.22.

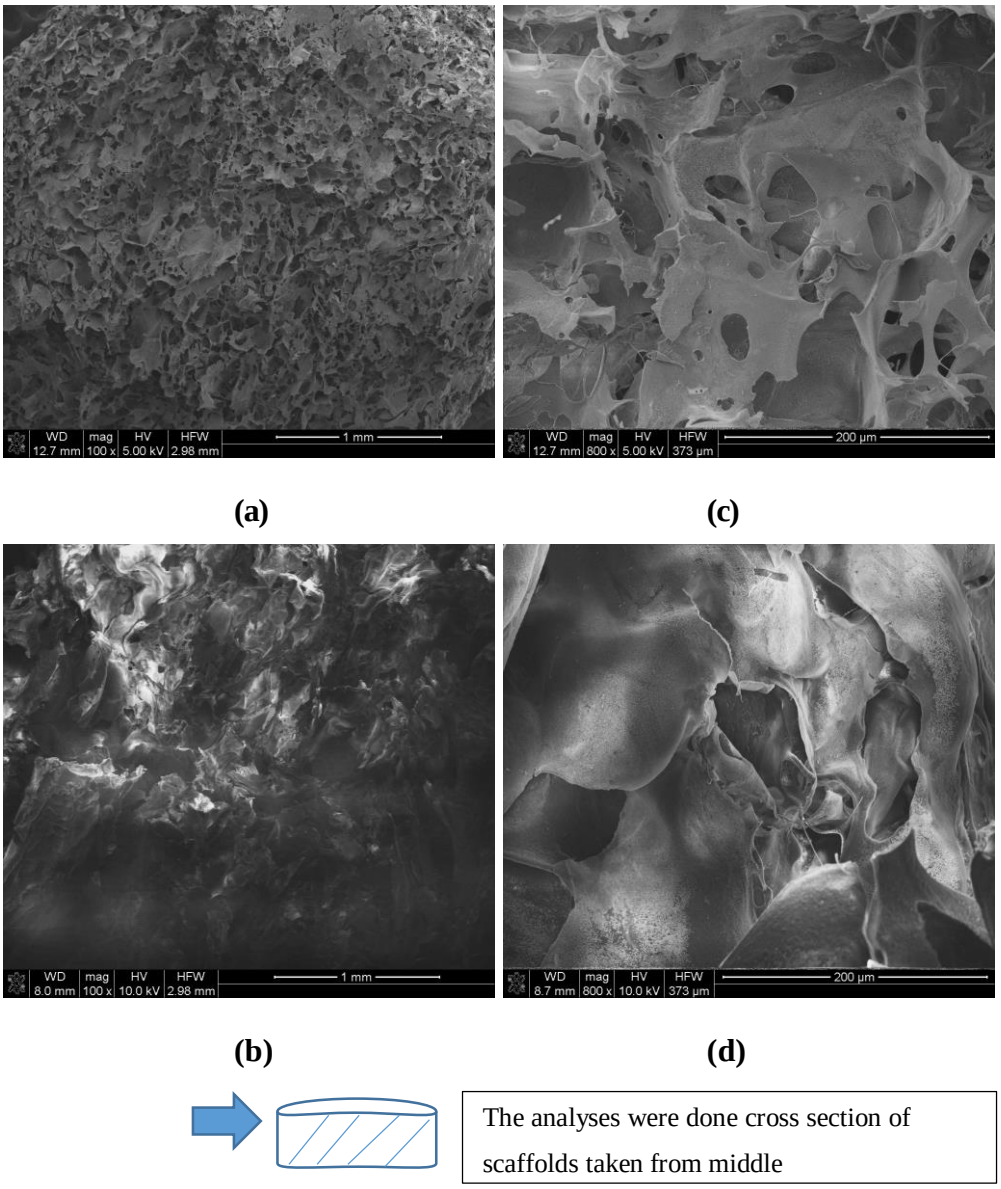

Figure 3.20 SEM images of SF:A.PEC (a) scale bar: 1 mm (c) scale bar: 200 µm, SF:A.PEC (MeOH+$CaCl_2$) (b) scale bar: 1mm, (d) scale bar: 200 µm after 1 day incubation in PBS at 37ºC

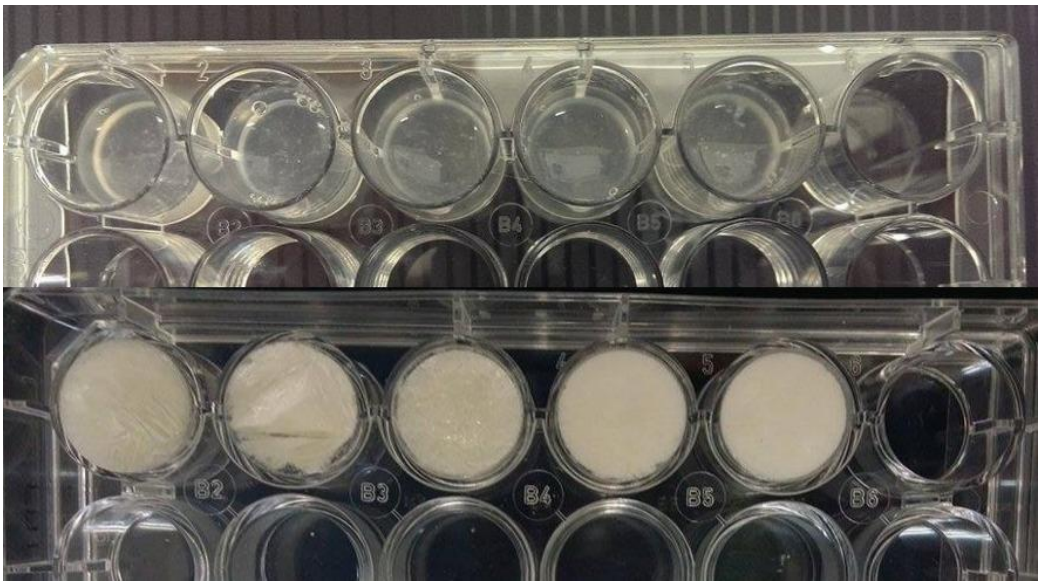

Figure 3.21 The gelation time study of borax containing experimental groups. Reaction mixture became opaque from left to right (wells at above) as borax concentration was increased. After freeze drying (wells at below), increasing gelation shows dimensional stability

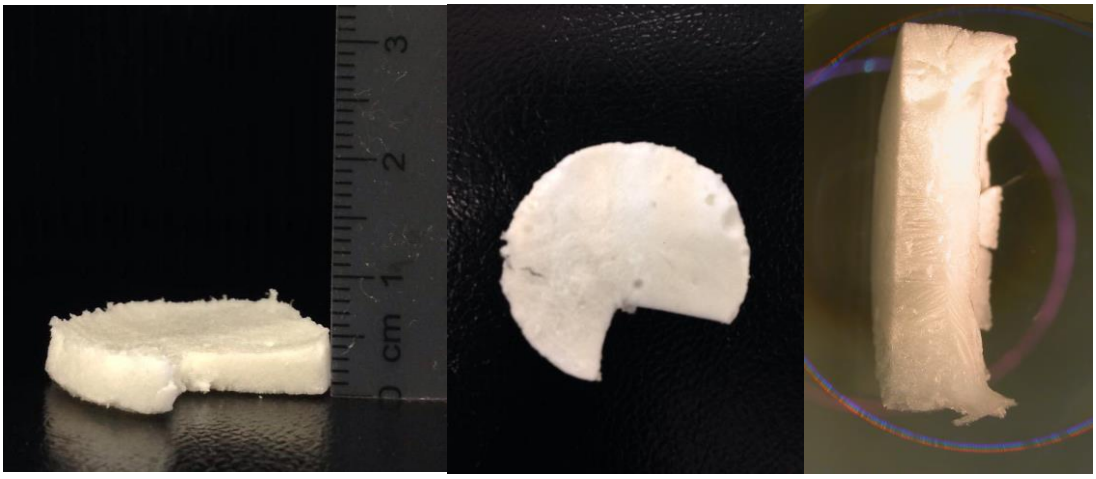

(a) **(b)** **(c)**

Figure 3.22 The macroscopic images of scaffolds crosslinked with 0.05 M borax (a) thickness, (b) top view, (c) lateral surface images obtained by a stereomicroscope (Nikon SMZ 1900, Japan).

As a result of degradation test, 0.015 M (pregelation employed), 0.025 M and 0.05 M borax containing experimental groups gave closer and lowest weight loss values among groups. SEM images of these groups were compared. In all borax containing groups, the lamellar interior structure was observed. After 1 day degradation, it was observed that the porosity of scaffolds increased, which could be due to loss of uncrosslinked pectin and /or crosslinkers from the polymeric matrix.

SEM images of 0.025 M borax containing experimental group was examined at different magnifications due to the collapse risk of samples after degradation (Figure 3.23). The images showed that the tubular structures became irregular due to penetration of water into structure which resulted with swelling of pectin. The lamellarity of scaffolds was lost to some extent and scaffolds became more microporous with 1 day incubation in PBS. More interconnectivity was observed in these scaffolds (Figure 3.24).

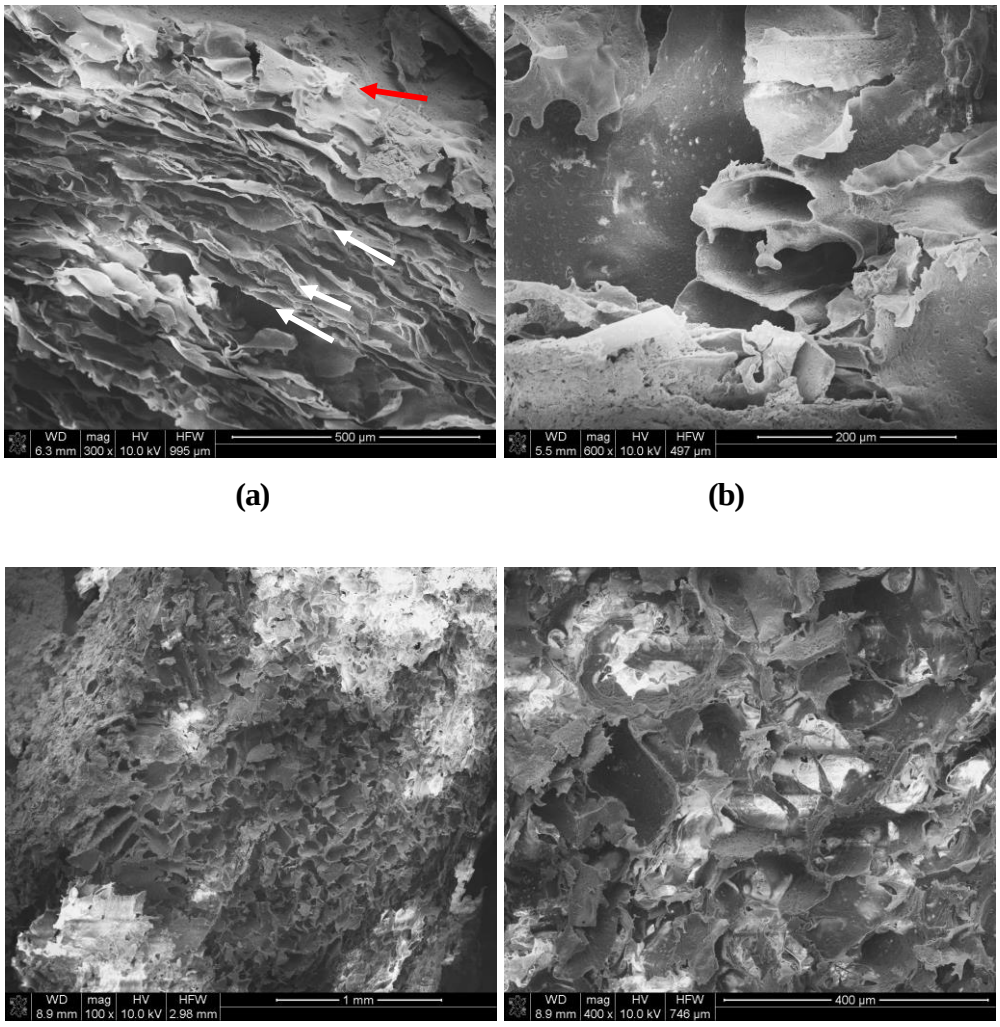

Figure 3.23 SEM images of scaffolds crosslinked with 0.025 M borax and treated with MeOH+$CaCl_2$ before degradation (a) scale bar: 500 µm (b) scale bar: 200 µm, after degradation (c) scale bar: 1 mm (d) scale bar: 400 µm. Red arrow show the surface of scaffolds, there was a skin layer formation. White arrows show the lamellae structure of scaffolds

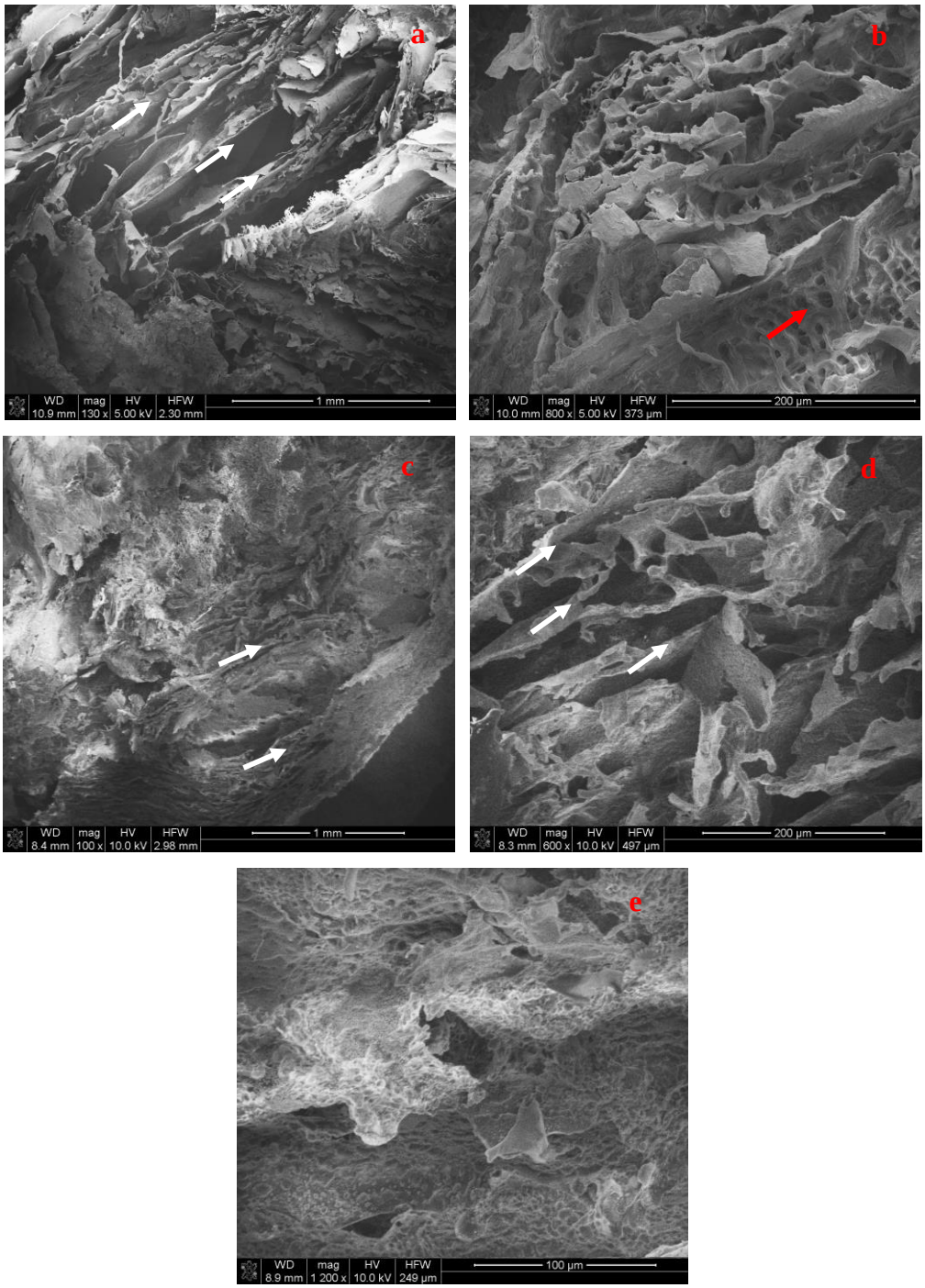

Figure 3.24 SEM images of scaffolds crosslinked with 0.05 M borax and treated with MeOH+$CaCl_2$ before degradation (a) scale bar: 1 mm (b) scale bar: 200 µm, after degradation test. (c) scale bar: 1mm (d) scale bar: 200µm (e) scale bar: 100µm. White arrows show lamella morphology of scaffolds. Red arrow was used to show interconnectivity of pores.

SEM images of 0.05 M borax containing scaffolds revealed they had surface texture which might enhance cell attachment and osteogenic differentiation. The pores observed might provide niches of cells apart from the textures surfaces (Figure 3.24). The interconnectivity and homogeneity on pore size distribution were confirmed.

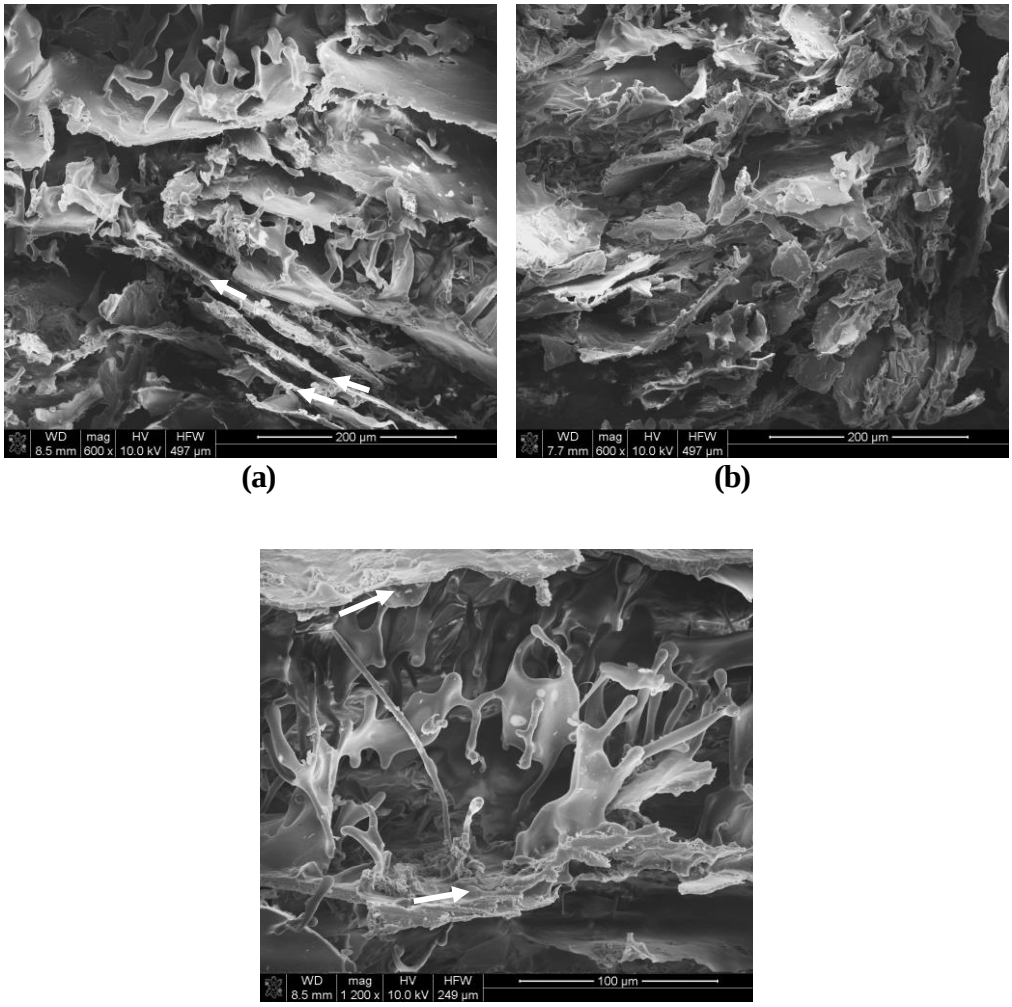

(a) **(b)**

(c)

Figure 3.25 SEM images of scaffolds prepared with 0.015 M borax and $CaCl_2$ pregelation which were treated with methanol after freze drying (a) scale bar: 200 µm (b) scale bar: 200 µm, (c) scale bar:100 µm. White arrows show lamella morphology of scaffolds

The experimental group with 0.015 M borax containing and pregelation employed showed similar interior structure as in other borax containing groups. The lamellar interior structure was clearly apparent as stated in above SEM images. (Figure 3.25).

PART III

3.3. Synthesis of Nano Sized Calcium Phosphate Particles Using Flame Spray Pyrolysis

3.3.1. Structural Analysis and Characterization of Particles

The prepared nanoparticle powder of calcium phosphates in FSP system was whitish color. Their specific surface area (SSA) measured by BET analysis between 40 to 50 m^2/g, depending on the Ca to P molar ratio (Table 3.5). Different Ca/P ratios were studied to investigate the feasibility of reactor system and compare the physical, chemical and biological differences based on composition difference.

Increasing Ca to P molar ratio caused a slight increase on the SSA due to the increasing calcium concentration in the main flame environment, which in turn provided larger number of seeds for particle formation, followed by their agglomeration and sintering before leaving the flame. Elemental analysis of particles (ICP-MS) was performed to determine calcium and phosphate amount in particles after synthesis which agreed with the Ca/P ratio in starting precursor solution (Table 3.5). To improve the analysis these results of Ca and P elements and their amounts in nanoparticles, scanning electron microscopy (SEM) was used for elemental microanalyses with energy dispersive spectrometry (EDS) technique. For all samples, Ca, P and O elements were detected. No contamination was observed.

Table 3.5 Elemental analysis results and specific surface area of particles

Ca/P molar ratio (experimental)	Ca/P ratio (ICP results)	Specific surface area (m^2/g) (BET results)
1.27	1.20	40.88±0.05
1.38	1.31	39.10±0.18
1.61	1.54	39.25±0.06
1.95	1.91	50.21±0.05
2.29	2.19	50.00 ±0.29

All calcium phosphate particles studied at different Ca/P ratios (1.20, 1.31, 1.54, 1.91, and 2.19) were at nano sizes. Representative low magnification SEM and TEM images of all Ca/P groups are given in Figure 3.26, in which polydisperse size distribution of particles can be seen. The particles had spherical shapes with loosely agglomerated structure. In FSP process, particle formation follows gas-to-particle and/or droplet-to-particle conversion mechanism depending on several parameters [153]. The most important of these parameters are; flame temperature which is decided by the heat of combustion of the solvent and premixed flame operating conditions, liquid precursor flow rate and concentration which affects the particle residence time and the degree of sintering, and dispersion oxygen flow rate which affects the liquid droplets size in the spray [153]. SEM and TEM results indicated that the primary particle formation in our system follows both gas-to-particle and droplet-to-particle mechanism under the processing conditions used. SEM and TEM pictures show agglomeration of the primary particles, which is generally the case for the FSP produced nanoparticle powders due to their need to minimize their surface free energy [188]. TEM images indicated spherical primary particles with necking and forming chain-like aggregate structures. This kind of morphology is desired in case for calcium phosphate based scaffolds because interconnective microporosity facilitates cell adhesion and body fluid circulation, and improves osteoconductive properties [79]. When solvent + precursor mixture is sprayed into the flame environment, precursors go through a series of reactions forming the particle nucleus. This is then followed by the particle growth through agglomeration and sintering depending on the residence time in the flame [88]. The existence of particle necking indicates that some particles stayed long enough at the high temperature regions of the flame to collide and stick together, and form chain-like aggregates.

SEM **SEM** **TEM**

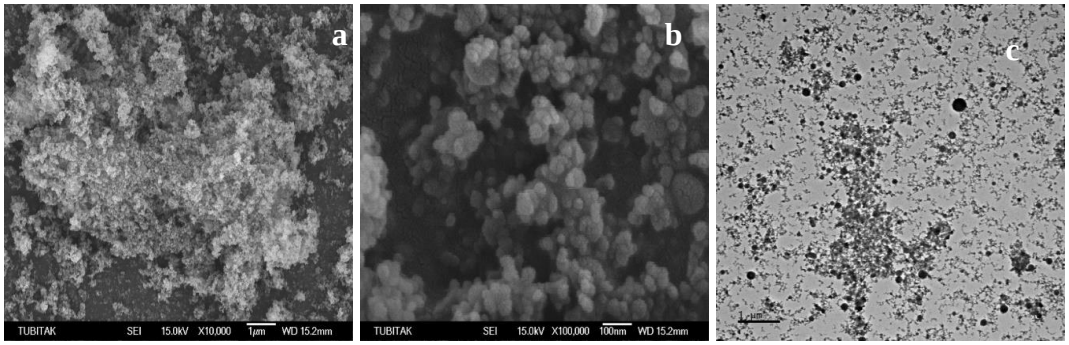

Ca/P:1.20

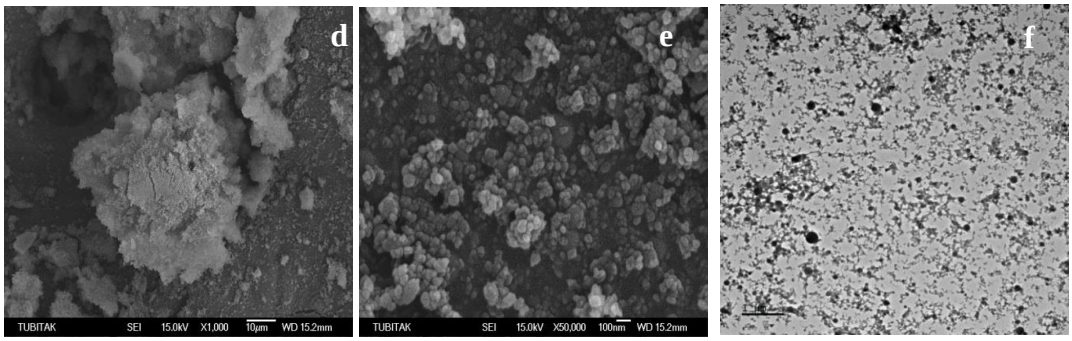

Ca/P:1.31

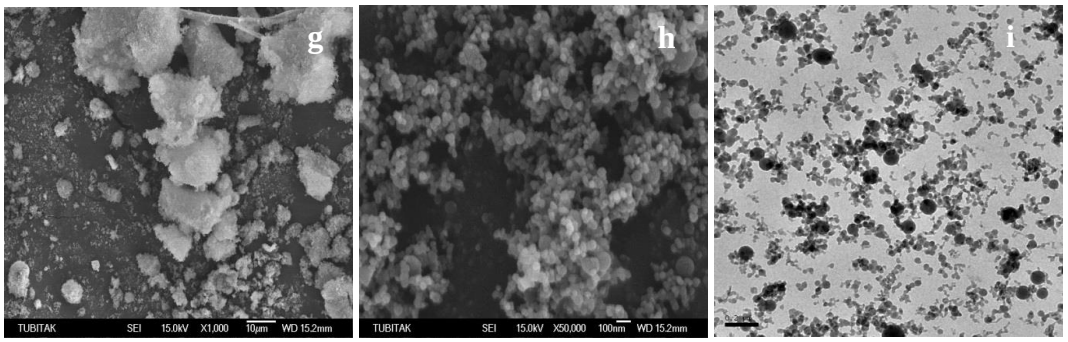

Ca/P:1.54

Figure 3.26 Representative low magnification SEM and TEM images. The scale bars of images are (Ca/P: 1.20), SEM (a) 1 μm, (b) 100 nm, TEM (c) 1 μm, SEM (d) 10 μm, (e) 100 nm, TEM (f) 1 μm, (Ca/P: 1.31), SEM (g) 10 μm, (h) 100 nm, and TEM (i) 0.2 μm, (Ca/P: 1.54), SEM (j) 10 μm, (k) 100 nm, and TEM (l) 0.2 μm, (Ca/P: 1.91), SEM (m) 10 μm, (n) 100 nm, and TEM (o) 0.2 μm, (Ca/P: 2.19) In all images loose agglomerations of particles were observed.

SEM **SEM** **TEM**

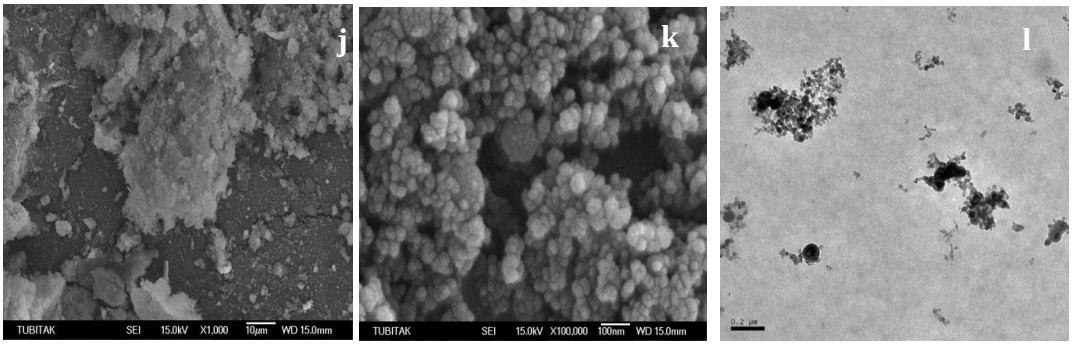

Ca/P:1.91

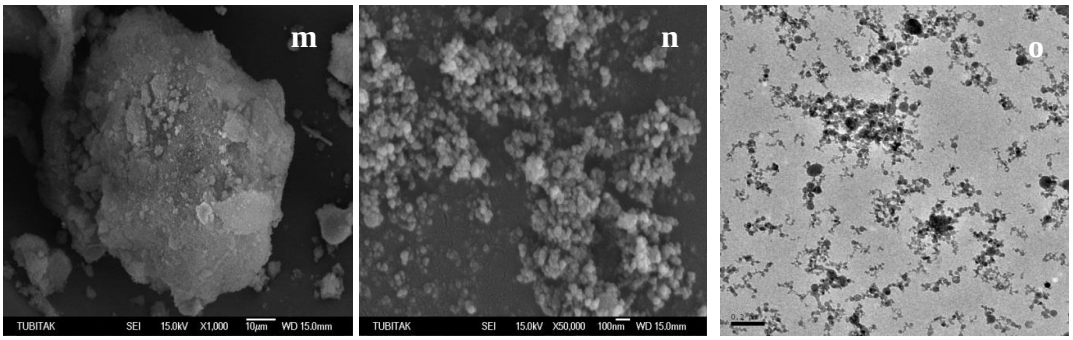

Ca/P:2.19

Figure 3.26 (continued)

TEM images of different calcium phosphate ratio samples are given in Figure 3.28. Majority of the particles were amorphous, indicating that the fast cooling of the particles after their formation, and leaving the flame without crystallizing. Yet, fused primary particles with sintered necks were also observed. In Figure 3.28 f, HRTEM-selected area electron diffraction (SAED) pattern for sample Ca/P: 1.31 is given, which shows the amorphous nature of the particles. HRTEM images of nanoparticles at low Ca/P ratios showed no atomic lattice fringes and corresponding FFT diffractograms in lower Ca/P ratios were considered as an evidence for amorphous structures. However, as the Ca/P ratio was increased, crystallinity increased as confirmed by XRD results. The last two composition showed gradual increase in crystallinity. The crystalline nanoparticle's HRTEM images and corresponding Fast Fourier transform (FFT) diffractogram for sample Ca/P: 1.91 and 2.19 are given in Figure 3.29. The last composition of calcium phosphate particles had the highest Ca/P ratio and crystallinity

among other compositions. However, relatively higher crystallinity was observed for the samples with Ca/P ratio higher than 1.54. This observation was also supported by XRD analysis.

The X-ray diffraction pattern of as prepared calcium phosphate powders showed broad HA reflections especially up to the Ca/P ratio of 1.54, indicating the mostly amorphous nature of the particles (Figure 3.27). In all the powders, sharp peaks corresponding to crystalline CaO, and broad reflections of amorphous beta-CPP and alpha-TCP existed.

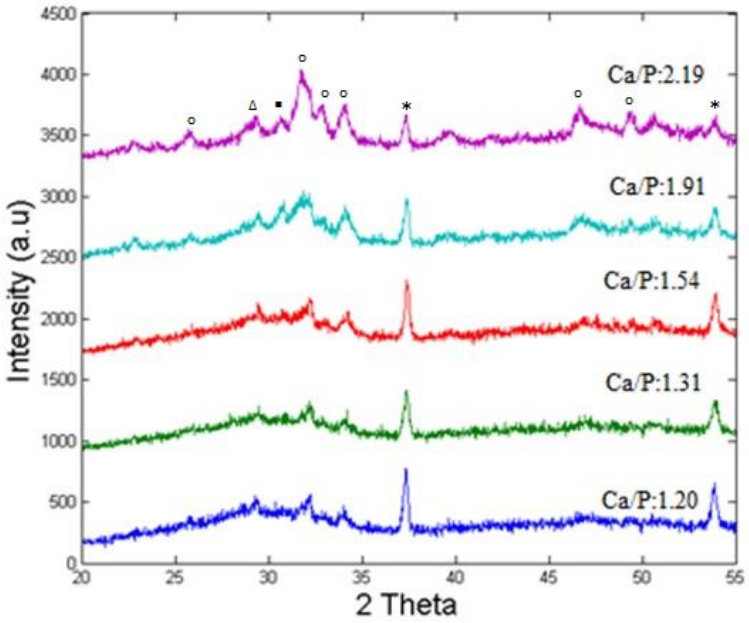

Figure 3.27 XRD spectra of as prepared calcium phosphate particles (o) hydroxyapatite, (Δ) beta-CPP, (▪) alpha TCP, (*) CaO

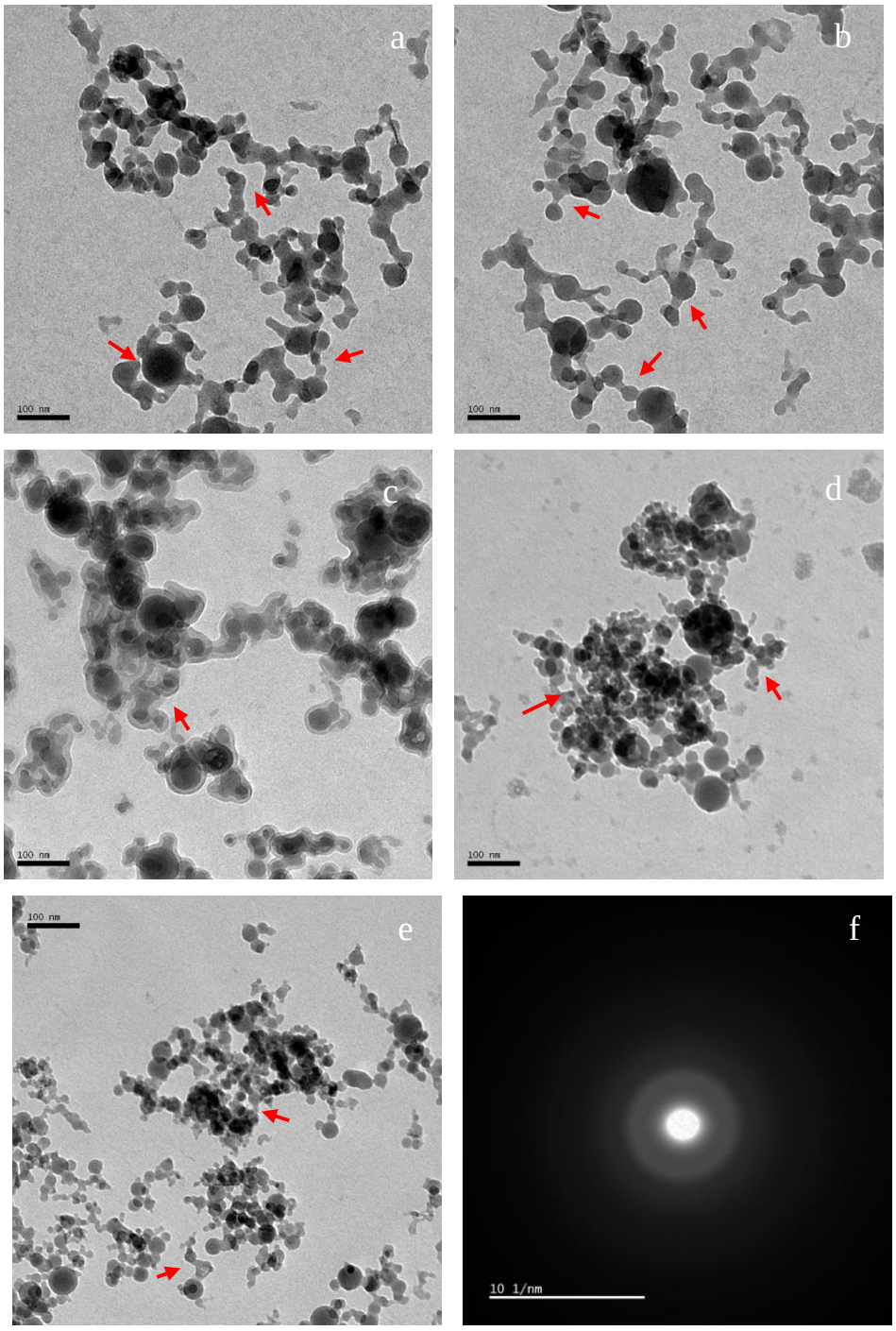

Figure 3.28 TEM images of different calcium phosphate ratio samples (a) 1.20, (b) 1.31, (c) 1.54, (d) 1.91, (e) 2.19 at 100 nm scalebar, (f) HRTEM-selected area electron diffraction (SAED) pattern for sample Ca/P: 1.31 that reveals amorphous phase. Red arrows show the necking between particles.

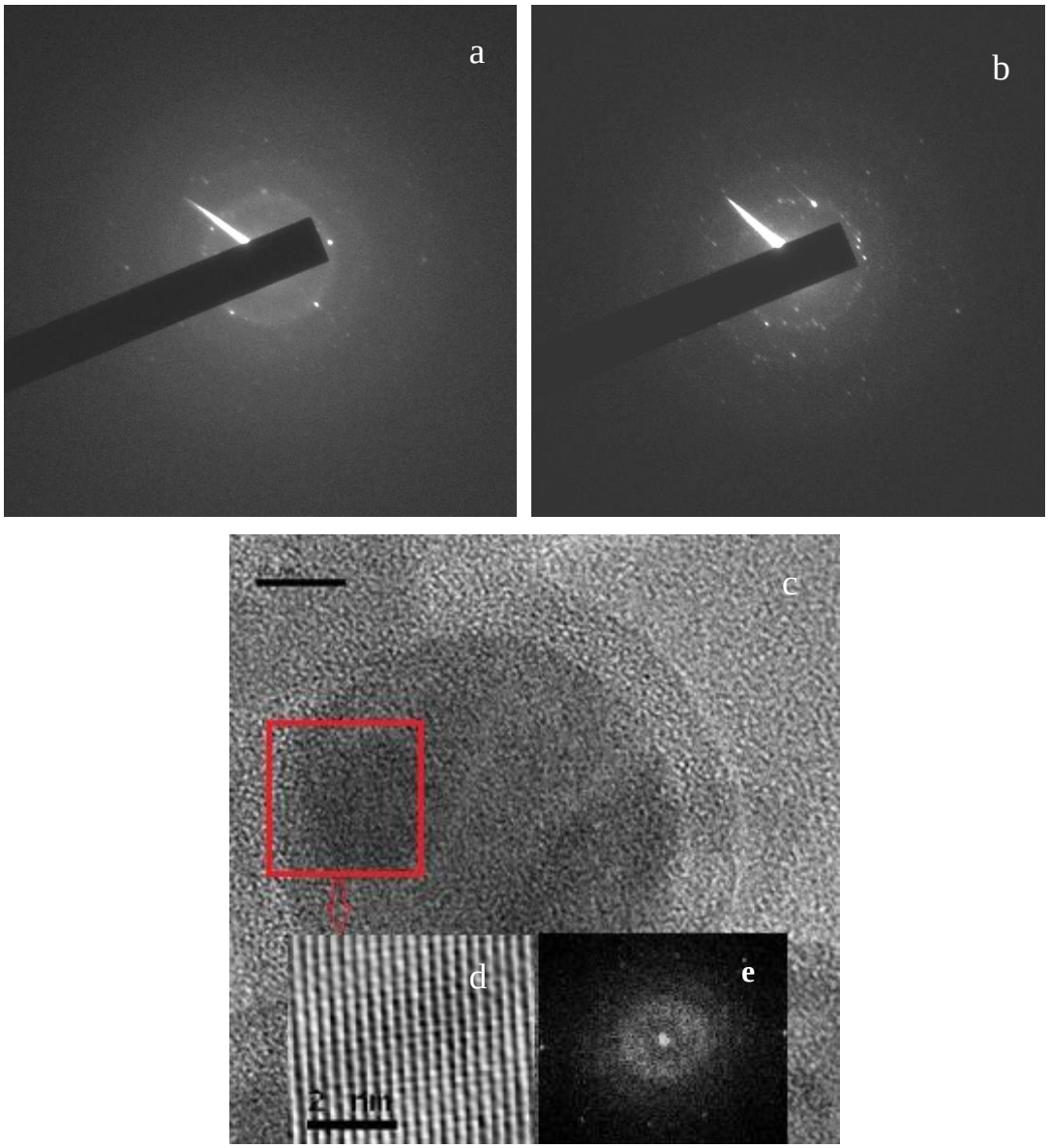

Figure 3.29 Selected Area Electron Diffraction (SAED) patterns of (a) Ca/P: 1.91 and (b) Ca/P:2.19, (c) HRTEM image of sample Ca/P: 2.19 (scale: 10 nm), (d) magnified and filtered view of the selected part in image c (scale: 2 nm) and (e) corresponding FFT diffractogram

The XRD data of all compositions showed that last composition with Ca/P: 2.19 had the most crystalline like diffraction peaks. Rietveld refinement of this composition revealed that with respect to Rigaku database there were four phases in this sample (Figure 3.27). The weight percentages of these phases were found as 70.7%

hydroxyapatite, 7.50% beta CPP, 12% alpha TCP and 9.50% calcium oxide. The primary particle diameter (d_{BET}) and crystallite size (d_{XRD}) of this composition were estimated in order to further discuss the particle size polydispersity (Table 3.6). The particles were assumed as spherical and the density was determined by considering the weight percentages of phases in the particles. Primary particle size was calculated using the equation.

$$\boldsymbol{dBET = 6/(\rho . SSA)}$$

The crystallite size was calculated from Schrerrer equation [189].

$$\boldsymbol{\tau = \frac{\kappa \lambda}{\beta cos\theta}}$$

Table 3.6 The primary particle size and crystallite size of sample Ca/P: 2.19

Ca/P molar ratio	Specific surface area (m^2/g)	Primary particle size d_{BET} (nm)	Crystallite size d_{XRD} (nm)
2.19	50.00 ±0.29	41.14	6.09

The particle size results were in correlation with literature [77,179,180]. In one of the studies the nano calcium phosphate particles were synthesized by spray drying process. The SSA of sample was measured as 50 m^2/g and primary particle size of as prepared sample was estimated at around 38 nm [190]. The primary particle size of nano TCP particles produced by FSP were estimated at around 13-40 nm in literature [191]. In another study, the crystallite size of FSP processed nano calcium phosphates with Ca/P: 2.0 ratio was measured as 19 nm [77]. Although these results did not give the exact particle sizes. We could conclude that our as prepared samples had a polydisperse particle size distribution. Increasing Ca amount in sample revealed the rise in crystalline particle and its size. The average primary particle size of Ca/P: 1.31 (selected as model) was determined as 23 nm by counting more than 500 particles in TEM pictures (Table 3.7). Average particle diameter was almost the same for all samples, which was expected, because the flame reactor operating conditions were kept the same in all the experiments. Smallest particle size was about 10 nm.

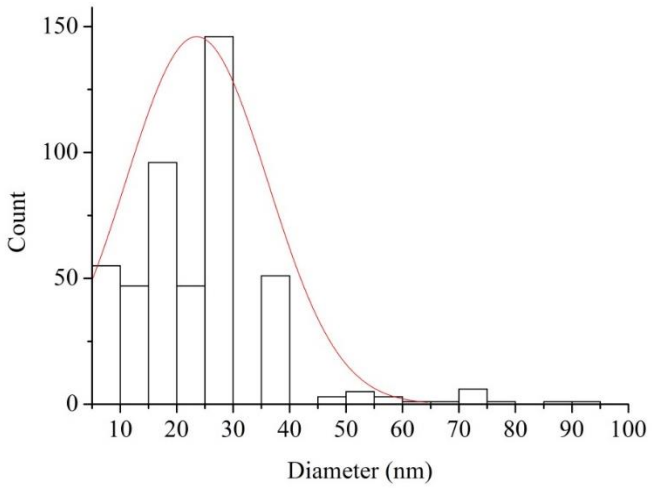

Table 3.7 Histogram of nanoparticle size distribution of Ca/P:1.31

The particle size distributions of amorphous compositions were determined in volume percentage by Zeta sizer analysis. All compositions gave similar size and volume percentage values at around 150-200 nm and 25%. This results gave no correlation with other particle size measurements. Since nano particles have higher surface interaction, to disperse particles, high amounts of energy or dispersant is required. If this energy is not overcome, particles are measured as an aggregate and result in higher sizes. In our samples, we confronted such challenge (Figure 3.30). For last composition (Ca/P: 2.19) particle size measurements could not be done.

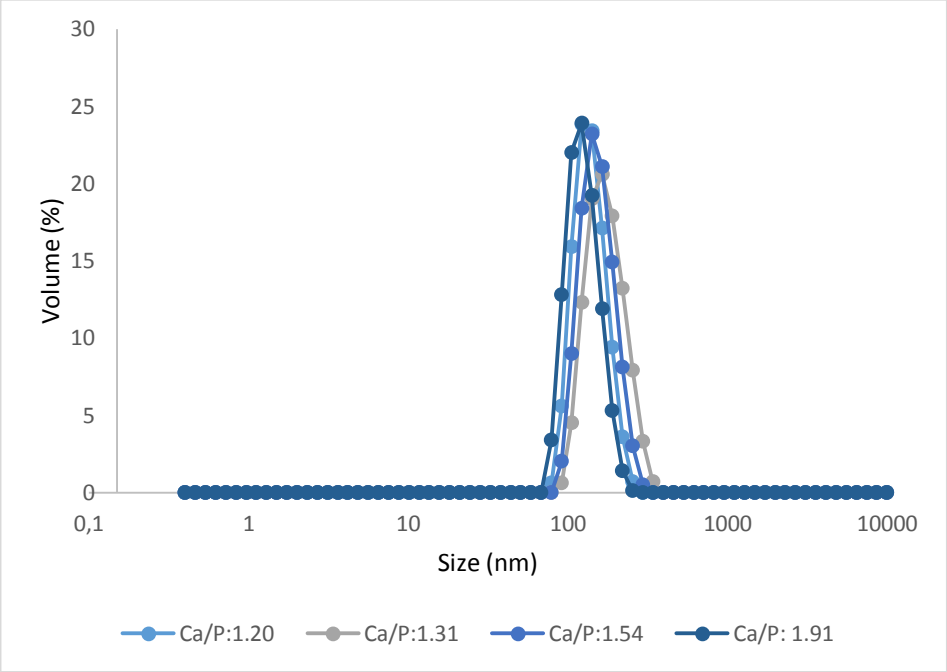

Figure 3.30 The size distribution diagrams of calcium phosphate particles produced by FSP at the different Ca/P ratios

In order to analyze the thermal behavior of synthesized calcium phosphate nanoparticles, thermogravimetric (TG) and differential thermal analysis (DTA) were performed. All five calcium phosphate compositions showed similar exothermic peaks and similar amount of weight losses, but the last two samples had another phase change around 800°C. The weight loss up to 200°C is an indicator of adsorbed water evaporation, and decrease up to ~400°C is thought to be due to the lattice water evaporation [190]. Decomposition temperature and crystallization onset temperature in TG analysis differ with respect to synthesis methods of calcium phosphates. In one of the studies of FSP processed particles, weight loss up to 600°C was defined as water evaporation and CO_2 loss from sample [79]. From 600°C to 1250°C it was interpreted as crystallization reaction and phase change. Thermal behavior of the synthesized particles was examined up to 900°C. The mass losses at ~200°C, ~500°C, 700°C and at around 800°C were more apparent for Ca/P ratios above 1.54 (Figure 3.31). 3-4% mass loss at ~200°C for all compositions were thought to be due to desorption of water in the samples. In our results, observation of phase change at about 800°C for higher

Ca/P ratios in DTA results suggested the formation of beta-TCP, which is a more stable form of alpha-TCP [192]. The onset of phase transition started at about 500ºC (Figure 3.31). After 700ºC, there was a plateau like gradual decrease on TGA curves suggesting the crystallization of the particles.

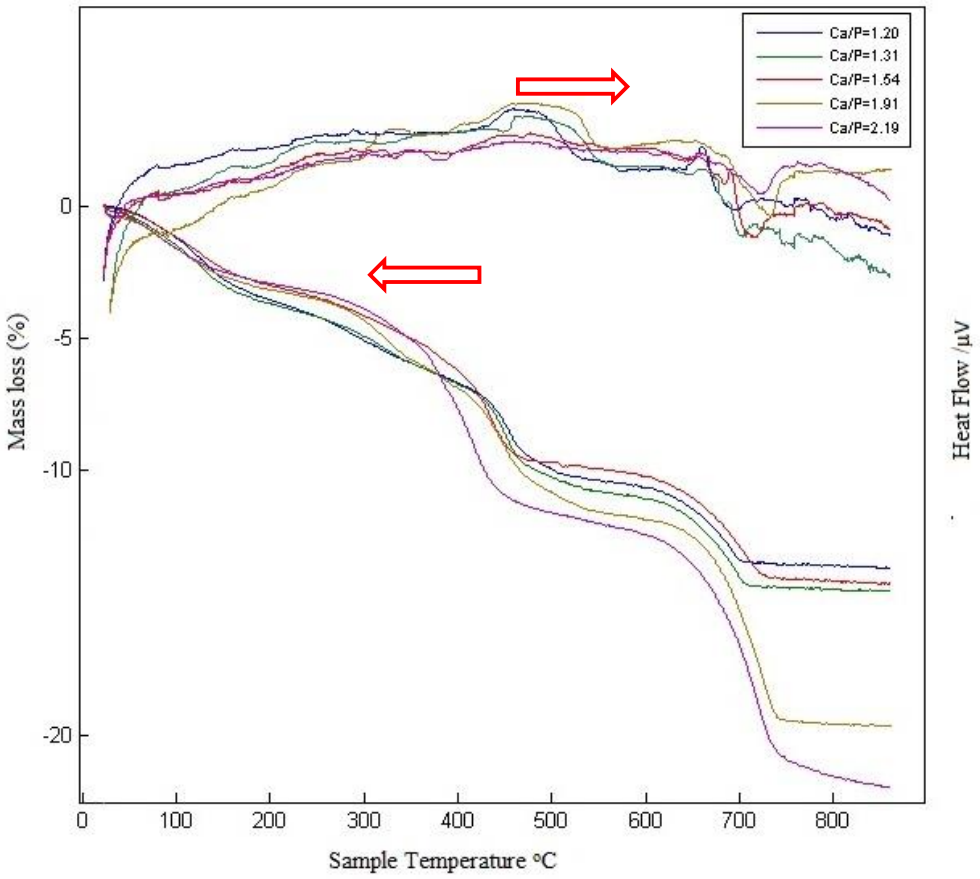

Figure 3.31 TGA-DTA curves of flame spray synthesized calcium phosphate nanoparticles at different Ca/P ratios

3.3.2. Biological Characterization of Particles

Physical and chemical properties of calcium phosphate particles determine the biological activity. The changes in chemical composition (calcium to phosphate molar ratio) and changes in structural properties such as crystallinity, porosity, and particle size result with differences in the behavior of particles [82]. In our study, properties of nanoparticles of calcium phosphates at different Ca/P molar ratios were studied.

Biological characterization of particles was conducted by cell viability and ALP activity studies using urine derived stem cells (USCs).

3.3.2.1. Isolation and Characterization of Urine Derived Stem Cells

3.3.2.1.1. Evaluation of Cell Morphology, Proliferative Capacity and Stem Cell Potential

A subpopulation of cells in human urine have been reported to have characteristics of mesenchymal stem cells, and they gained an attention afterwards [27,30]. The biological characterizations of these type of cells have already been studied [28,30,193]. As stated in introduction part, the tissue engineering applications of these cells were already assessed. With the ease of isolation, high proliferative capacity and osteogenic differentiation of these cells in mind, we favored to isolate and employ urine derived stem cells in our study. The morphology, proliferation capacity and surface marker expression were evaluated and compared with previous studies. The mesenchymal stem cell features of urine derived cells were assessed. The proliferation rate, self-renewal capacity and potency of isolated cells were examined.

The isolation was performed from spontaneously voided urine samples of several different age and sex group of donors. Urine derived stem cells isolated and expanded from two healthy men donors and used in the study (24 years old). Although same medium and conditions were supplied to isolates, cells from other donors did not expand. At different passage numbers they became giant and proliferation declined. In one of the studies on urine derived stem cells, it is stated that in urine there are three types of cells which named as terminally differentiated, differentiating and urine derived stem cells [29]. Such kind of expansion problem was encountered in this study and this type of cells with lower expansion capacity were categorized as differentiating group of cells in urine. The morphology of cells from both healthy two donors resembled with those in previous studies [28,30,31]. They showed fibroblastic like morphology. The single cell adhered to plate and formed a colony in few days (Figure 3.32). They robustly expanded in same morphology (conducted up to 8^{th} passage) which shows the self-renewal capacity of cells. The cells in first adherence and in

colony showed round like morphology. In studies, this morphology is defined as rice-grain like morphology [28].

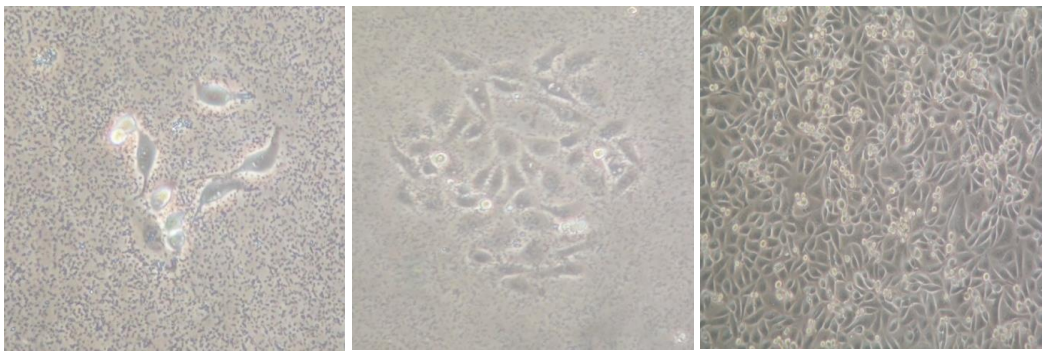

(a) (b) (c)

Figure 3.32 Phase contrast micrographs of cells in culture (a) First appearance of cells at day 5 (b) first colony formation at day 7 (c) confluency at day 10.

For experiments, cells were passaged until 8th passage. The morphology changed after 8th passage; cells became giant and their proliferation rate declined. The parameters like medium ingredients, trypsin concentration and trypsin incubation time influenced the cell morphology. Moreover, the contact of cells to neighbor cells determines the proliferation capacity [34]. In case of low seeding density, the duplication time of cells increased, cells turned to ghost like morphology in order to conform cell to cell contact. We optimized cultivation conditions for cells and conducted studies with respect to them. Urine derived stem cells showed higher proliferation capacity as stated in previous studies [27,28,194]. The proliferation rate of 1st passage of cells was studied by Alamar Blue viability assay. An increase in percent reduction shows increase in cell number. The viability test revealed that cells proliferated with time (Figure 3.33).

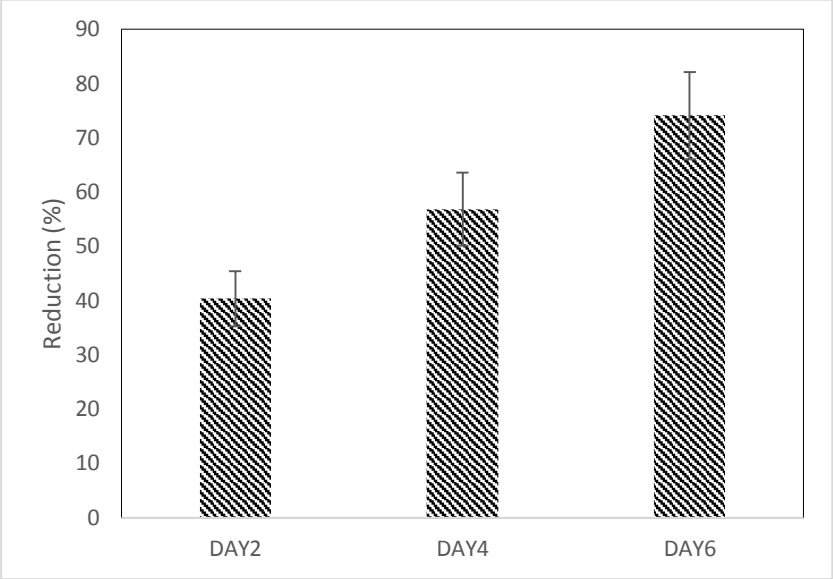

Figure 3.33 Growth curve of USCs cultured in growth medium (KSFM:EFM)

Immunophenotyping of cells were performed by flow cytometry for expression of surface antigens. Pericyte and mesenchymal stem cell markers CD44 (hyaluronan receptor), CD73, CD90 (Thy-1), CD105 (endoglin), endothelial cell marker CD31, hemaotopoietic cell marker CD45 were used for assessing the mesenchymal origin of cells. The mesenchymal markers; CD73 and CD44 were expressed on cell surface of USCs around 80%. CD105 expression level was 42.2%. In one of urine derived stem cell characterization study, CD44 was considered as urothelial basal cell marker and was used to demonstrate the urothelial origin of the isolated cells [28]. With this in mind we can confirm the urothelial origin of cells by these results. Cells were positive for mesenchymal markers (CD73, CD44 and CD 105 expression) and negative for hematopoietic, endothelial and osteogenic markers (CD45, CD31, osteopontin, respectively) (Figure 3.34).

However, CD90 expression was unexpectedly low (Figure 3.34). One possibility could be due to experimental errors like staining problems or antibody stock solution. Moreover, in characterization papers, the flow cytometry results did not show exactly same expression levels for USCs. In one of these studies, CD105 expression was measured at low levels (around 1%) and even cell source was admitted as mesenchymal stem cells [27].

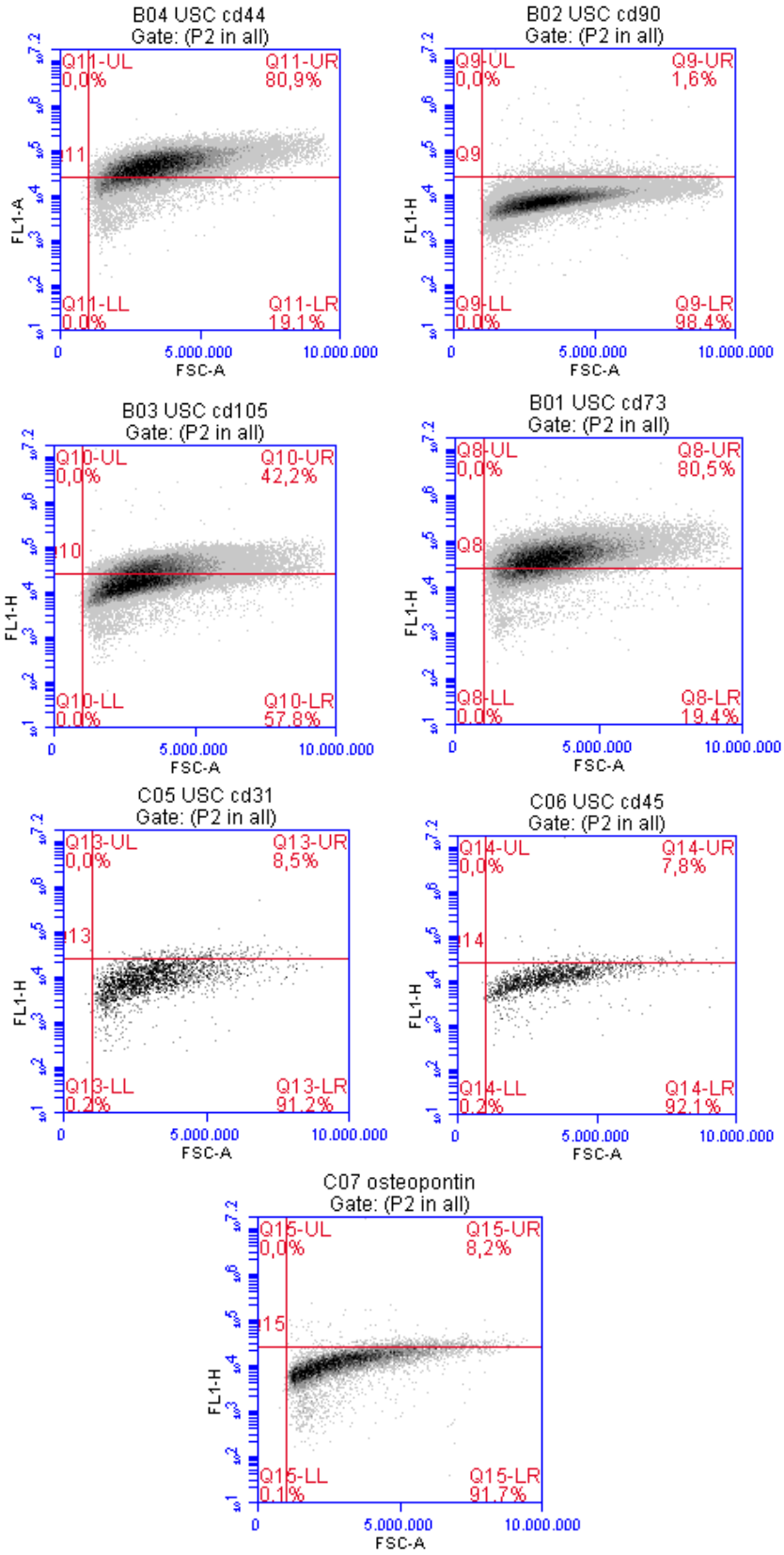

Figure 3.34 Flow cytometry analysis results of urine derived stem cells.

3.3.2.1.2. Evaluation of Multilineage Differentiation Potential of USCs

The multilineage differentiation capacity of urine derived stem cells was previously studied on osteogenic, chondrogenic, adipogenic, myogenic and urogenic lineage differentiation [29,30,193]. We also studied differentiation capacity of isolated urine derived cells towards osteogenic, adipogenic and chondrogenic lineages to show their multipotential differentiation capacity as mesenchymal stem cells [29,30].

Multilineage differentiation potential of these cells was only conducted on cells of one donor by incubating with particular differentiation media. The morphology of cells during differentiation was controlled by light microscopy images (Figure 3.35). Urine derived stem cells were in cobblestone like morphology in basal medium. The cells in differentiation media contained less dividing cells relative to cells in basal medium. There was less bright cells than control groups which was a sign for the onset of differentiation. In osteogenic medium cells were elongated (Figure 3.35b). The morphology of cells in osteogenic differentiation was similar with previous studies [30,195]. Osteogenic differentiation was further confirmed by Alkaline Phosphatase enzyme activity level and Alizarin Red S staining. Alkaline phosphatase enzyme exists in several tissues, however, excess amount of this enzyme is found in mineralized tissues. It is stated that this enzyme was found on cell surface and in matrix vesicles of mineralized tissues [196]. This enlightens the fact that alkaline phosphatase enzyme should be expressed in early stages of cells that differentiate into hard tissue and then is expressed on cell surface or in matrix vesicles [197]. This early expression of ALP enzyme makes it specific marker for osteogenic differentiation of cells. Therefore, it has been reported that the gene responsible to express alkaline phosphatase enzyme is usually up-regulated at around 7 days of in vitro cultivation and declines, since genes for other specific proteins like osteocalcin are upregulated and expressed in cells [196–198]. In our results, the alkaline phosphatase enzyme levels were studied after 7 and 14 days of incubations. The results revealed that urine derived stem cells had higher intracellular ALP enzyme level at day 7 than observed at day 14 (Figure 3.37).The decrease in enzyme level at day 14 showed that alkaline phosphatase specific gene expression was downregulated and other osteogenic specific proteins like osteopontin and osteocalcin were expressed in cells. It can be interpreted that cells were in late

osteogenic developmental stage. This result correlated with previous osteogenesis induced urine derived stem cells [35,193]. The human mesenchymal stem cells and adipose derived stem cells also showed similar osteogenic differentiation profile [26,195].

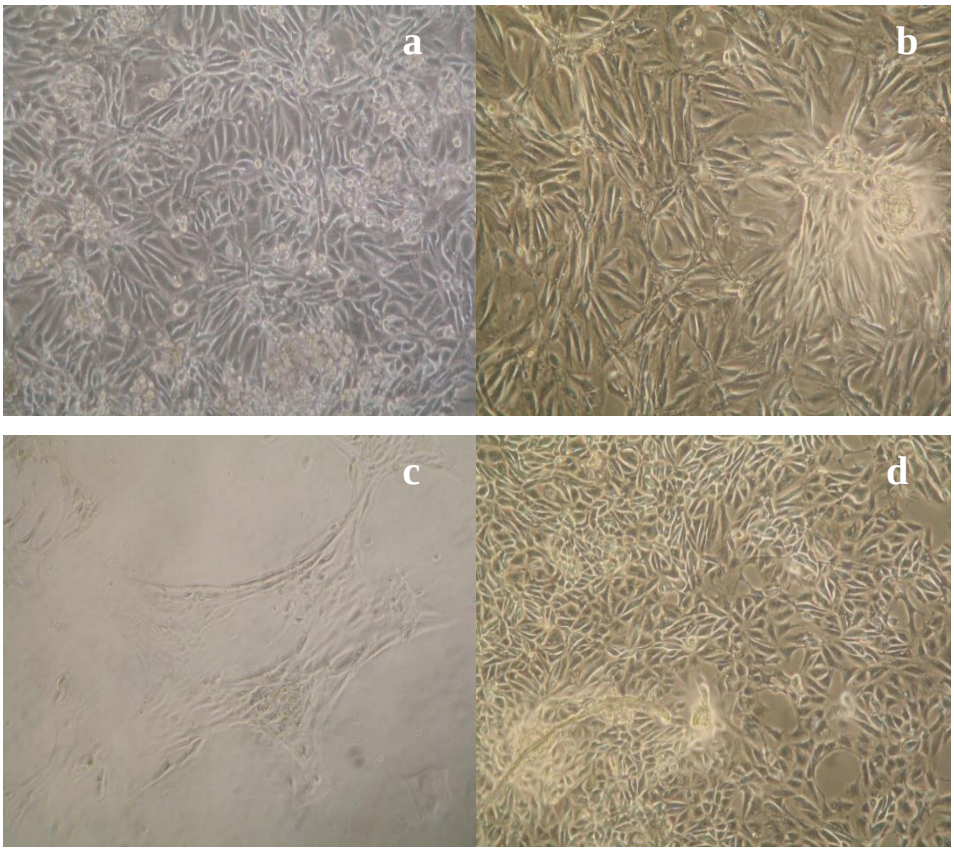

Figure 3.35 The phase contrast light microscopy images of cells in (a) basal medium, (b) osteogenic medium, (c) chondrogenic medium, and (d) adipogenic medium. Magnification 10X.

The Alizarin Red S staining was performed after 14 days of incubation in osteogenic media. The results showed that cells had a tendency for initial mineral deposition. The calcium deposits were stained in red like color. The heamatoxylin counterstaining highlighted the dot like tiny mineral deposits in cells (Figure 3.38). The previous study on multipotential differentiation profile of urine derived stem cells was examined osteogenesis via Alizarin Red staining at day 21 [193]. The osteogenic differentiation

of urine derived stem cells was further confirmed by measuring osteopontin expression level of cells. The cells were incubated in osteogenic medium for 21 days and flow cytometry analyses were performed to measure the osteopontin level in cells. The analysis was performed without lysing cells although it requires lysis. However, when compared with undifferentiated USCs osteopontin level, there was a remarkable increase in level from 8.2% to 43.8% (Figure 3.36). In literature, there was no study specifically on osteopontin expression analysis of osteogenic differentiated human urine derived stem cells. Therefore, the comparison was interpreted with respect to human mesenchymal stem cell osteogenic differentiation characterization by osteopontin expression. It is stated in one of the studies, osteopontin expression was analyzed with RT-PCR at day 7 and 14, the level increased as 1.5 fold at day 14 with respect to day 7 [199]. In our results, we observed about 5 fold increase in expression ration although cells were not lyzed.

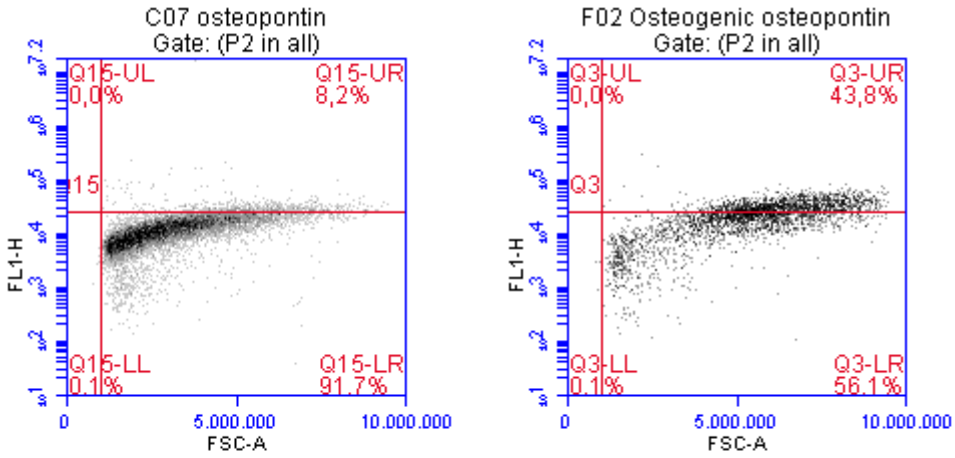

Figure 3.36 Flow cytometry analysis results of urine derived stem cells for osteopontin expression level.

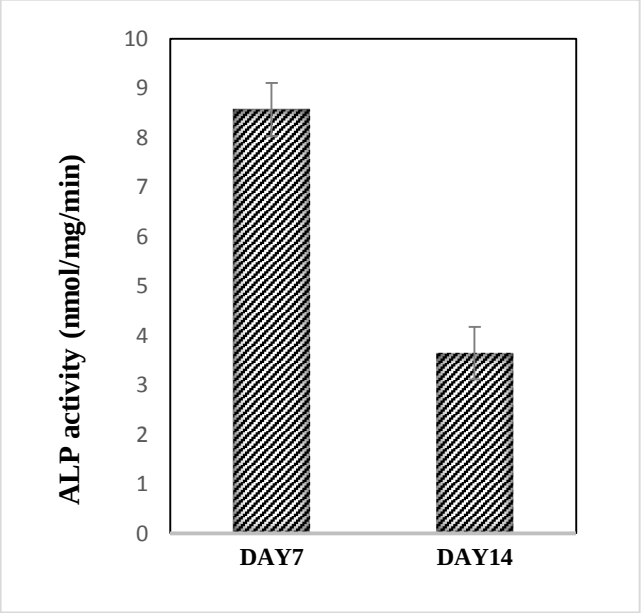

Figure 3.37 The alkaline phosphatase enzyme activity of osteogenic differentiation induced urine derived stem cells at different time points. At day 7 ALP activity was statistically higher than that observed at day14 ($p<0.05$).

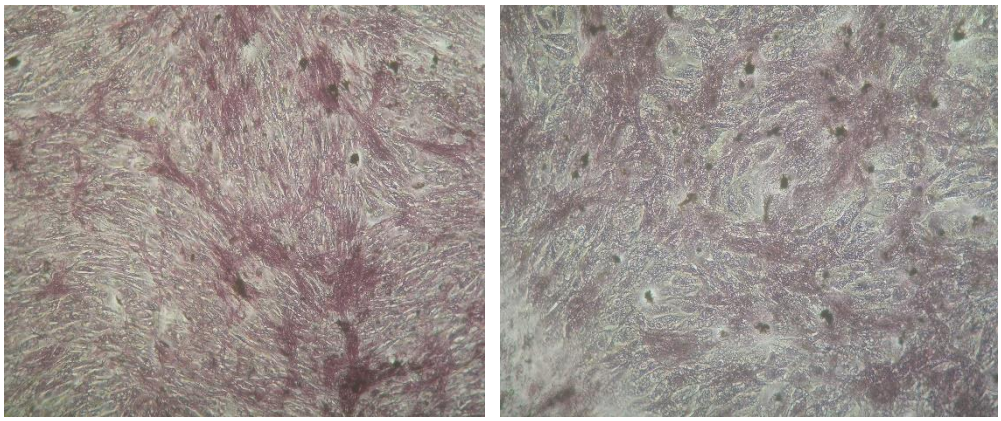

Figure 3.38 The Alizarin Red S staining images of cells incubated in osteogenic medium for 14 days. Red stained regions notify the calcium deposition by the cells. Magnification 10X.

Adipogenic differentiation was confirmed by the morphology change of cells and Oil Red S staining. The cells got more rounded like shape in adipogenic differentiation medium for 2 weeks since they begin to form oil droplets. In Figure 3.35 c, more round

like shaped cells were observed. This was a sign for adipogenic differentiation as shown in other studies [30]. The Oil Red S staining revealed small oil droplets after 2 weeks of incubation (Figure 3.39). Chondrogenic differentiation was studied in monolayer culture of urine derived stem cells in chondrogenic inductive medium supplied with TGF-β3. The pellet cultured in chondrogenic differentiation medium would have been better to obtain the chondrogenic differentiation of cells. In monolayer culture, the cells detached from plate and lost during medium changes. However the phase contrast microscopy images of monolayer cells showed that morphology of cells were similar to these cells. (Figure 3.35c) [193]. For chondrogenic differentiation, USCs of 3 donors were used in their differentiation towards chondrocyte. The authors reported that each clone showed specific capacity to multipotency; one donor's cells differentiated into restricted lineages, one was differentiated into multiple lineages and other showed mixed of capacity. In the light of this finding, the authors pointed out that in clone, the stages of cells vary. This type of cells with restricted differentiation capacity was categorized as differentiating cells among differentiated, differentiating and urine derived stem cells types [193].

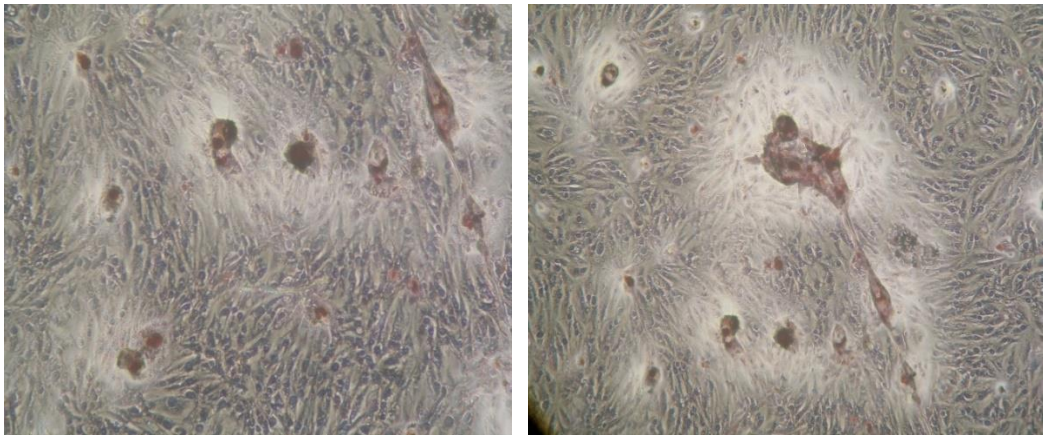

Figure 3.39 The Oil Red S staining images of cells incubated in adipogenic medium for 21 days. Magnification 10X.

In consideration of these results, isolated cells from urine was examined, urine derived stem cells were isolated and expanded. The expansion capacity, self-renewability, multi lineage differentiation potential of our cells gave consistency with stem cells.

The higher yield was obtained in these cells with noninvasive low cost and simple isolation method.

3.3.2.2. In Vitro Cytotoxicity and Osteogenic Effect of Calcium Phosphate Nanoparticles

The cellular viability of urine derived stem cells was determined after incubation with nano calcium phosphate particles at different incubation periods. Relative viabilities of all compositions with respect to control were determined (Figure 3.40). There was no statistically significant difference among different compositions. For all time periods percent cell viabilities of all groups were around 85%. The morphology of cells proved the viability of cells. The cells kept their morphology during assay. In our XRD data (Figure 3.27) the presence of calcium oxide was apparent. Although in previous studies, the cytotoxic effect of CaO impurity was observed with a decrease in cell viability [77,82], Our nanoparticles with CaO impurity showed no cytotoxic effect on urine derived stem cells when added to the culture media at different concentrations.

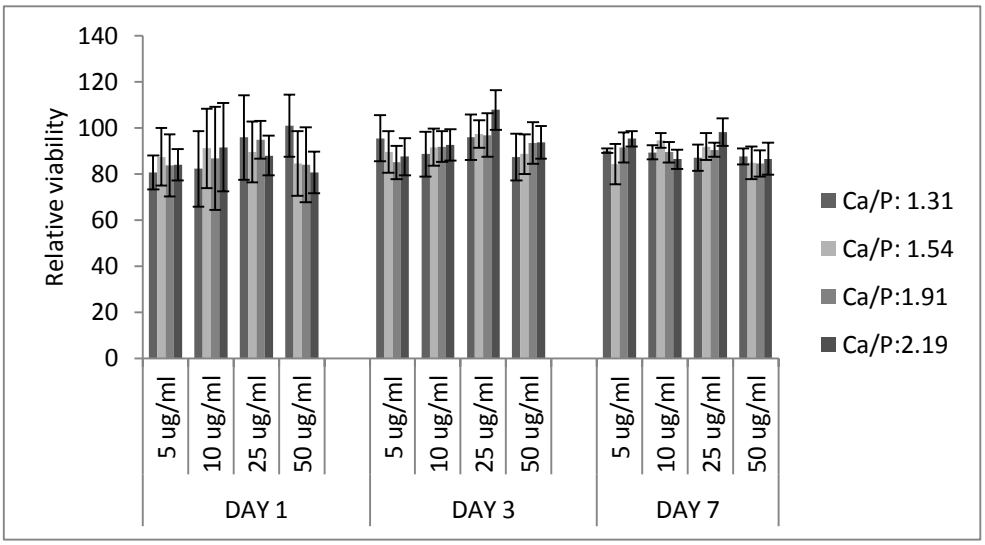

Figure 3.40 Relative cell viability of USCs exposed to different concentrations of calcium phosphate nanoparticles at different Ca/P ratios. Cells that were not exposed to nanoparticles were used as control (n=5)

The effect of as prepared flame synthesized particles on osteogenic differentiation of USCs was studied by measuring alkaline phosphatase (ALP) enzyme activity. To test particles have a positive effect on osteogenic differentiation of urine derived stem cells, biochemical ALP assay was performed and results are given as specific enzyme activity (nmol/min/mg protein). The effect of different concentrations (5, 10, 25 and 50 μg/ ml) of all compositions of calcium phosphate particles (1.20-2.19 Ca/P ratio range) on osteogenic differentiation of cells was studied. A slight decrease in ALP activity of cells treated with two highest Ca:P ratios at 50 μg/ml concentration was observed at day 7 (Figure 3.41). There were no statistically significant differences among concentrations and compositions at two-time points. However, ALP activities of cells for all groups decreased at day 14 in each group. ALP activity at day 7 was statistically higher than observed at day 14 showing that cells progressed to next stage in differentiation [200]. Among all concentrations studied, for 50 μg/ml dose of calcium phosphate, relatively higher enzyme activity level than control was observed. Meanwhile, there was a slight decrease in enzyme activity with increasing calcium to phosphate ratio in 50 μg/ml dose groups. As stated above, physical properties of nanoparticles influence the biological properties of material. Characterization results revealed that particles with increasing calcium to phosphate ratio had more agglomeration, and showed more crystalline behaviors according to XRD patterns, HRTEM images and FFT diffractograms. Increasing crystallinity decreases the dissolution rate of calcium phosphate particles [201].

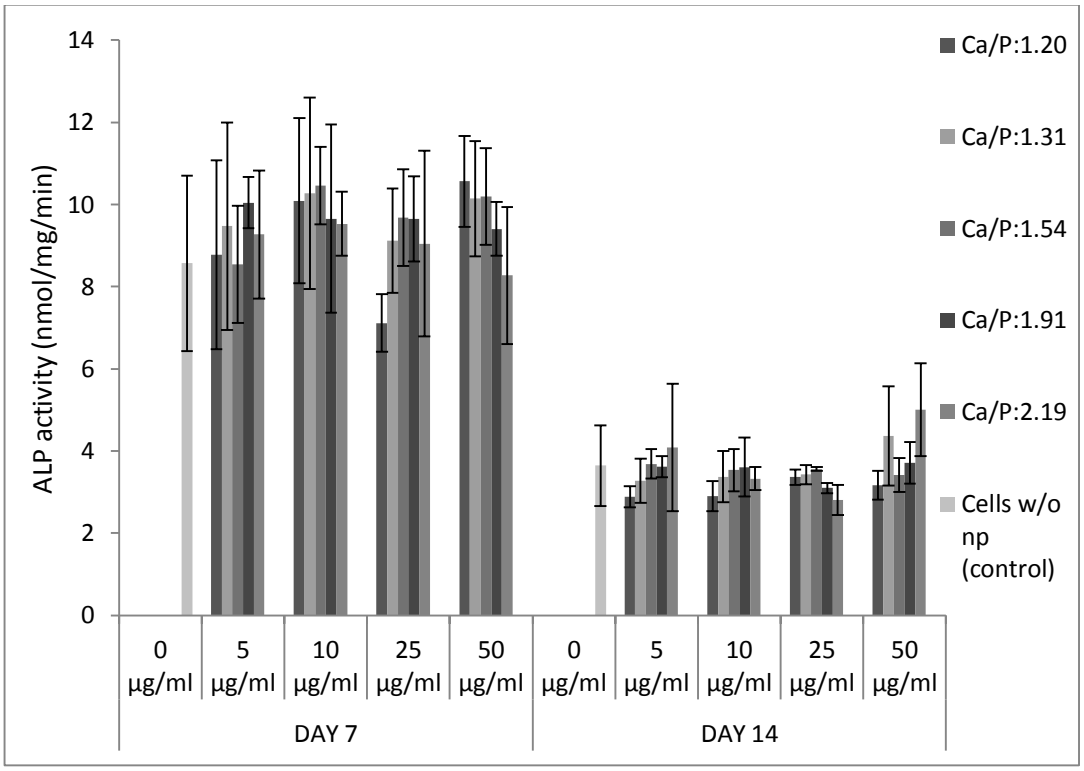

Figure 3.41 ALP activity of USCs that were exposed to different concentrations of CaP nanoparticles of different compositions in osteogenic medium. Cells unexposed to nanoparticles were used as control (n=4). ALP activities of USCs at day 7 were statistically higher than that observed at day14 among all groups ($p<0.05$).

CHAPTER 4

CONCLUSION

In this study, a novel silk fibroin and citrus pectin based porous three-dimensional scaffolds were designed and studied for bone tissue engineering applications. To best of our knowledge silk fibroin and citrus pectin was crosslinked for the first time in literature. The scaffolds were chemically crosslinked with three different methods, namely click reactions, carbodiimide reactions and imine formation reactions. The click chemistry reactions were accomplished and conjugation was characterized, however mixture could not be molded in stabile three dimensional structures. Among all experimental groups the scaffolds crosslinked with 0.015 M borax and treated with methanol and calcium chloride retained structural stability with the lowest weight loses among all groups and high water uptake values.

In this study, urine derived stem cells were isolated and characterized as an alternative stem cell source for bone tissue engineering applications. Additionally, amorphous nano calcium phosphates with different Ca/P ratios (1.20-2.19) were synthesized using Flame Spray Pyrolysis method to reinforce the scaffolds for future studies. An increase in the specific surface area and crystallinity were observed with increasing Ca/P ratios. Human urine derived stem cells were used for testing the *in vitro* biocompatibility of synthesized particles. The results revealed that there was no cytotoxic effect of nanoparticles on stem cells at the 5-50 μg/ml concentration range. Cells treated with prepared nanoparticles had higher alkaline phosphatase (ALP) enzyme activity than the control cells.

As a conclusion, future studies are suggested to be investigated on use of urine derived stem cells (differentiated towards osteogenic lineage) seeded silk fibroin and citrus pectin based scaffolds by incorporating calcium phosphate nanoparticles as a potential engineered construct for regeneration of bone.

REFERENCES

[1] Stevens R. Gray's Anatomy for Students. Ann R Coll Surg Engl 2006;88:513–4. doi:10.1308/003588406X116873b.

[2] Mistry AS, Mikos AG. Tissue Engineering Strategies for Bone Regeneration. In: Ioannis V. Yannas, editor. Regen. Med. II, Springer Berlin Heidelberg; 2005, p. 1–22. doi:10.1007/b99997.

[3] Clarke B. Normal bone anatomy and physiology. Clin J Am Soc Nephrol 2008;3 (supp.):131–9. doi:10.2215/CJN.04151206.

[4] Van Gaalen S, Kruyt M, Meijer G, Mistry A, Mikos A, Beucken J van den, et al. Tissue Engineering of Bone. In: Van Blitterswijk CA, editor. Tissue Eng. 1st ed., London: Academic Press, Elsevier; 2008, p. 559–610. doi:10.1016/B978-0-12-370869-4.00019-7.

[5] Sadat-Shojai M, Khorasani M-T, Dinpanah-Khoshdargi E, Jamshidi A. Synthesis methods for nanosized hydroxyapatite with diverse structures. Acta Biomater 2013;9:7591–621. doi:10.1016/j.actbio.2013.04.012.

[6] Currey JD. The structure and mechanics of bone. J Mater Sci 2012;47:41–54. doi:10.1007/s10853-011-5914-9.

[7] Martin RB. Bones: structure and mechanics: John D. Currey (Ed.), Princeton University Press or Amazon.com, Princeton, NJ. J Biomech 2003;36:893. doi:10.1016/S0021-9290(03)00033-2.

[8] Barrère F, van Blitterswijk C, de Groot K. Bone regeneration: molecular and cellular interactions with calcium phosphate ceramics. Int J Nanomedicine 2006;1:317–32.

[9] O' Keefe RJ, Mao J. Bone Tissue Engineering and Regeneration : From Discovery to the Clinic — An Overview. Tissue Eng Part B 2011;17:389–92. doi:10.1089/ten.teb.2011.0475.

[10] Le C, Bao M, Teo EY, Chong MSK, Liu Y, Choolani M, et al. Advances in Bone Tissue Engineering. In: Andrades JA, editor. Regen. Med. Tissue Eng. 1st ed., Intech; 2013, p. 599–613.

[11] Muschler GF, Nakamoto C, Griffith LG. Engineering principles of clinical cell-based tissue engineering. J Bone Joint Surg Am 2004;86-A:1541–58.

[12] Altman GH, Diaz F, Jakuba C, Calabro T, Horan RL, Chen J, et al. Silk-based biomaterials. Biomaterials 2003;24:401–16.

[13] Lanza R, Langer R, Vacanti J. Principles of Tissue Engineering. 3rd ed. California: Elsevier Inc.; 2007.

[14] Amini AR, Laurencin CT, Nukavarapu ST. Bone Tissue Engineering: Recent Advances and Challenges. Crit Rev Biomed Eng 2013;40:363–408. doi:10.1615/CritRevBiomedEng.v40.i5.10.

[15] Burdick JA, Anseth KS. Photoencapsulation of osteoblasts in injectable RGD-modified PEG hydrogels for bone tissue engineering. Biomaterials 2002;23:4315–23. doi:10.1016/S0142-9612(02)00176-X.

[16] Schimming R, Schmelzeisen R. Tissue-engineered bone for maxillary sinus augmentation. J Oral Maxillofac Surg 2004;62:724–9. doi:10.1016/j.joms.2004.01.009.

[17] Blau HM, Brazelton TR, Weimann JM. The evolving concept of a stem cell: Entity or function? Cell 2001;105:829–41. doi:10.1016/S0092-8674(01)00409-3.

[18] Yu J, Thomson JA. Embryonic Stem Cells : Derivation and Properties. Princ. Regen. Med. Second Edi, Elsevier Inc.; 2011, p. 199–214. doi:10.1016/B978-0-12-381422-7.10010-0.

[19] Thomson JA. Embryonic Stem Cell Lines Derived from Human Blastocysts. Science (80-) 1998;282:1145–7. doi:10.1126/science.282.5391.1145.

[20] Kawaguchi J, Mee PJ, Smith AG. Osteogenic and chondrogenic differentiation of embryonic stem cells in response to specific growth factors. Bone 2005;36:758–69. doi:10.1016/j.bone.2004.07.019.

[21] Salgado AJ, Coutinho OP, Reis RL. Bone tissue engineering: state of the art and future trends. Macromol Biosci 2004;4:743–65. doi:10.1002/mabi.200400026.

[22] Seong JM, Kim B-C, Park J-H, Kwon IK, Mantalaris A, Hwang Y-S. Stem cells in bone tissue engineering. Biomed Mater 2010;5:062001. doi:10.1088/1748-6041/5/6/062001.

[23] Colnot C. Cell Sources for Bone Tissue Engineering: Insights from Basic Science. Tissue Eng Part B Rev 2011;17:449–57. doi:10.1089/ten.teb.2011.0243.

[24] Meijer GJ, De Bruijn JD, Koole R, Van Blitterswijk CA. Cell-based bone tissue engineering. J PLoS Med 2007;4:0260–4. doi:10.1371/journal.pmed.0040009.

[25] Shin M, Yoshimoto H, Vacanti JP. In vivo bone tissue engineering using mesenchymal stem cells on a novel electrospun nanofibrous scaffold. Tissue Eng 2004;10:33–41. doi:10.1089/107632704322791673.

[26] Correia C, Bhumiratana S, Yan L-P, Oliveira AL, Gimble JM, Rockwood D, et al. Development of silk-based scaffolds for tissue engineering of bone from human adipose-derived stem cells. Acta Biomater 2012;8:2483–92. doi:10.1016/j.actbio.2012.03.019.

[27] Bharadwaj S, Liu G, Shi Y, Markert C, Andersson K-E, Atala A, et al. Characterization of urine-derived stem cells obtained from upper urinary tract for use in cell-based urological tissue engineering. Tissue Eng Part A 2011;17:2123–32. doi:10.1089/ten.tea.2010.0637.

[28] Zhang Y, McNeill E, Tian H, Soker S, Andersson KE, Yoo JJ, et al. Urine Derived Cells are a Potential Source for Urological Tissue Reconstruction. J Urol 2008;180:2226–33. doi:10.1016/j.juro.2008.07.023.

[29] Liu G, Deng C, Zhang Y. Stem Cells: Current Challenges and New Directions 2013:19–29. doi:10.1007/978-1-4614-8066-2.

[30] Guan, J J , Niu, X , Gong, F , Guo SC. Biological Characteristics of Human-Urine-Derived Stem Cells : Potential for Cell Based Therapy in Neurology. Tissue Eng Part A 2014;20:1–13. doi:10.1089/ten.tea.2013.0584.

[31] Liu G, Deng C, Zhang Y. Urine-Derived Stem Cells: Biological Characterization and Potential Clinical Applications. In: Turksen K, editor. Stem Cells Curr. Challenges New Dir., New York, NY: Springer New York; 2013, p. 19–29. doi:10.1007/978-1-4614-8066-2.

[32] Bodin A, Bharadwaj S, Wu S, Gatenholm P, Atala A, Zhang Y. Tissue-engineered conduit using urine-derived stem cells seeded bacterial cellulose polymer in urinary reconstruction and diversion. Biomaterials 2010;31:8889–901. doi:10.1016/j.biomaterials.2010.07.108.

[33] Liu G, Wang X, Sun X, Deng C, Atala A, Zhang Y. The effect of urine-derived stem cells expressing VEGF loaded in collagen hydrogels on myogenesis and innervation following after subcutaneous implantation in nude mice. Biomaterials 2013;34:8617–29. doi:10.1016/j.biomaterials.2013.07.077.

[34] Wang L, Wang L, Huang W, Su H, Xue Y, Su Z, et al. Generation of integration-free neural progenitor cells from cells in human urine. Nat Methods 2013;10:84–9. doi:10.1038/nmeth.2283.

[35] Qin H, Zhu C, An Z, Jiang Y, Zhao Y, Wang J, et al. Silver nanoparticles promote osteogenic differentiation of human urine-derived stem cells at noncytotoxic concentrations. Int J Nanomedicine 2014;9:2469–78. doi:10.2147/IJN.S59753.

[36] Hollister SJ, Murphy WL. Scaffold Translation: Barriers Between Concept and Clinic. Tissue Eng Part B Rev 2011;17:459–74. doi:10.1089/ten.teb.2011.0251.

[37] Correlo VM, Oliveira JM, Mano JF, Neves NM, Reis RL. Natural Origin Materials for Bone Tissue Engineering – Properties, Processing, and Performance. In: Atala A, Lanza R, Thomson J, Nerem R, editors. Princ. Regen. Med. Second Edi, Elsevier Inc.; 2011, p. 557–86. doi:10.1016/B978-0-12-381422-7.10032-X.

[38] Mano JF, Silva GA, Azevedo HS, Malafaya PB, Sousa RA, Silva SS, et al. Natural origin biodegradable systems in tissue engineering and regenerative medicine: present status and some moving trends. J R Soc Interface 2007;4:999–1030. doi:10.1098/rsif.2007.0220.

[39] Ige OO, Umoru LE, Aribo S. Natural Products: A Minefield of Biomaterials. ISRN Mater Sci 2012;2012:1–20. doi:10.5402/2012/983062.

[40] Hacker MC, Mikos AG. Synthetic Polymers. In: Atala A, Lanza R, Thomson J, Nerem R, editors. Princ. Regen. Med. Second Edi, Elsevier Inc.; 2011, p. 587–622. doi:10.1016/B978-0-12-381422-7.10033-1.

[41] Fakhry A, Schneider GB, Zaharias R, Senel S. Chitosan supports the initial attachment and spreading of osteoblasts preferentially over fibroblasts. Biomaterials 2004;25:2075–9. doi:10.1016/j.biomaterials.2003.08.068.

[42] Alsberg E, Anderson KW, Albeiruti A, Franceschi RT, Mooney DJ. Cell-interactive alginate hydrogels for bone tissue engineering. J Dent Res 2001;80:2025–9. doi:10.1177/00220345010800111501.

[43] Gravel M, Gross T, Vago R, Tabrizian M. Responses of mesenchymal stem cell to chitosan-coralline composites microstructured using coralline as gas forming agent.Biomaterials2006;27:1899–906. doi:10.1016/j.biomaterials.2005.10.020.

[44] Kenny SM, Buggy M. Bone cements and fillers: A review. J Mater Sci Mater Med 2003;14:923–38. doi:10.1023/A:1026394530192.

[45] Cao H, Kuboyama N. A biodegradable porous composite scaffold of PGA/beta-TCP for bone tissue engineering. Bone 2010;46:386–95. doi:10.1016/j.bone.2009.09.031.

[46] Mistry AS, Pham QP, Schouten C, Yeh T, Christenson EM, Mikos AG, et al. In vivo bone biocompatibility and degradation of porous fumarate-based polymer/alumoxane nanocomposites for bone tissue engineering. J Biomed Mater Res - Part A 2010;92:451–62. doi:10.1002/jbm.a.32371.

[47] Rockwood DN, Preda RC, Yücel T, Wang X, Lovett ML, Kaplan DL. Materials fabrication from Bombyx mori silk fibroin. Nat Protoc 2011;6:1612–31. doi:10.1038/nprot.2011.379.

[48] Murphy AR, Kaplan DL. Biomedical applications of chemically-modified silk fibroin. J Mater Chem 2009;19:6443–50. doi:10.1039/b905802h.

[49] Gomes M, Azevedo H, Malafaya P, Silva S, Oliveira J, Silva G, et al. Natural Polymers in Tissue Engineering Applications. In: van Blitterswijk C, Thomsen P, Lindahl A, Hubbell J, Williams D, Cancedda R, et al., editors. Tissue Eng. 1st ed., Elsevier Inc.; 2008, p. 145–92. doi:10.1016/B978-0-12-370869-4.00006-9.

[50] Jmol: an open-source Java viewer for chemical structures in 3D n.d. http://jmol.sourceforge.net/#How to cite Jmol (accessed December 07, 2014).

[51] He YX, Zhang NN, Li WF, Jia N, Chen BY, Zhou K, et al. N-terminal domain of Bombyx mori fibroin mediates the assembly of silk in response to pH decrease. J Mol Biol 2012;418:197–207. doi:10.1016/j.jmb.2012.02.040.

[52] Omenetto FG, Kaplan DL. New opportunities for an ancient material. Science 2010;329:528–31. doi:10.1126/science.1188936.

[53] Kim HJ, Kim UJ, Kim HS, Li C, Wada M, Leisk GG, et al. Bone tissue engineering with premineralized silk scaffolds. Bone 2008;42:1226–34. doi:10.1016/j.bone.2008.02.007.

[54] Li C, Vepari C, Jin H-J, Kim HJ, Kaplan DL. Electrospun silk-BMP-2 scaffolds for bone tissue engineering. Biomaterials 2006;27:3115–24. doi:10.1016/j.biomaterials.2006.01.022.

[55] Bhumiratana S, Grayson WL, Castaneda A, Rockwood DN, Gil ES, Kaplan DL, et al. Nucleation and growth of mineralized bone matrix on silk-hydroxyapatite composite scaffolds. Biomaterials 2011;32:2812–20. doi:10.1016/j.biomaterials.2010.12.058.

[56] Parenteau-Bareil R, Gauvin R, Berthod F. Collagen-based biomaterials for tissue engineering applications. Materials (Basel) 2010;3:1863–87. doi:10.3390/ma3031863.

[57] Bella J, Eaton M, Brodsky B, Berman HM. Crystal and molecular structure of a collagen-like peptide at 1.9 A resolution. Science 1994;266:75–81. doi:10.1126/science.7695699.

[58] Lee CH, Singla A, Lee Y. Biomedical applications of collagen. Int J Pharm 2001;221:1–22. doi:10.1016/S0378-5173(01)00691-3.

[59] Inzana J a, Olvera D, Fuller SM, Kelly JP, Graeve O a, Schwarz EM, et al. 3D printing of composite calcium phosphate and collagen scaffolds for bone regeneration. Biomaterials 2014;35:4026–34. doi:10.1016/j.biomaterials.2014.01.064.

[60] Coimbra P, Ferreira P, de Sousa HC, Batista P, Rodrigues MA, Correia IJ, et al. Preparation and chemical and biological characterization of a pectin/chitosan polyelectrolyte complex scaffold for possible bone tissue engineering applications. Int J Biol Macromol 2011;48:112–8. doi:10.1016/j.ijbiomac.2010.10.006.

[61] Liu L, Won YJ, Cooke PH, Coffin DR, Fishman ML, Hicks KB, et al. Pectin/poly(lactide-co-glycolide) composite matrices for biomedical applications. Biomaterials 2004;25:3201–10. doi:10.1016/j.biomaterials.2003.10.036.

[62] Munarin F, Guerreiro SG, Grellier MA, Tanzi MC, Barbosa MA, Petrini P, et al. Pectin-based injectable biomaterials for bone tissue engineering. Biomacromolecules 2011;12:568–77. doi:10.1021/bm101110x.

[63] Takei T, Sato M, Ijima H, Kawakami K. In situ gellable oxidized citrus pectin for localized delivery of anticancer drugs and prevention of homotypic cancer cell aggregation. Biomacromolecules 2010;11:3525–30. doi:10.1021/bm1010068.

[64] Kokkonen H. Aspects of bone sugar biology. University of Oulu, 2009.

[65] Alborzi S, Lim LT, Kakuda Y. Electrospinning of sodium alginate-pectin ultrafine fibers. J Food Sci 2010;75:100–7. doi:10.1111/j.1750-3841.2009.01437.x.

[66] Ichibouji T, Miyazaki T, Ishida E, Sugino A, Ohtsuki C. Apatite mineralization abilities and mechanical properties of covalently cross-linked pectin hydrogels. Mater Sci Eng C 2009;29:1765–9. doi:10.1016/j.msec.2009.01.027.

[67] Sun J, Tan H. Alginate-Based Biomaterials for Regenerative Medicine Applications. Materials (Basel) 2013;6:1285–309. doi:10.3390/ma6041285.

[68] Franklin MJ, Nivens DE, Weadge JT, Lynne Howell P. Biosynthesis of the pseudomonas aeruginosa extracellular polysaccharides, alginate, Pel, and Psl. Front Microbiol 2011;2. doi:10.3389/fmicb.2011.00167.

[69] Kuo CK, Ma PX. Ionically crosslinked alginate hydrogels as scaffolds for tissue engineering: Part 1. Structure, gelation rate and mechanical properties. Biomaterials 2001;22:511–21. doi:10.1016/S0142-9612(00)00201-5.

[70] Li Z, Ramay HR, Hauch KD, Xiao D, Zhang M. Chitosan-alginate hybrid scaffolds for bone tissue engineering. Biomaterials 2005;26:3919–28. doi:10.1016/j.biomaterials.2004.09.062.

[71] Suárez-González D, Barnhart K, Saito E, Vanderby R, Hollister SJ, Murphy WL. Controlled nucleation of hydroxyapatite on alginate scaffolds for stem cell-based bone tissue engineering. J Biomed Mater Res - Part A 2010;95:222–34. doi:10.1002/jbm.a.32833.

[72] Lin H-R, Yeh Y-J. Porous alginate/hydroxyapatite composite scaffolds for bone tissue engineering: preparation, characterization, and in vitro studies. J Biomed Mater Res B Appl Biomater 2004;71:52–65. doi:10.1002/jbm.b.30065.

[73] Chen F, Zhu Y, Wu J, Huang P, Cui D. Nanostructured Calcium Phosphates : Preparation and Their Application in Biomedicine. Nano Biomed Eng 2012;1:41–9. doi:10.5101/nbe.v4i1.p41-49.1.

[74] Lobo SE, Livingston Arinzeh T. Biphasic Calcium Phosphate Ceramics for Bone Regeneration and Tissue Engineering Applications. Materials (Basel) 2010;3:815–26. doi:10.3390/ma3020815.

[75] Mohn D, Ege D, Feldman K, Schneider OD, Imfeld T, Boccaccini AR, et al. Spherical Calcium Phosphate Nanoparticle Fillers Allow Polymer Processing of Bone Fixation Devices with High Bioactivity. Polym Eng Sci 2010;50:952–60. doi:10.1002/pen.

[76] Thein-Han WW, Misra RDK. Biomimetic chitosan-nanohydroxyapatite composite scaffolds for bone tissue engineering. Acta Biomater 2009;5:1182–97. doi:10.1016/j.actbio.2008.11.025.

[77] Mohn D, Doebelin N, Tadier S, Bernabei RE, Luechinger N a., Stark WJ, et al. Reactivity of calcium phosphate nanoparticles prepared by flame spray synthesis as precursors for calcium phosphate cements. J Mater Chem 2011;21:13963. doi:10.1039/c1jm11977j.

[78] Cho JS, Ko YN, Jung DS, Jang HC, Lee M-J, Kang YC. Characteristics of size controlled hydroxyapatite powders with nanometer size prepared by flame spray pyrolysis. J Ceram Soc Japan 2009;117:1060–4. doi:10.2109/jcersj2.117.1060.

[79] Loher S, Stark WJ, Maciejewski M, Baiker A, Pratsinis SE, Reichardt D, et al. Fluoro-apatite and Calcium Phosphate Nanoparticles by Flame Synthesis. Chem Mater 2005;1999:725–31. doi:10.1021/cm048776c.

[80] Buzea C, Blandino IIP, Robbie K. Nanomaterials and nanoparticles : Sources and toxicity. Biointerphase 2007;2:1–103.

[81] Stark WJ. Nanoparticles in biological systems. Angew Chem Int Ed Engl 2011;50:1242–58. doi:10.1002/anie.200906684.

[82] Liu H, Yazici H, Ergun C, Webster TJ, Bermek H. An in vitro evaluation of the Ca/P ratio for the cytocompatibility of nano-to-micron particulate calcium phosphates for bone regeneration. Acta Biomater 2008;4:1472–9. doi:10.1016/j.actbio.2008.02.025.

[83] Zhou H, Lee J. Nanoscale hydroxyapatite particles for bone tissue engineering. Acta Biomater 2011;7:2769–81. doi:10.1016/j.actbio.2011.03.019.

[84] Hild N, Schneider OD, Mohn D, Luechinger N a, Koehler FM, Hofmann S, et al. Two-layer membranes of calcium phosphate/collagen/PLGA nanofibres: in vitro biomineralisation and osteogenic differentiation of human mesenchymal stem cells. Nanoscale 2011;3:401–9. doi:10.1039/c0nr00615g.

[85] Schneider OD, Loher S, Brunner TJ, Uebersax L, Simonet M, Grass RN, et al. Cotton Wool-Like Nanocomposite Biomaterials Prepared by Electrospinning : In vitro Bioactivity and Osteogenic Differentiation of Human Mesenchymal Stem Cells. J Biomed Mater Res Part B Appl Biomater 2007;84:350–62. doi:10.1002/jbmb.

[86] Dorozhkin S V. Nanosized and nanocrystalline calcium orthophosphates. Acta Biomater 2010;6:715–34. doi:10.1016/j.actbio.2009.10.031.

[87] Hoppe A, Güldal NS, Boccaccini AR. A review of the biological response to ionic dissolution products from bioactive glasses and glass-ceramics. Biomaterials 2011;32:2757–74. doi:10.1016/j.biomaterials.2011.01.004.

[88] Teoh WY, Amal R, Mädler L. Flame spray pyrolysis: An enabling technology for nanoparticles design and fabrication. Nanoscale 2010;2:1324–47. doi:10.1039/c0nr00017e.

[89] Madler L, Kammler HK, Mueller R, Pratsinis SE. Controlled synthesis of nanostructured particles by flame spray pyrolysis. J Aerosol Sci 2002;33:369–89. doi:10.1016/S0021-8502(01)00159-8.

[90] Pratsinis SE. Flame aerosol synthesis of ceramic powders. Prog Energy Combust Sci 1998;24:197–219. doi:10.1016/S0360-1285(97)00028-2.

[91] Maciejewski M, Brunner TJ, Loher SF, Stark WJ, Baiker A. Phase transitions in amorphous calcium phosphates with different Ca/P ratios. Thermochim Acta 2008;468:75–80. doi:10.1016/j.tca.2007.11.022.

[92] Cho JS, Kang YC. Nano-sized hydroxyapatite powders prepared by flame spray pyrolysis. J Alloys Compd 2008;464:282–7. doi:10.1016/j.jallcom.2007.09.092.

[93] Tofighi A, Palazzolo R. Calcium Phosphate Bone Cement Preparation Using Mechano-Chemical Process. Key Eng Mater 2005;284-286:101–4. doi:10.4028/www.scientific.net/KEM.284-286.101.

[94] Combes C, Rey C. Amorphous calcium phosphates: synthesis, properties and uses in biomaterials. Acta Biomater 2010;6:3362–78. doi:10.1016/j.actbio.2010.02.017.

[95] El Briak-Benabdeslam H, Ginebra MP, Vert M, Boudeville P. Wet or dry mechanochemical synthesis of calcium phosphates? Influence of the water content on DCPD-CaO reaction kinetics. Acta Biomater 2008;4:378–86. doi:10.1016/j.actbio.2007.07.003.

[96] Fathi M., Hanifi A, Mortazavi V. Preparation and bioactivity evaluation of bone-like hydroxyapatite nanopowder. J Mater Process Technol 2008;202:536–42. doi:10.1016/j.jmatprotec.2007.10.004.

[97] Hench LL, Polak JM. Third-generation biomedical materials. Science 2002;295:1014–7. doi:10.1126/science.1067404.

[98] Sarkar MR, Wachter N, Patka P, Kinzl L. First histological observations on the incorporation of a novel calcium phosphate bone substitute material in human cancellous bone. J Biomed Mater Res 2001;58:329–34.

[99] Deville S, Saiz E, Tomsia AP. Freeze casting of hydroxyapatite scaffolds for bone tissue engineering. Biomaterials 2006;27:5480–9. doi:10.1016/j.biomaterials.2006.06.028.

[100] Liu X, Smith LA, Hu J, Ma PX. Biomimetic nanofibrous gelatin/apatite composite scaffolds for bone tissue engineering. Biomaterials 2009;30:2252–8. doi:10.1016/j.biomaterials.2008.12.068.

[101] Holzwarth JM, Ma PX. Biomimetic nanofibrous scaffolds for bone tissue engineering. Biomaterials 2011;32:9622–9. doi:10.1016/j.biomaterials.2011.09.009.

[102] Bergmann C, Lindner M, Zhang W, Koczur K, Kirsten A, Telle R, et al. 3D printing of bone substitute implants using calcium phosphate and bioactive glasses. J Eur Ceram Soc 2010;30:2563–7. doi:10.1016/j.jeurceramsoc.2010.04.037.

[103] Seitz H, Rieder W, Irsen S, Leukers B, Tille C. Three-dimensional printing of porous ceramic scaffolds for bone tissue engineering. J Biomed Mater Res B Appl Biomater 2005;74:782–8. doi:10.1002/jbm.b.30291.

[104] Fierz FC, Beckmann F, Huser M, Irsen SH, Leukers B, Witte F, et al. The morphology of anisotropic 3D-printed hydroxyapatite scaffolds. Biomaterials 2008;29:3799–806. doi:10.1016/j.biomaterials.2008.06.012.

[105] Zorlutuna P, Annabi N, Camci-Unal G, Nikkhah M, Cha JM, Nichol JW, et al. Microfabricated biomaterials for engineering 3D tissues. Adv Mater 2012;24:1782–804. doi:10.1002/adma.201104631.

[106] McCullen SD, Miller PR, Gittard SD, Gorga RE, Pourdeyhimi B, Narayan RJ, et al. In situ collagen polymerization of layered cell-seeded electrospun scaffolds for bone tissue engineering applications. Tissue Eng Part C Methods 2010;16:1095–105. doi:10.1089/ten.tec.2009.0753.

[107] Brun P, Ghezzo F, Roso M, Danesin R, Palù G, Bagno A, et al. Electrospun scaffolds of self-assembling peptides with poly(ethylene oxide) for bone tissue engineering. Acta Biomater 2011;7:2526–32. doi:10.1016/j.actbio.2011.02.025.

[108] Ramakrishna S, Fujihara K, Teo W, Lim T, Ma Z. An introduction to Electrospinning and Nanofibers. Singapore: World Scientific Publishing; 2005.

[109] Greiner A, Wendorff JH. Electrospinning: A fascinating method for the preparation of ultrathin fibers. Angew Chemie - Int Ed 2007;46:5670–703. doi:10.1002/anie.200604646.

[110] Lee W-Y, Cheng W-Y, Yeh Y-C, Lai C-H, Hwang S-M, Hsiao C-W, et al. Magnetically directed self-assembly of electrospun superparamagnetic fibrous bundles to form three-dimensional tissues with a highly ordered architecture. Tissue Eng Part C Methods 2011;17:651–61. doi:10.1089/ten.tec.2010.0621.

[111] Liu X, Ma PX. Polymeric Scaffolds for Bone Tissue Engineering. Ann Biomed Eng 2004;32:477–86.

[112] Liu X, Jin X, Ma PX. Nanofibrous hollow microspheres self-assembled from star-shaped polymers as injectable cell carriers for knee repair. Nat Mater 2011;10:398–406. doi:10.1038/nmat2999.

[113] Liu X, Ma PX. Phase separation, pore structure, and properties of nanofibrous gelatin scaffolds. Biomaterials 2009;30:4094–103. doi:10.1016/j.biomaterials.2009.04.024.

[114] Elbert DL, Hubbell JA. Conjugate addition reactions combined with free-radical cross-linking for the design of materials for tissue engineering. Biomacromolecules 2001;2:430–41. doi:10.1021/bm0056299.

[115] Hennink WE, van Nostrum CF. Novel crosslinking methods to design hydrogels. Adv Drug Deliv Rev 2012;64:223–36. doi:10.1016/j.addr.2012.09.009.

[116] Yokoyama F, Masada I, Shimamura K, Ikawa T, Monobe K. Morphology and structure of highly elastic poly(vinyl alcohol) hydrogel prepared by repeated freezing-and-melting. Colloid Polym Sci 1986;264:595–601. doi:10.1007/BF01412597.

[117] Pieper JS, Hafmans T, Veerkamp JH, Van Kuppevelt TH. Development of tailor-made collagen-glycosaminoglycan matrices: EDC/NHS crosslinking, and ultrastructural aspects. Biomaterials 2000;21:581–93. doi:10.1016/S0142-9612(99)00222-7.

[118] Kim KJ, Lee SB, Han NW. Kinetics of crosslinking reaction of PVA membrane with glutaraldehyde. Korean J Chem Eng 1994;11:41–7. doi:10.1007/BF02697513.

[119] Lin W-H, Tsai W-B. In situ UV-crosslinking gelatin electrospun fibers for tissue engineering applications. Biofabrication 2013;5:035008. doi:10.1088/1758-5082/5/3/035008.

[120] Gupta B, Tummalapalli M, Deopura BL, Alam MS. Preparation and characterization of in-situ crosslinked pectin-gelatin hydrogels. Carbohydr Polym 2014;106:312–8. doi:10.1016/j.carbpol.2014.02.019.

[121] Weng L, Chen X, Chen W. Rheological characterization of in situ crosslinkable hydrogels formulated from oxidized dextran and N-carboxyethyl chitosan. Biomacromolecules 2007;8:1109–15. doi:10.1021/bm0610065.

[122] Speer DP, Chvapil M, Eskelson CD, Ulreich J. Biological effects of residual glutaraldehyde in glutaraldehyde-tanned collagen biomaterials. J Biomed Mater Res 1980;14:753–64. doi:10.1002/jbm.820140607.

[123] Kolb HC, Finn MG, Sharpless KB. Click Chemistry: Diverse Chemical Function from a Few Good Reactions. Angew Chemie - Int Ed 2001;40:2004–21.doi:10.1002/1521-3773(20010601)40:11<2004::AID-NIE2004>3.0.CO;2-5.

[124] Huisgen R. 1,3-Dipolar Cycloadditions. Past and Future. Angew Chemie Int Ed English 1963;2:565–98. doi:10.1002/anie.196305651.

[125] Hermanson GT. Bioconjugate techniques. Second. London: Elsevier; 2008.

[126] Lin F. Preparing Polymeric Biomaterials using "Click" Chemistry Techniques. University of Akron, 2014.

[127] Nimmo CM. Diels-Alder Click Cross-Linked Hyaluronic Acid Hydrogels for Tissue Engineering by Diels-Alder Click-Crosslinked Hyaluronic Acid Hydrogels for Tissue Engineering. University of Toronto, 2011.

[128] Baskin JM, Bertozzi CR. Copper-Free Click Chemistry. Click Chem. Biotechnol. Mater. Sci., 2009, p. 29–51. doi:10.1002/9780470748862.ch3.

[129] Jewett JC, Bertozzi CR. Cu-free click cycloaddition reactions in chemical biology. Chem Soc Rev 2010;39:1272–9. doi:10.1039/b901970g.

[130] Zhao H, Heusler E, Jones G, Li L, Werner V, Germershaus O, et al. Decoration of silk fibroin by click chemistry for biomedical application. J Struct Biol 2014. doi:10.1016/j.jsb.2014.02.009.

[131] Kulbokaite R, Ciuta G, Netopilik M, Makuska R. N-PEG'ylation of chitosan via "click chemistry" reactions. React Funct Polym 2009;69:771–8. doi:10.1016/j.reactfunctpolym.2009.06.010.

[132] Crescenzi V, Di Chiara M, Galesso D. Hyaluronic acid derivatives obtained via "click chemistry" crosslinking., 2008.

[133] Sampaio S, Miranda TMR, Santos JG, Soares GMB. Preparation of silk fibroin-poly(ethylene glycol) conjugate films through click chemistry. Polym Int 2011;60:1737–44. doi:10.1002/pi.3143.

[134] Gotoh Y, Tsukada M, Baba T, Minoura N. Physical properties and structure of poly(ethylene glycol)-silk fibroin conjugate films. Polymer (Guildf) 1997;38:487–90. doi:10.1016/S0032-3861(96)00665-9.

[135] Li G, Liu H, Li T, Wang J. Surface modification and functionalization of silk fibroin fibers/fabric toward high performance applications. Mater Sci Eng C 2012;32:627–36. doi:10.1016/j.msec.2011.12.013.

[136] Galeotti F, Andicsova A, Bertini F, Botta C. A versatile click-grafting approach to surface modification of silk fibroin films. J Mater Sci 2013;48:7004–10. doi:10.1007/s10853-013-7509-0.

[137] Das S, Pati D, Tiwari N, Nisal A, Sen Gupta S. Synthesis of silk fibroin-glycopolypeptide conjugates and their recognition with lectin. Biomacromolecules 2012;13:3695–702. doi:10.1021/bm301170u.

[138] Truong VX, Ablett MP, Gilbert HTJ, Bowen J, Richardson SM, Hoyland J a., et al. In situ-forming robust chitosan-poly(ethylene glycol) hydrogels prepared by copper-free azide–alkyne click reaction for tissue engineering. Biomater Sci 2014;2:167. doi:10.1039/c3bm60159e.

[139] Breger J, Fisher B, Samy R, Pollack S, Wang NS, Isayeva I. Synthesis of "click" alginate hydrogel capsules and comparison of their sta...: METUnique Search. J Biomed Mater Res B Appl Biomater 2014. doi:doi: 10.1002/jbm.b.33282.

[140] Pahimanolis N, Vesterinen AH, Rich J, Seppala J. Modification of dextran using click-chemistry approach in aqueous media. Carbohydr Polym 2010;82:78–82. doi:10.1016/j.carbpol.2010.04.025.

[141] Evans HL, Slade RL, Carroll L, Smith G, Nguyen Q-D, Iddon L, et al. Copper-free click—a promising tool for pre-targeted PET imaging. Chem Commun 2012;48:991. doi:10.1039/c1cc16220a.

[142] Singh I, Heaney F. Solid phase strain promoted "click" modification of DNA via [3+2]-nitrile oxide-cyclooctyne cycloadditions. Chem Commun (Camb) 2011;47:2706–8. doi:10.1039/c0cc03985c.

[143] Yamamoto Y, Kurihara K, Yamada A, Takahashi M, Takahashi Y, Miyaura N. Intramolecular allylboration of γ-(ω-formylalkoxy)allylboronates for syntheses of trans- or cis-2-(ethenyl)tetrahydropyran-3-ol and 2-(ethenyl)oxepan-3-ol. Tetrahedron 2003;59:537–42. doi:10.1016/S0040-4020(02)01557-0.

[144] Sylvester KT, Chirik PJ. Iron-catalyzed, hydrogen-mediated reductive cyclization of 1,6-enynes and diynes: Evidence for bis(imino)pyridine ligand participation. J Am Chem Soc 2009;131:8772–4. doi:10.1021/ja902478p.

[145] O'Neil EJ, DiVittorio KM, Smith BD. Phosphatidylcholine-derived bolaamphiphiles via click chemistry. Org Lett 2007;9:199–202. doi:10.1021/ol062557a.

[146] Loka RS, Sadek CM, Romaniuk NA, Cairo CW. Conjugation of synthetic N-acetyl-lactosamine to azide-containing proteins using the staudinger ligation. Bioconjug Chem 2010;21:1842–9. doi:10.1021/bc100209r.

[147] Grajkowski A, Cies J. Convenient Synthesis of a Propargylated Cyclic (3′-5′) Diguanylic Acid and Its " Click " Conjugation to a Biotinylated Azide. Bioconjug Chem 2010;21:2147–52.

[148] Dodge JA, Nissen JS, Presnell M. A General Procedure for Mitsunobu Inversion of Sterically Hindered Alcohols:Inversıon Of Menthol. (1s,2s,5r)-5-Methyl-2-(1-Methylethyl) Cyclohexyl 4-Nıtrobenzoate. Org Synth Coll 1996;73:110. doi:10.15227/orgsyn.073.0110.

[149] Li X, Zhang C, Wang L, Ma C, Yang W, Li M. Acylation modification of Antheraea pernyi silk fibroin using succinic anhydride and its effects on enzymatic degradation behavior. J Chem 2013;2013:1–7. doi:10.1155/2013/640913.

[150] Gupta B, Tummalapalli M, Deopura BL, Alam MS. Functionalization of pectin by periodate oxidation. Carbohydr Polym 2013;98:1160–5. doi:10.1016/j.carbpol.2013.06.069.

[151] Deshmukh M, Singh Y, Gunaseelan S, Gao D, Stein S, Sinko PJ. Biodegradable poly(ethylene glycol) hydrogels based on a self-elimination degradation mechanism. Biomaterials 2010;31:6675–84. doi:10.1016/j.biomaterials.2010.05.021.

[152] Fink T, Lund P, Pilgaard L, Rasmussen JG, Duroux M, Zachar V. Instability of standard PCR reference genes in adipose-derived stem cells during propagation, differentiation and hypoxic exposure. BMC Mol Biol 2008;9:98. doi:10.1186/1471-2199-9-98.

[153] Sel S, Duygulu O, Kadiroglu U, Machin NE. Synthesis and characterization of nano-V2O5 by flame spray pyrolysis, and its cathodic performance in Li-ion rechargeable batteries. Appl Surf Sci 2014. doi:10.1016/j.apsusc.2014.02.061.

[154] Biochem D of C and. IR Chart. Univ Color Boulder 2011:155–64. http://orgchem.colorado.edu/Spectroscopy/specttutor/irchart.html (accessed December 27, 2014).

[155] Gómez-Ordóñez E, Rupérez P. FTIR-ATR spectroscopy as a tool for polysaccharide identification in edible brown and red seaweeds. Food Hydrocoll 2011;25:1514–20. doi:10.1016/j.foodhyd.2011.02.009.

[156] Alvira M, Eritja R. Synthesis of oligonucleotides carrying 5’-5' linkages using copper-catalyzed cycloaddition reactions. Chem Biodivers 2007;4:2798–809. doi:10.1002/cbdv.200790229.

[157] Sun S, Wu P. Mechanistic Insights into Cu (I) -Catalyzed Azide - Alkyne “ Click ” Cycloaddition Monitored by Real Time Infrared Spectroscopy. J Phys Chem A 2010;114:8331–6. doi:10.1021/jp105034m.

[158] Tsukada M, Gotoh Y, Nagura M, Minoura N, Kasai N, Freddi G. Structural changes of silk fibroin membranes induced by immersion in methanol aqueous solutions. J Polym Sci Part B Polym Phys 1994;32:961–8. doi:10.1002/polb.1994.090320519.

[159] Malkoch M, Vestberg R, Gupta N, Mespouille L, Dubois P, Mason AF, et al. Synthesis of well-defined hydrogel networks using Click chemistry. Chem Commun 2006:2774. doi:10.1039/b603438a.

[160] Nimmo CM, Shoichet MS. Regenerative biomaterials that "click": Simple, aqueous-based protocols for hydrogel synthesis, surface immobilization, and 3D patterning. Bioconjug Chem 2011;22:2199–209. doi:10.1021/bc200281k.

[161] Wang Y, Kim H-J, Vunjak-Novakovic G, Kaplan DL. Stem cell-based tissue engineering with silk biomaterials. Biomaterials 2006;27:6064–82. doi:10.1016/j.biomaterials.2006.07.008.

[162] Furuzono T, Ishihara K, Nakabayashi N, Tamada Y. Chemical modification of silk fibroin with 2-methacryloyloxyethyl phosphorylcholine . II . Graft-polymerization onto fabric through 2-methacryloyloxyethyl isocyanate and interaction between fabric and platelets. Biomaterials 2000;21:327–33.

[163] Gotoh Y, Tsukada M, Aiba S, Minoura N. Chemical modification of silk fibroin with N-acetyl-chito-oligosaccharides. Int J Biol Macromol 1996;18:19–26.

[164] Cumpstey I. Chemical modification of polysaccharides. ISRN Org Chem 2013;2013:417672. doi:10.1155/2013/417672.

[165] Sinitsya A, Čopíková J, Prutyanov V, Skoblya S, MacHovič V. Amidation of highly methoxylated citrus pectin with primary amines. Carbohydr Polym 2000;42:359–68. doi:10.1016/S0144-8617(99)00184-8.

[166] Synytsya A, Copikova J, Marounek M, Mlcochova P, Sihelnihoca L, Blafkova P, et al. Preparation of N -alkylamides of Highly Methylated (HM) Citrus Pectin. Czech J Food Sci 1995;21:162–6.

[167] Rosenbohm C, Lundt I, Christensen TMIE, Young NWG. Chemically methylated and reduced pectins: Preparation, characterisation by 1H NMR spectroscopy, enzymatic degradation, and gelling properties. Carbohydr Res 2003;338:637–49. doi:10.1016/S0008-6215(02)00440-8.

[168] Zhong-Hou Z, Ming-Zhong L, Ting Z, Shu-Qin Y, Xu-Jia C. Preparation of silk fibroin film cross-linked by carbodiimide (EDC). Res Progresses Mod Technol Silk, Text Mech I 2007:346–51\n492.

[169] Fraeye I, Colle I, Vandevenne E, Duvetter T, Van Buggenhout S, Moldenaers P, et al. Influence of pectin structure on texture of pectin-calcium gels. Innov Food Sci Emerg Technol 2010;11:401–9. doi:10.1016/j.ifset.2009.08.015.

[170] Tibbits CW, MacDougall AJ, Ring SG. Calcium binding and swelling behaviour of a high methoxyl pectin gel. Carbohydr Res 1998;310:101–7. doi:10.1016/S0008-6215(98)00172-4.

[171] Kim U-J, Park J, Kim HJ, Wada M, Kaplan DL. Three-dimensional aqueous-derived biomaterial scaffolds from silk fibroin. Biomaterials 2005;26:2775–85. doi:10.1016/j.biomaterials.2004.07.044.

[172] Bhardwaj N, Kundu SC. Silk fibroin protein and chitosan polyelectrolyte complex porous scaffolds for tissue engineering applications. Carbohydr Polym 2011;85:325–33. doi:10.1016/j.carbpol.2011.02.027.

[173] Pamuła E, Dobrzyński P, Bero M, Paluszkiewicz C. Hydrolytic degradation of porous scaffolds for tissue engineering from terpolymer of l-lactide, ε-caprolactone and glycolide. J Mol Struct 2005;744-747:557–62. doi:10.1016/j.molstruc.2004.11.016.

[174] Davidenko N, Campbell JJ, Thian ES, Watson CJ, Cameron RE. Collagen-hyaluronic acid scaffolds for adipose tissue engineering. Acta Biomater 2010;6:3957–68. doi:10.1016/j.actbio.2010.05.005.

[175] Rosellini E, Cristallini C, Barbani N, Vozzi G, Giusti P. Preparation and characterization of alginate/gelatin blend films for cardiac tissue engineering. J Biomed Mater Res A 2009;91:447–53. doi:10.1002/jbm.a.32216.

[176] Zhu J, Marchant RE. Design properties of hydrogel tissue-engineering scaffolds. Expert Rev Med Devices 2011;8:607–26. doi:10.1586/erd.11.27.

[177] Kwon H, Sun L, Cairns DM, Rainbow RS, Preda RC, Kaplan DL, et al. The influence of scaffold material on chondrocytes under inflammatory conditions. Acta Biomater 2013;9:6563–75. doi:10.1016/j.actbio.2013.01.004.

[178] Kurita O, Fujiwara T, Yamazaki E. Characterization of the pectin extracted from citrus peel in the presence of citric acid. Carbohydr Polym 2008;74:725–30. doi:10.1016/j.carbpol.2008.04.033.

[179] Shi J, Xing MMQ, Zhong W. Development of hydrogels and biomimetic regulators as tissue engineering scaffolds. Membranes (Basel) 2012;2:70–90. doi:10.3390/membranes2010070.

[180] Mishra RK, Banthia AK, Majeed ABA. Pectin based formulations for biomedical applications: A review. Asian J Pharm Clin Res 2012;5:1–7.

[181] Archana D, Upadhyay L, Tewari RP, Dutta J, Huang YB, Dutta PK. Chitosan-pectin-alginate as a novel scaffold for tissue engineering applications. Indian J Biotechnol 2013;12:475–82.

[182] Sun L, Li H, Qu L, Zhu R, Fan X, Xue Y, et al. Immobilized lentivirus vector on chondroitin sulfate-hyaluronate acid-silk fibroin hybrid scaffold for tissue-engineered ligament-bone junction. Biomed Res Int 2014;2014:1–10. doi:10.1155/2014/816979.

[183] Nwe N, Furuike T, Tamura H. The mechanical and biological properties of chitosan scaffolds for tissue regeneration templates are significantly enhanced by chitosan from Gongronella butleri. Materials (Basel) 2009;2:374–98. doi:10.3390/ma2020374.

[184] O'Brien FJ, Harley BA, Waller MA, Yannas I V, Gibson LJ, Prendergast PJ. The effect of pore size on permeability and cell attachment in collagen scaffolds for tissue engineering. Technol Health Care 2007;15:3–17.

[185] Jin H-J, Fridrikh S V., Rutledge GC, Kaplan DL. Electrospinning Bombyx mori Silk with Poly(ethylene oxide). Biomacromolecules 2002;3:1233–9. doi:10.1021/bm025581u.

[186] Oliveira AL, Sun L, Kim HJ, Hu X, Rice W, Kluge J, et al. Aligned silk-based 3-D architectures for contact guidance in tissue engineering. Acta Biomater 2012;8:1530–42. doi:10.1016/j.actbio.2011.12.015.

[187] Kumbar S, Laurencin C, Deng M, editors. Natural and Synthetic Biomedical Polymers. 1st ed. San Diego: Elsevier; 2014.

[188] Stark WJ. Nanoparticles in biological systems. Angew Chemie - Int Ed 2011;50:1242–58. doi:10.1002/anie.200906684.

[189] Monshi A. Modified Scherrer Equation to Estimate More Accurately Nano-Crystallite Size Using XRD. World J Nano Sci Eng 2012;02:154–60. doi:10.4236/wjnse.2012.23020.

[190] Sun L, Chow L, Frukhtbeyn SA, Bonevich J. Preparation and Properties of Nanoparticles of Calcium Phosphates With Various Ca/P Ratios. J Res Natl Inst Stand Technol 2010;115:243–55.

[191] Brunner TJ, Grass RN, Bohner M, Stark WJ. Effect of particle size, crystal phase and crystallinity on the reactivity of tricalcium phosphate cements for bone reconstruction. J Mater Chem 2007;17:4072. doi:10.1039/b707171j.

[192] Cho JS, Jung DS, Han JM, Kang YC. Nano-sized α and β-TCP powders prepared by high temperature flame spray pyrolysis. Mater Sci Eng C 2009;29:1288–92. doi:10.1016/j.msec.2008.10.020.

[193] Bharadwaj S, Liu G, Shi Y, Wu R, Yang B, He T, et al. Multipotential differentiation of human urine-derived stem cells: potential for therapeutic applications in urology. Stem Cells 2013;31:1840–56. doi:10.1002/stem.1424.

[194] Lang R, Liu G, Shi Y, Bharadwaj S, Leng X, Zhou X, et al. Self-Renewal and Differentiation Capacity of Urine-Derived Stem Cells after Urine Preservation for 24 Hours. PLoS One 2013;8. doi:10.1371/journal.pone.0053980.

[195] Matsuoka F, Takeuchi I, Agata H, Kagami H, Shiono H, Kiyota Y, et al. Morphology-Based Prediction of Osteogenic Differentiation Potential of Human Mesenchymal Stem Cells. PLoS One 2013;8. doi:10.1371/journal.pone.0055082.

[196] Golub EE, Harrison G, Taylor AG, Camper S, Shapiro IM. The role of alkaline phosphatase in cartilage mineralization. Bone Miner 1992;17:273–8. doi:10.1016/0169-6009(92)90750-8.

[197] Golub EE, Boesze-Battaglia K. The role of alkaline phosphatase in mineralization. Curr Opin Orthop 2007;18:444–8. doi:10.1097/BCO.0b013e3282630851.

[198] SIFFERT RS. The role of alkaline phosphatase in osteogenesis. J Exp Med 1951;93:415–26. doi:10.1084/jem.93.5.415.

[199] Machado C, Correa C, Medrado G, Leite M, Goes A. Ectopic expression of telomerase enhances osteopontin and osteocalcin expression during osteogenic differentiation of human mesenchymal stem cells from elder donors. J Stem Cells Regen Med 2009;5:49–57.

[200] Lock J, Liu H. Nanomaterials enhance osteogenic differentiation of human mesenchymal stem cells similar to a short peptide of BMP-7. Int J Nanomedicine 2011;6:2769–77. doi:10.2147/IJN.S24493.

[201] Chai YC, Carlier A, Bolander J, Roberts SJ, Geris L, Schrooten J, et al. Current views on calcium phosphate osteogenicity and the translation into effective bone regeneration strategies. Acta Biomater 2012;8:3876–87. doi:10.1016/j.actbio.2012.07.002.

APPENDIX A

ETHICS COMMITTEE APPROVAL REPORT

UYGULAMALI ETİK ARAŞTIRMA MERKEZİ
APPLIED ETHICS RESEARCH CENTER

ORTA DOĞU TEKNİK ÜNİVERSİTESİ
MIDDLE EAST TECHNICAL UNIVERSITY

DUMLUPINAR BULVARI 06800
ÇANKAYA ANKARA/TURKEY
T: +90 312 210 22 91
F: +90 312 210 79 59
ueam@metu.edu.tr
www.ueam.metu.edu.tr

Sayı: 28620816/ 23 -109

14.01.2014

Gönderilen : Doç. Dr. Ayşen Tezcaner
Biyomedikal Mühendisliği

Gönderen : Prof. Dr. Canan Özgen
IAK Başkanı

İlgi : Etik Onayı

Danışmanlığını yapmış olduğunuz Biyomedikal Mühendisliği Bölümü öğrencisi Sibel Ataol'un "; Kemik Hasarlarının Tedavisine Yönelik Nanohidroksiapatit İle Güçlendirilmiş Üç Boyutlu Fibroin Ve Pektin Taşıyıcılarının Geliştirilmesi Ve İn Vitro Karakterizasyonu" isimli araştırması "İnsan Araştırmaları Komitesi" tarafından uygun görülerek gerekli onay verilmiştir.

Bilgilerinize saygılarımla sunarım.

Etik Komite Onayı

Uygundur

14/01/2014

Prof.Dr. Canan Özgen
Uygulamalı Etik Araştırma Merkezi
(UEAM) Başkanı
ODTÜ 06531 ANKARA

APPENDIX B

SPECTRAL DATA

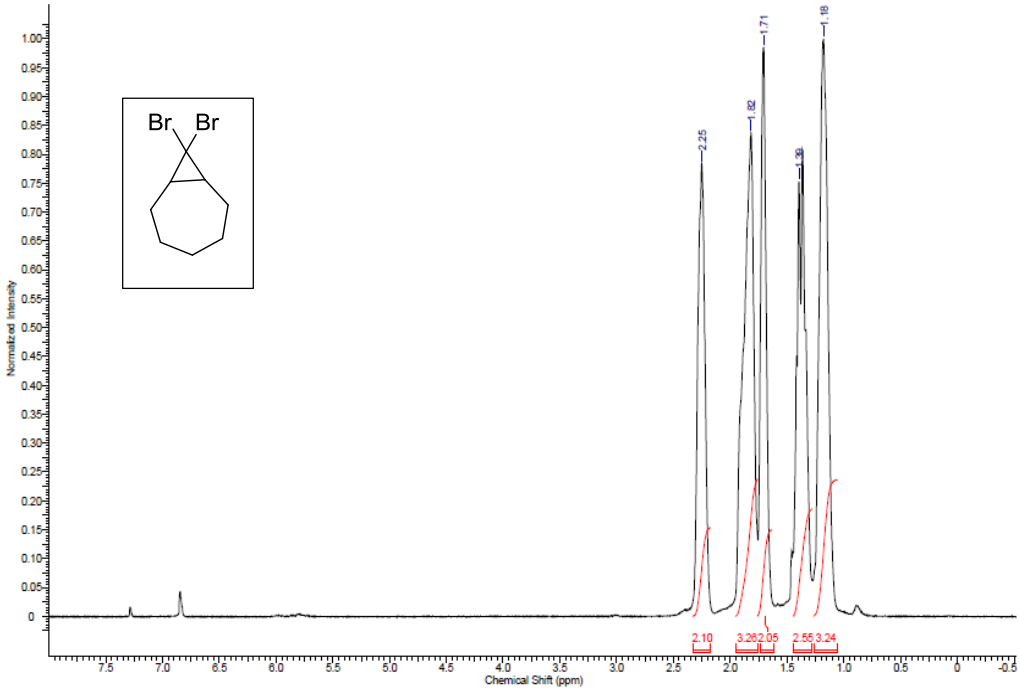

Figure B.1 ^{1}H NMR spectrum of Compound 1

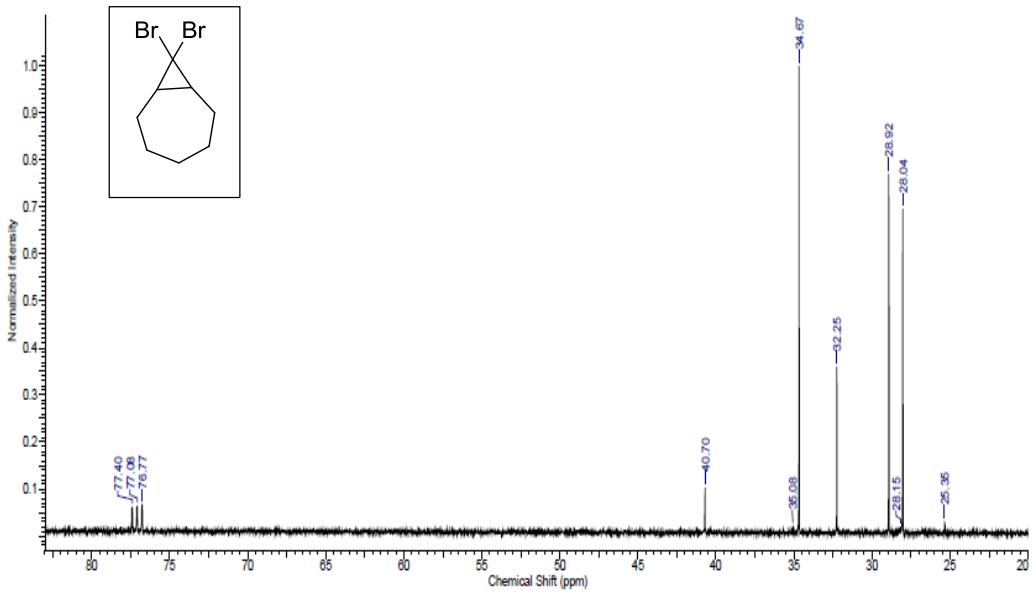

Figure B.2 ^{13}C NMR spectrum of Compound 1

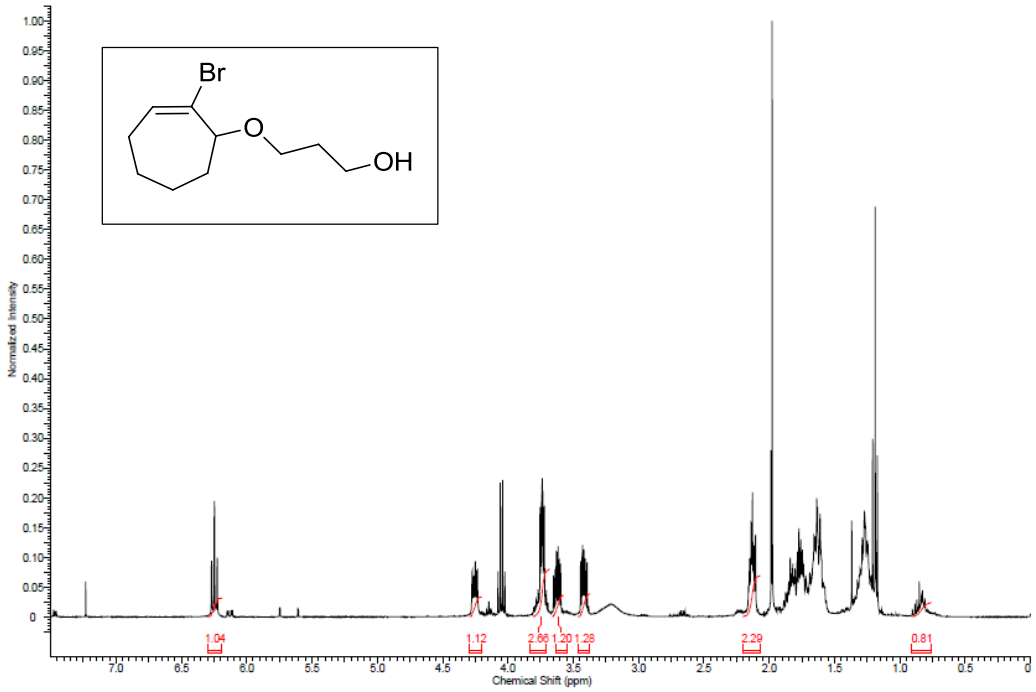

Figure B.3 ^{1}H NMR spectrum of Compound 2

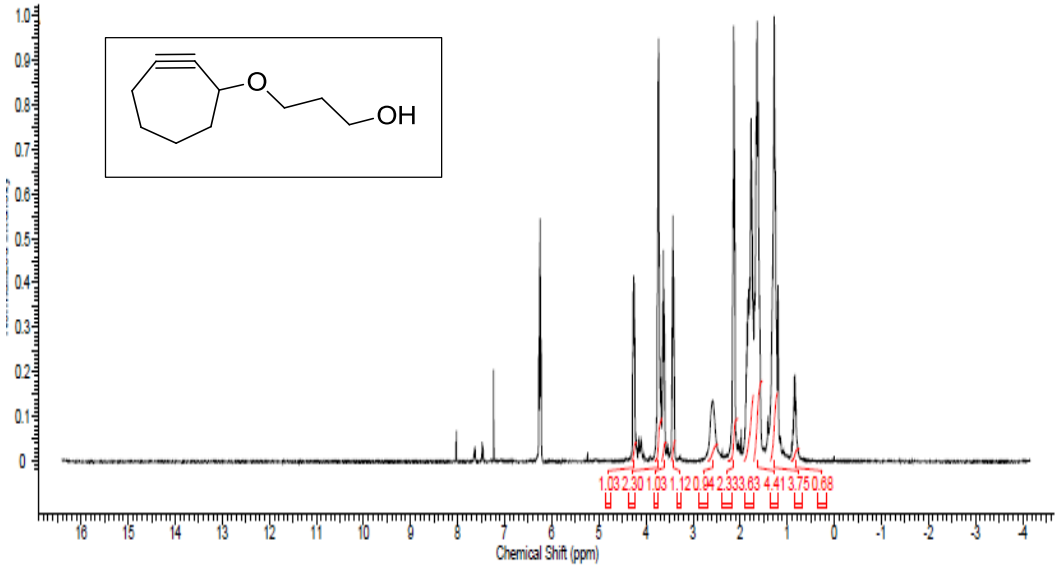

Figure B.4 ^{1}H NMR spectrum of Compound 3

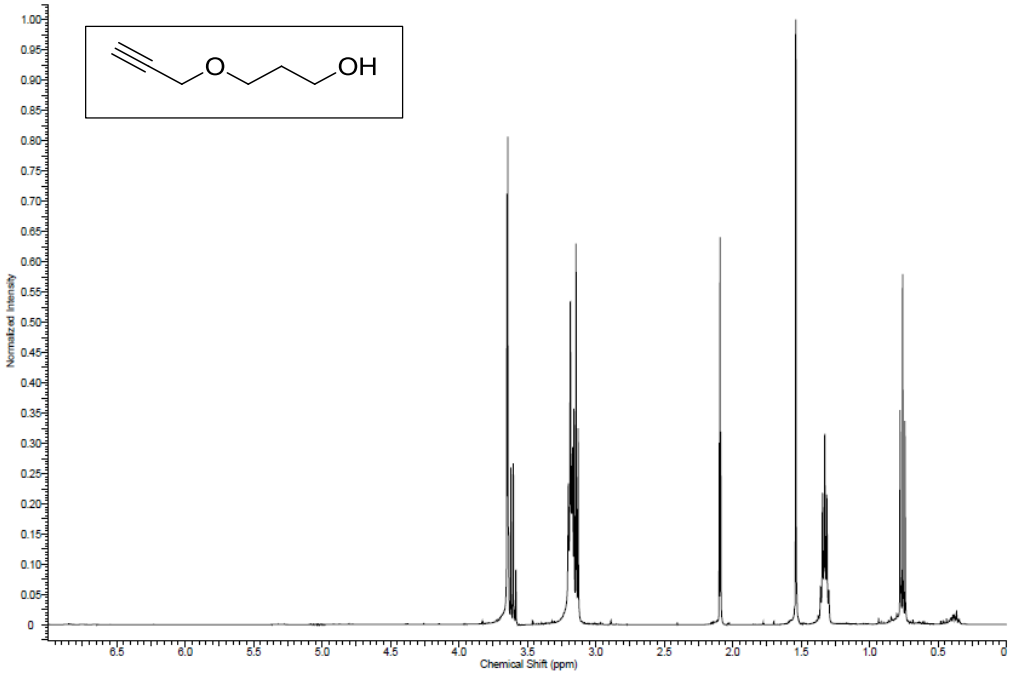

Figure B.5 ^{1}H NMR spectrum of Compound 4

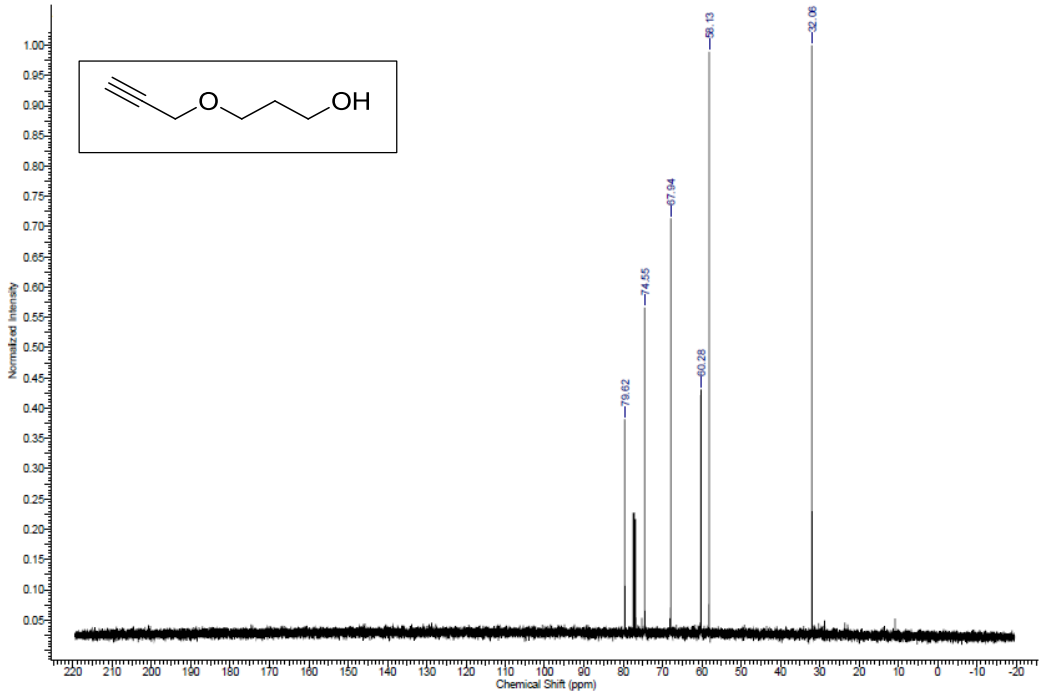

Figure.B.6 ^{13}C NMR spectrum of Compound 4

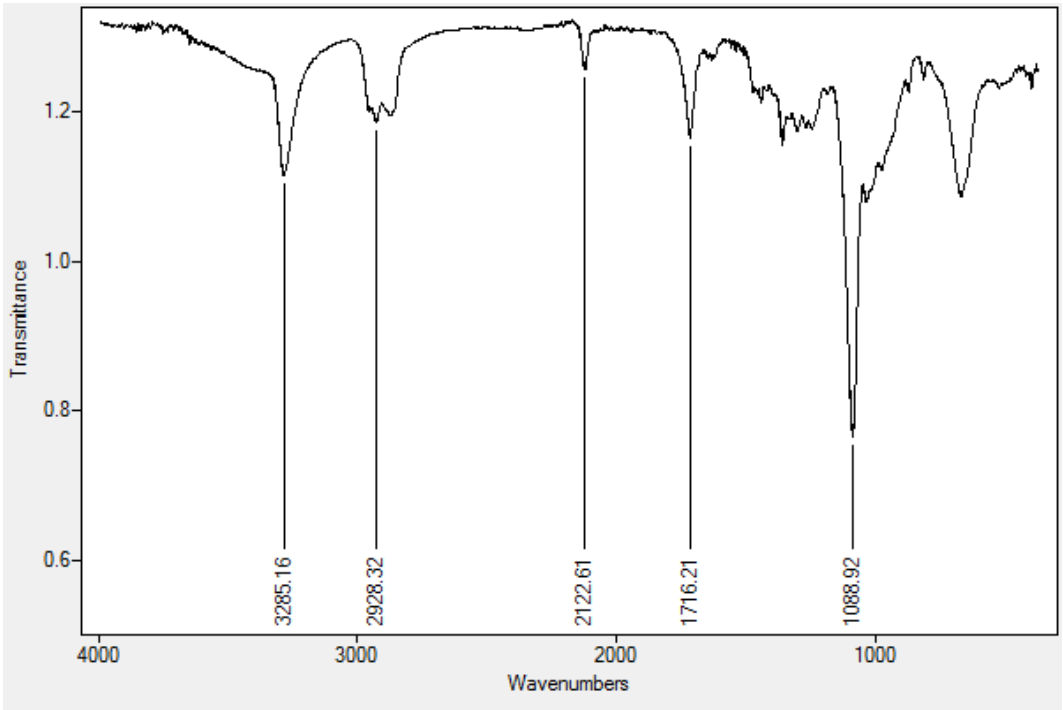

Figure.B.7 FTIR ATR spectrum of Compound 4

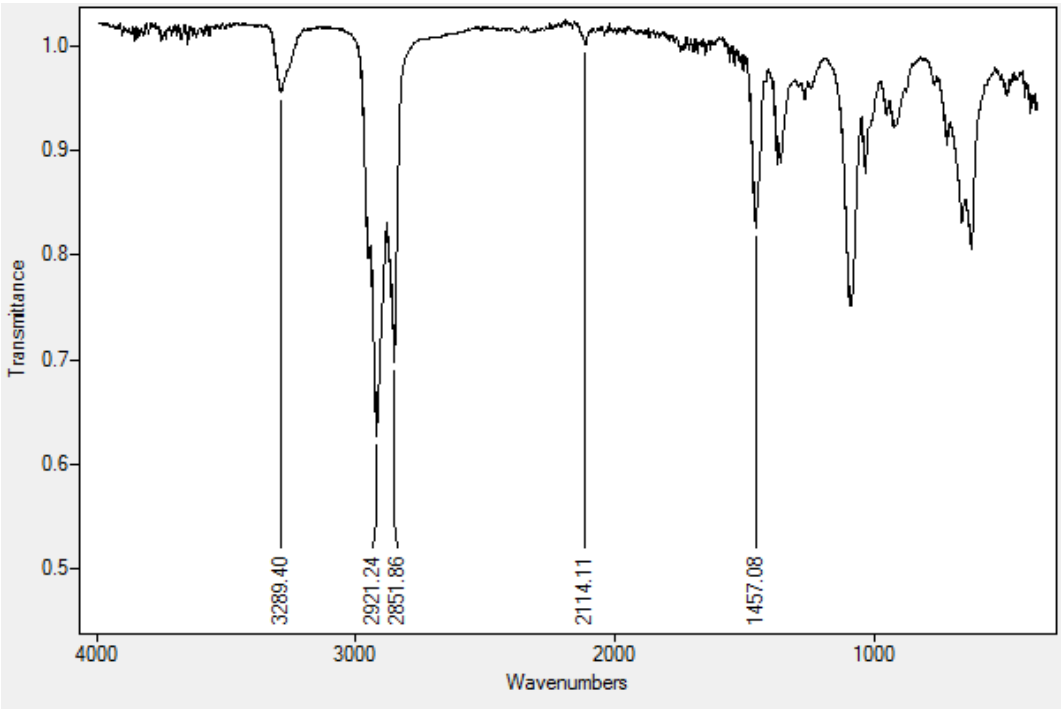

Figure.B.8 FTIR ATR spectrum of Compound 5

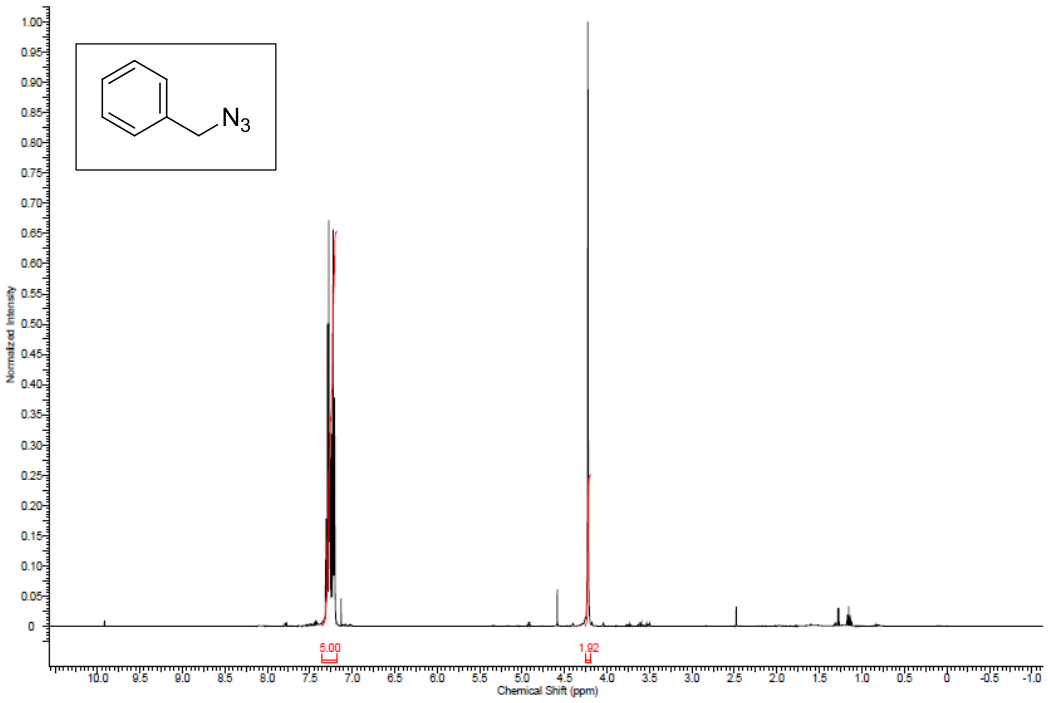

Figure.B.9 ^{1}H NMR spectrum of Compound 7

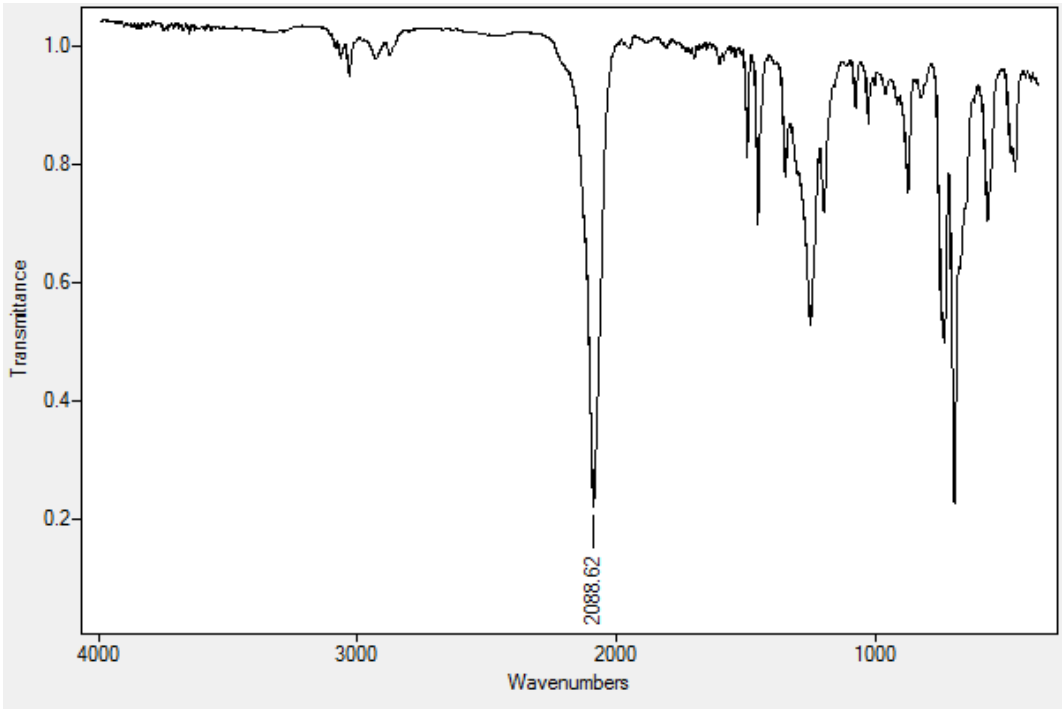

Figure.B.10 FTIR ATR spectrum of Compound 7

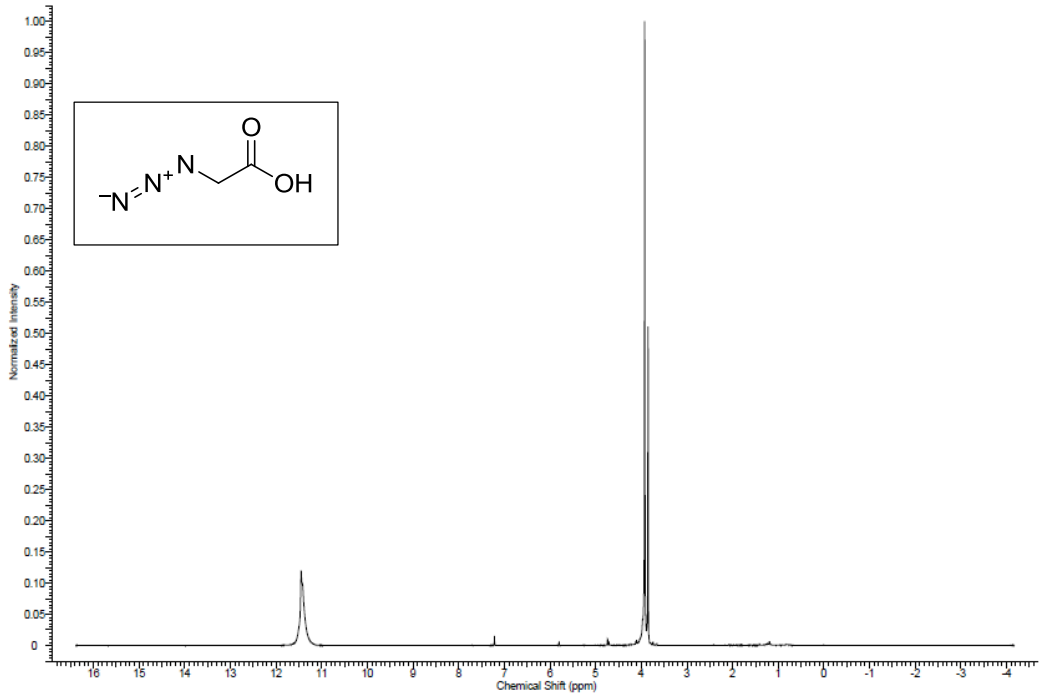

Figure B.11 ^{1}H NMR spectrum of Compound 8

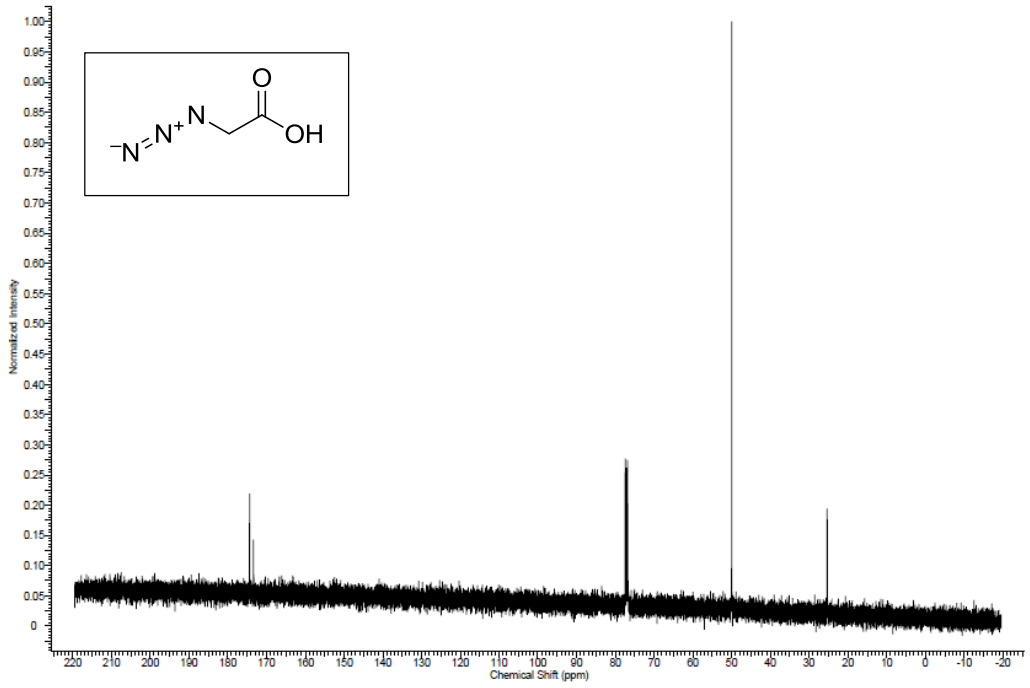

Figure B.12 ^{13}C NMR spectrum of Compound 8

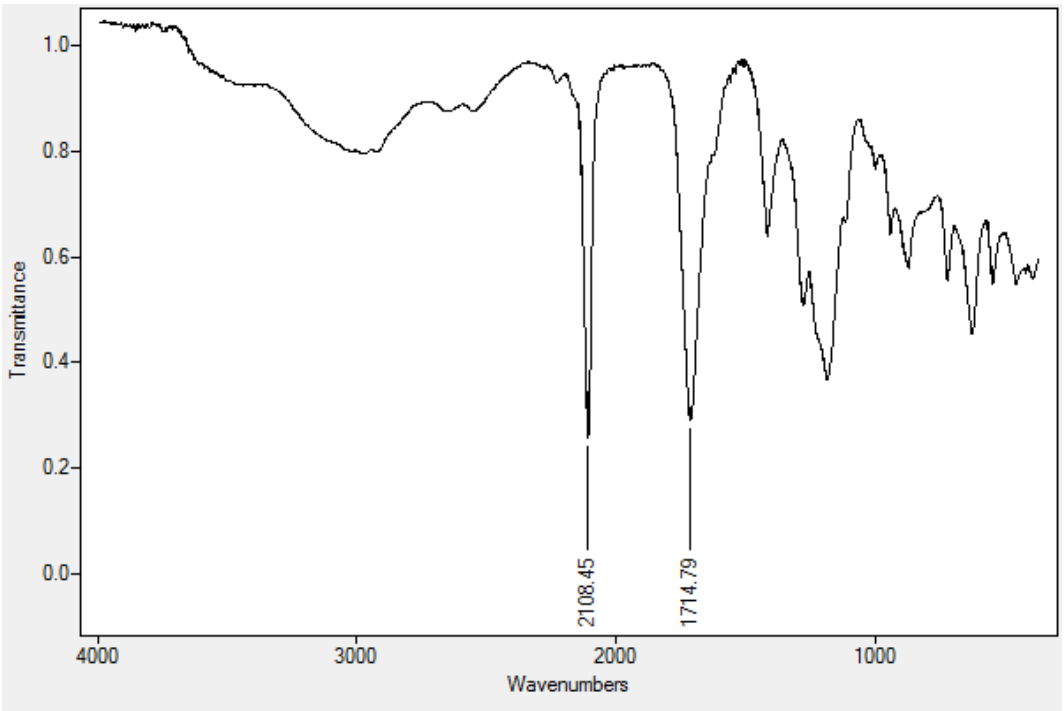

Figure B.13 FTIR ATR spectrum of Compound 8

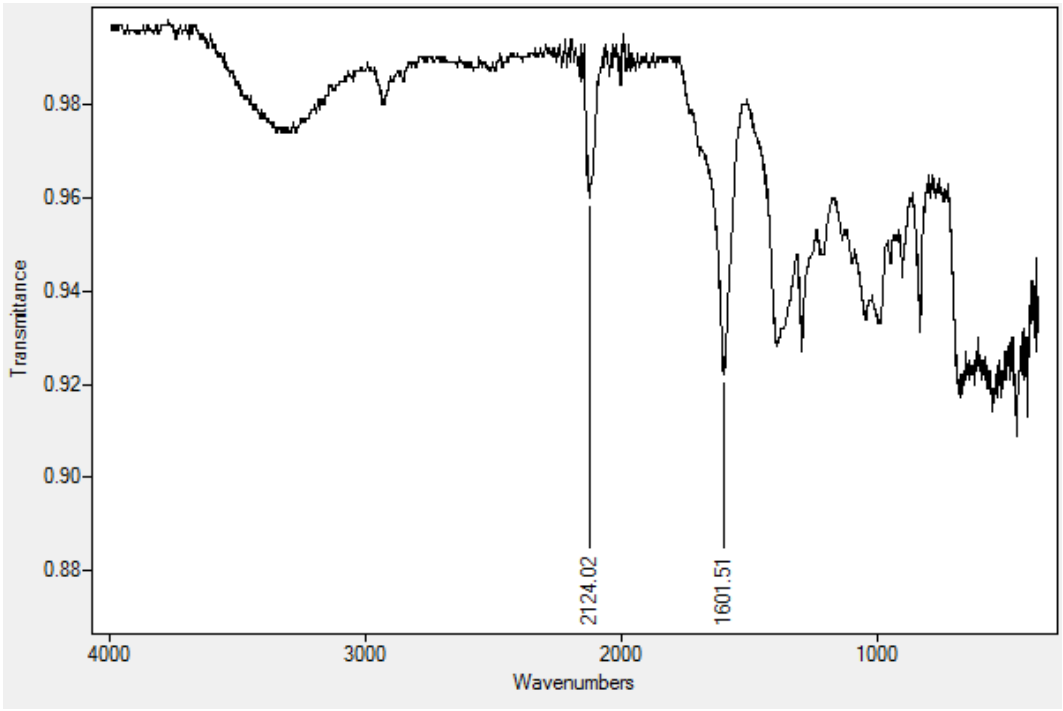

Figure B.14 FTIR ATR spectrum of Compound 9

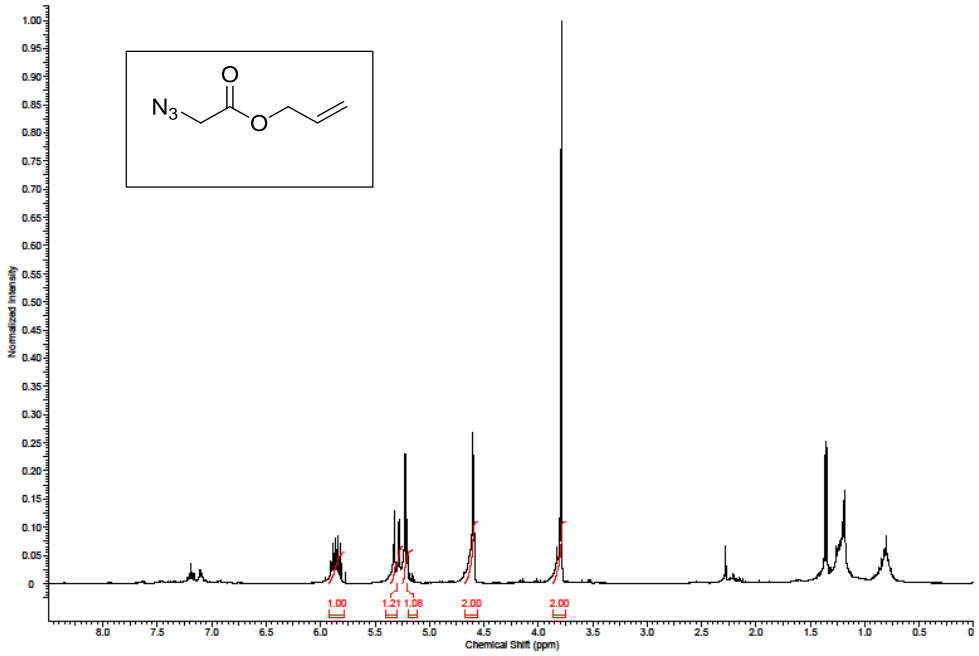

Figure B.15 ^{1}H NMR spectrum of Compound 11

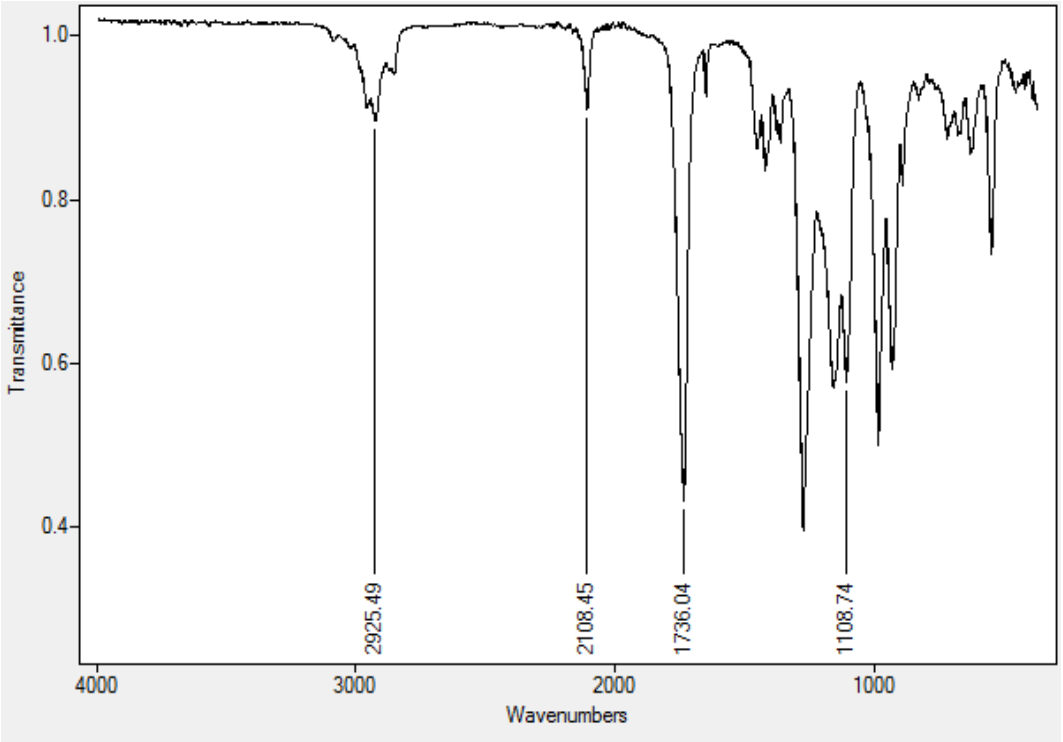

Figure B.16 FTIR ATR spectrum of Compound 11

APPENDIX C

CALIBRATION CURVES

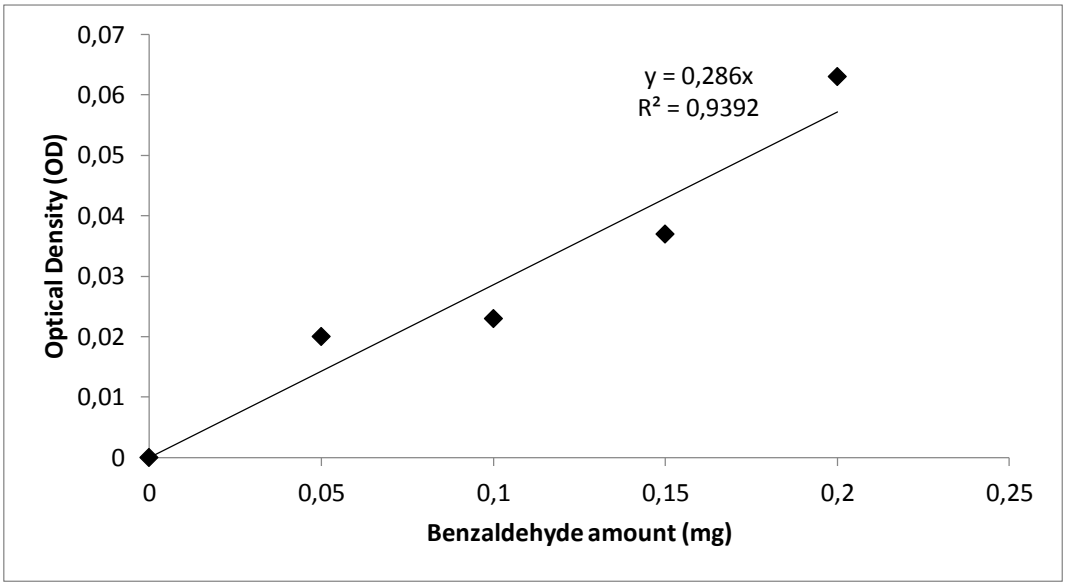

Figure C.1 The calibration curve for determining degree of oxidation using benzaldehyde as standard

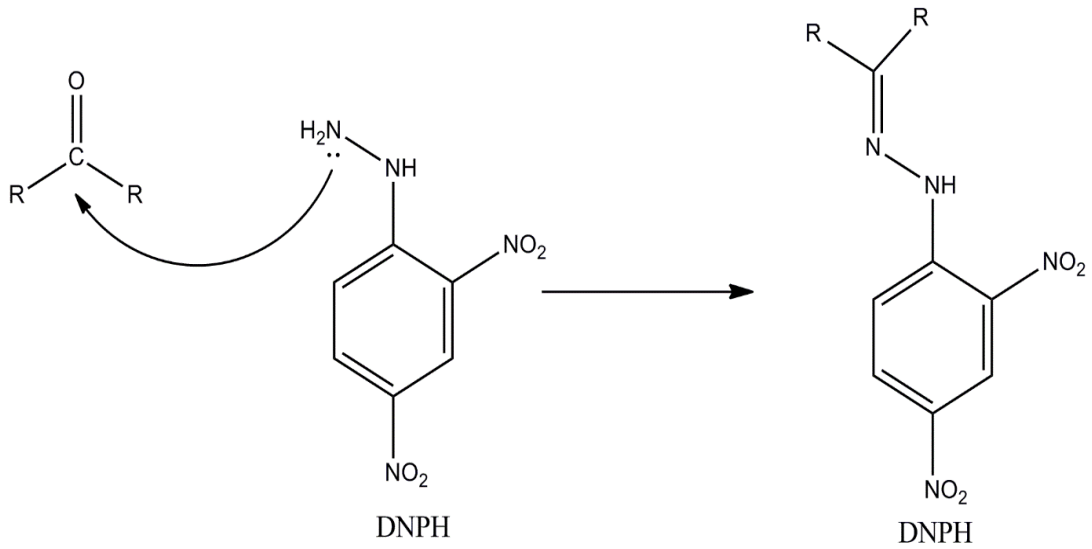

Figure C.2 The reaction scheme of dinitrophenylhydrazine with aldehyde and conversion to dinitrophenylhydrazone

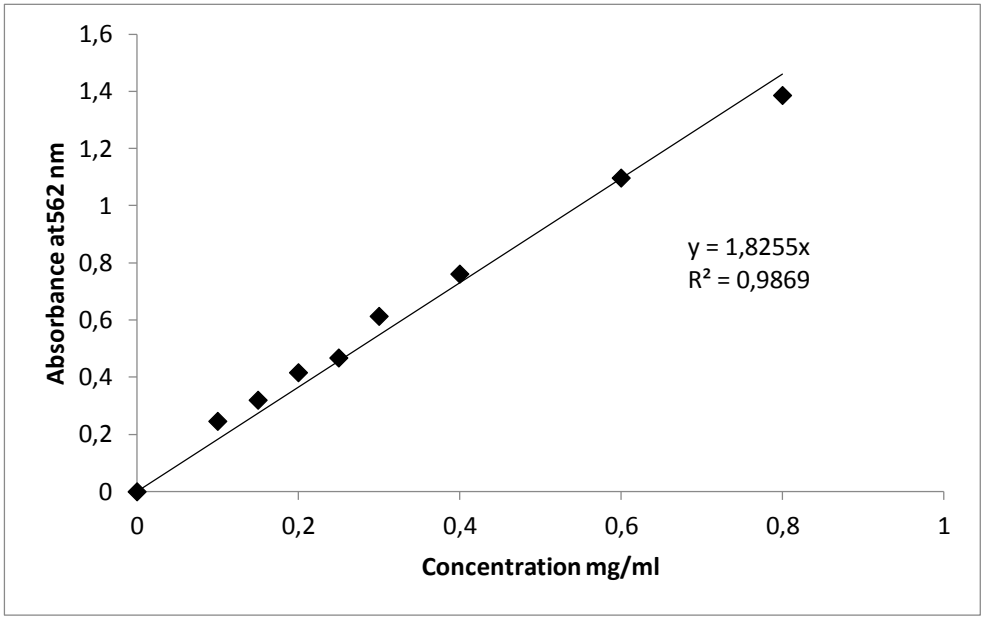

Figure C.3 The calibration curve of BCA assay constructed with bovine serum albumin as standard for protein amount determination

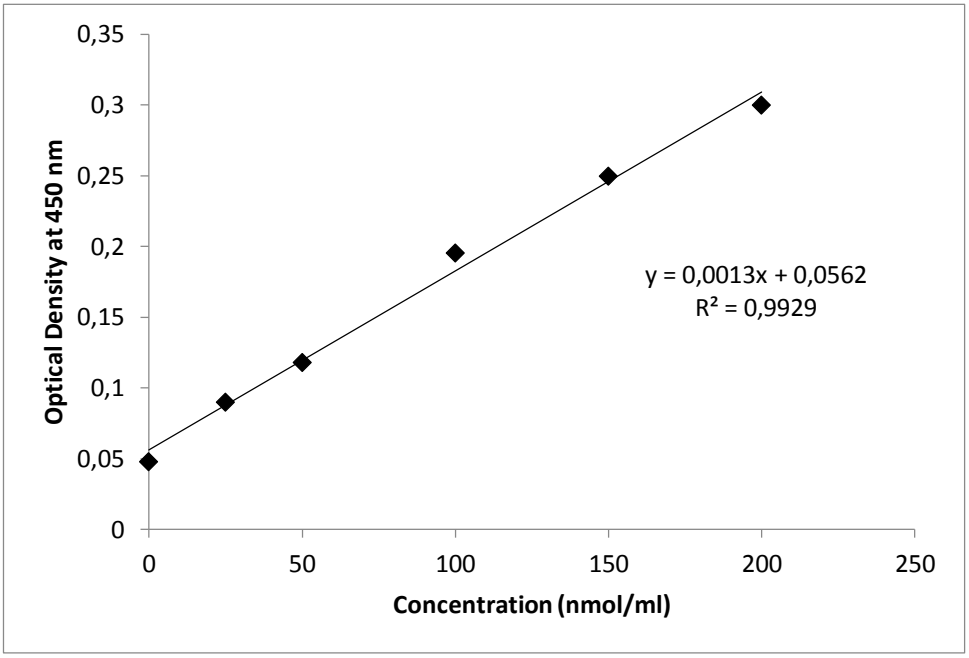

Figure C.4 The calibration curve constructed with p-nitrophenol for ALP activity assay